TECHNISCHE UNIVERSITÄT DARMSTADT

The Interplay of Signaling Dynamics and Cell Cycle Regulation in Single Cells

vom Fachbereich Biologie

der Technischen Universität Darmstadt

zur Erlangung des Grades

Doctor rerum naturalium

(Dr. rer. nat.)

Dissertation

von Stefan Jürgen Bohn

Erstgutachter: Prof. Dr. Alexander Löwer

Zweitgutachterin: Prof. Dr. Ulrike A. Nuber

Darmstadt 2021

Bohn, Stefan Jürgen: The Interplay of Signaling Dynamics and Cell Cycle Regulation in Single Cells

Darmstadt, Technische Universität Darmstadt
Jahr der Veröffentlichung der Dissertation auf TUprints: 2021
Tag der mündlichen Prüfung: 11.06.2021

CONTENTS

ABSTRACT

Signaling pathways that control cellular responses such as proliferation, quiescence, migration and apoptosis are crucial for embryonic development, tissue homeostasis and regeneration. Dysregulation of these signaling processes can result in severe human diseases including cancer. Therefore, to maintain a balance between the above-mentioned cell fates and to prevent pathological events, an interplay between different signaling pathways is indispensable. For instance, mitogenic signaling induced by the mitogen-activated protein kinase (MAPK) and phosphatidylinositol 3-kinase (PI3K)-AKT networks is required for cells to enter the cell cycle and divide. However, to prevent uncontrolled proliferation, anti-mitogenic signals such as those transmitted by mothers against decapentaplegic homologue (SMAD) proteins are essential. To gain a deeper understanding of these pathway interactions, I employed quantitative time-resolved measurements of fluorescent reporters and computer-aided data analysis.

In the first part of the present study, I examined how the MAPK and PI3K/AKT pathways synergize to regulate cell cycle entry and progression. Although these networks have been well characterized in earlier studies, their relative contribution, especially at later cell cycle stages, remains largely unexplored. In order to investigate the response of cells outside of an active cell cycle to acute mitogenic signals, untransformed human breast epithelial cells were first arrested in a quiescent state by growth factor deprivation. Afterwards, epidermal growth factor (EGF)-induced signal processing in individual cells was quantified over time, which revealed that both pathways were necessary for initial cell cycle entry, whereas only PI3K/AKT affected the duration of S-phase at later stages of mitogenic signaling. My results provide evidence that the high metabolic demands of replication are unmet in the absence of AKT signaling, which results in a strongly prolonged S-phase of the cell cycle.

In the second part, I investigated how the cell cycle and mitogenic signals influence the SMAD signaling pathway. I uncovered that ligands of the transforming growth factor beta (TGFb) superfamily signaled very differently in quiescent versus proliferating cells. While TGFb mediated a stronger SMAD2 response in proliferating cells compared to quiescent cells, the opposite was observed upon growth differentiation factor 11 (GDF11) stimulation. I was able to show that MAPK activity was responsible for the switch in ligand sensitivity, most likely through regulation of target genes. Therefore, the question arose whether a single key player or a complete pathway-rewiring were accountable. As RNA sequencing revealed considerable changes in the expression of multiple SMAD-associated genes and single perturbations of SMAD signaling regulators could not explain the observed phenomenon, I hypothesized that a more wide-ranging rewiring of the network is necessary to shift the sensitivity to

different ligands of the TGFb superfamily. However, further studies using genome-scale knockout or activation screenings need to be carried out to validate this idea and recreate the pathway-rewiring in proliferating cells. Besides the switch in ligand sensitivity, I observed different SMAD-mediated cell fates in proliferating and quiescent cells. While apoptosis was only induced in quiescent cells, epithelial to mesenchymal transition (EMT) and cytostasis were found in dividing cells. Interestingly, cellular responses correlated well with the dynamics of SMAD signaling, which suggested that ligands mediate diverse cellular outcomes through different dynamical patterns of SMAD2 nuclear accumulation. This quantitative nature of the pathway was later validated by real-time quantitative PCR (RT-qPCR) and RNA sequencing.

ZUSAMMENFASSUNG

Signalwege, die zelluläre Prozesse wie Proliferation, Quieszenz, Migration und Apoptose steuern, sind entscheidend für Embryonalentwicklung, Gewebehomöostase und Regeneration. Eine Fehlregulation dieser Signalprozesse kann zu schweren Erkrankungen wie Krebs führen. Daher ist eine Wechselwirkung verschiedener Signalwege unerlässlich, um das Gleichgewicht zwischen den oben genannten Zellschicksalen aufrechtzuerhalten und pathologische Ereignisse zu verhindern. Beispielsweise sind mitogene Signale, die durch das MAPK-Netzwerk vermittelt werden, erforderlich, damit Zellen in den Zellzyklus eintreten und sich teilen können. Allerdings sind anti-mitogene Signale, wie sie von SMAD-Proteinen übertragen werden, essenziell, um unkontrollierte Zellteilung zu verhindern. In der vorliegenden Arbeit wurden quantitative zeitaufgelöste Messungen von Reporterzelllinien durchgeführt und die entstandenen Daten mittels computergestützter Analyse evaluiert, um ein besseres Verständnis dieser Wechselwirkungen zu erhalten.

Im ersten Teil meiner Dissertation untersuchte ich wie die MAPK und PI3K/AKT-Signalwege zusammenarbeiten, um den Eintritt und das Fortschreiten des Zellzyklus zu regulieren. Obwohl diese Netzwerke in früheren Studien gut charakterisiert wurden, ist ihr relativer Beitrag, insbesondere in Bezug auf spätere Zellzyklusstadien, noch weitgehend unerforscht. Aus diesem Grund wurde die Reaktion quieszenter Zellen auf akute mitogene Stimuli untersucht. Hierfür wurden zunächst nicht transformierte humane Brustepithelzellen durch den Entzug von Wachstumsfaktoren in Quieszenz gebracht. Danach wurde die EGF-induzierte Signalverarbeitung in einzelnen Zellen über die Zeit quantifiziert, was zeigte, dass beide Signalwege für den Eintritt in den Zellzyklus notwendig sind, aber nur PI3K/AKT die Dauer der S-Phase beeinflusste. Meine Ergebnisse deuten darauf hin, dass die hohen Stoffwechselanforderungen der S-Phase ohne funktionsfähiges AKT nicht erfüllt werden, wodurch es zu einer stark verlängerten Zellzyklusphase kommt.

Im zweiten Teil meiner Arbeit untersuchte ich, wie der Zellzyklus und mitogene Signale den SMAD-Signalweg beeinflussen. Dabei ergab sich, dass Liganden der TGFb-Superfamilie in ruhenden und sich teilenden Zellen sehr unterschiedliche Auswirkungen haben. Während TGFb eine stärkere SMAD2-Antwort in proliferierenden Zellen im Vergleich zu quieszenten Zellen induzierte, hatte GDF11 einen gegenteiligen Effekt. Ich konnte zeigen, dass der Grund für den Wechsel der Liganden-Empfindlichkeit die MAPK-Aktivität war, welche vermutlich die Regulation der Zielgene veränderte. Daher stellte sich als nächstes die Frage, ob ein einzelnes Gen oder eine vollständige Neuverschaltung des Signalweges für diesen Effekt verantwortlich war. Da RNA-Sequenzierung deutliche Veränderungen in der Expression mehrerer SMAD-assoziierter Gene zeigte und einzelne

Störungen der SMAD-Signalregulatoren das beobachtete Phänomen nicht nachbilden konnten, stellte ich die Hypothese auf, dass eine umfassendere Neuverschaltung des Netzwerks erforderlich ist, um die Empfindlichkeit gegenüber verschiedener Liganden zu verändern. Allerdings müssten weitere Studien, die beispielsweise Knockout- oder Aktivierungsscreenings im genomischen Maßstab verwenden, durchgeführt werden, um diese Hypothese zu validieren. Zusätzlich zur Änderung der Liganden-Empfindlichkeit beobachtete ich verschiedene SMAD-vermittelte Zellschicksale in proliferierenden und ruhenden Zellen. Während Apoptose nur in Zellen außerhalb eines aktiven Zellzyklus festgestellt wurde, wurden EMT und Zytostase nur in sich teilenden Zellen nachgewiesen. Die zellulären Reaktionen korrelierten sehr stark mit der Dynamik der SMAD-Signalübertragung, was darauf hindeutet, dass Liganden unterschiedliche zelluläre Auswirkungen durch Variationen in den SMAD2-Dynamiken vermitteln. Diese quantitativen Eigenschaften des Signalweges wurden später durch RT-qPCR und RNA-Sequenzierung bestätigt.

1 INTRODUCTION

1.1 THE DEVELOPMENT OF THE MAMMARY GLAND

According to current estimations, the human body is composed of 3.72×10^{13} cells (Bianconi et al., 2013). In adult organisms, most of these cells are non-dividing and outside of an active cell cycle. The non-dividing state can be separated into two groups, irreversibly arrested and reactivatable cells. Irreversibly arrested cells, such as senescent or terminally differentiated cells, can no longer re-enter and progress through the cell cycle. In comparison, reactivatable cells are capable of resuming proliferation under appropriate physiological conditions (Figure 1A). These cells are often referred to as quiescent or G0 cells and occur, for example, in the liver (hepatocytes), blood (lymphocytes) or connective tissue (fibroblasts). Additionally, adult stem cells and some epithelial cells can reside in a quiescent cell state. The switch between proliferation and quiescence is essential for regeneration and tissue homeostasis of higher organisms (Yao, 2014). For example, hepatocytes are highly differentiated cells that are usually in a quiescent state but resume proliferation for liver regeneration and repair (Fausto, 2004). Another prime example for a tissue that alternates between proliferation states is the mammary gland. The rudiment of the gland is present at birth and remains in a quiescent state until the final stages of its development occur during puberty. Under the control of hormones, proliferation and migration is induced and enables the gland epithelium to invade into the mammary fat pad (Figure 1B). This process is referred to as branching morphogenesis and results in a bilayered ductal structure composed of an inner layer of luminal epithelial cells and an outer layer of myoepithelial cells. During each estrous cycle, the cells of the bilayered ductal structure proliferate and die. Due to hormonal changes throughout pregnancy and lactation, the epithelium is remodeled to form secretory alveoli through proliferation and migration. Upon weaning, a process called involution restructures the epithelium once again and returns the mammary gland to its quiescent state. This highlights that from birth to adulthood, the mammary gland undergoes enormous morphological changes that are controlled by hormones and paracrine signals. Each cycle of pregnancy, lactation and involution is accompanied by an interplay of proliferation, differentiation, migration and apoptosis (Inman et al., 2015).

These developmental features make the mammary gland a versatile tissue, but at the same time prone to diseases such as cancer. Apart from some types of skin cancer, breast cancer is the most common malignancy in woman. In 2020 it even surpassed lung cancer as the most diagnosed cancer with over two million cases worldwide (Sung et al., 2021). In the mammary gland, malignancies arise predominantly from the luminal epithelial cells. Given the frequency with which cells divide in this tissue, it is not inconceivable that, despite low endogenous mutations rates, around one in eight women is expected to develop breast cancer. During a woman's life, the breast can undergo

approximately 450 cycles of proliferation and involution in response to hormonal changes induced by each menstrual cycle. Another tissue that comprises epithelial cells with a high turnover rate (3-5 days) is the intestine. Therefore, it is not surprising that two of the most common cancers in human occur in breast and colonic epitheliums (Barker, 2014; Hinck and Näthke, 2014).

To prevent diseases such as cancer but still enable plasticity and regeneration in tissues like the mammary gland, pathways controlling proliferation, cytostasis, apoptosis, adhesion and migration need to be tightly and highly regulated. For example, to maintain the balance between quiescence and proliferation, the rate and timing of cell divisions need to be precisely coordinated by intracellular signaling pathways and extracellular stimuli. Crucial regulators of cell cycle entry and progression are the mitogen-activated protein kinase (MAPK) and phosphatidylinositol 3-kinase (PI3K)-AKT pathways (Seger and Krebs, 1995; Liang and Slingerland, 2003). In the breast, hormones such as estradiol and progesterone or growth factors like epidermal growth factor (EGF) can stimulate cell proliferation by activation of MAPK and PI3K. Moreover, approximately half of breast tumors show increased activity of MAPK pathways and around 70 % exhibit mutations of the PI3K network, making the two pathways key regulators in breast cancer growth (Simoncini et al., 2000; Santen et al., 2002; Hernandez-Aya and Gonzalez-Angulo, 2011). To oppose the effects of mitogenic signaling, anti-proliferative signals such as those transmitted by transforming growth factor beta (TGFb) superfamily ligands are indispensable to balance proliferation and cytostasis (Massagué and Polyak, 1995). For instance, the branching process is inhibited by endogenous production of the cytokine TGFb once the fat pad of the breast is filled with the ductal epithelium (Nelson et al., 2006). Besides regulating cell cycle progression, pathways involved in mammary gland development coordinate migration and apoptosis to remodel the epithelium. Again, TGFb signaling is crucial in regulating these cellular responses. For example, weaning-induced involution is TGFb dependent as the cytokine initiates apoptosis and subsequently cell clearance through phagocytosis (Nguyen and Pollard, 2000; Kolek et al., 2003; Fornetti et al., 2016; Guo et al., 2017). Furthermore, TGFb signaling plays an important role in the transdifferentiation of epithelial cells to mesenchymal cells (epithelial to mesenchymal transition, EMT), a process that is utilized by the mammary gland tissue to facilitate branching morphogenesis (Miettinen et al., 1994; Robson et al., 2006). As TGFb signaling is essential for the development of the breast, dysregulations of the pathway have severe consequences. While cytostatic and apoptosis-inducing effects contribute to a tumor suppressive role of TGFb during early oncogenic events, EMT is associated with increased cancer cell motility, invasion and metastasis in later stages of tumor progression. Thus, paradoxically, TGFb can function as a tumor suppressor as well as a tumor promotor in breast cancer (Zarzynska, 2014).

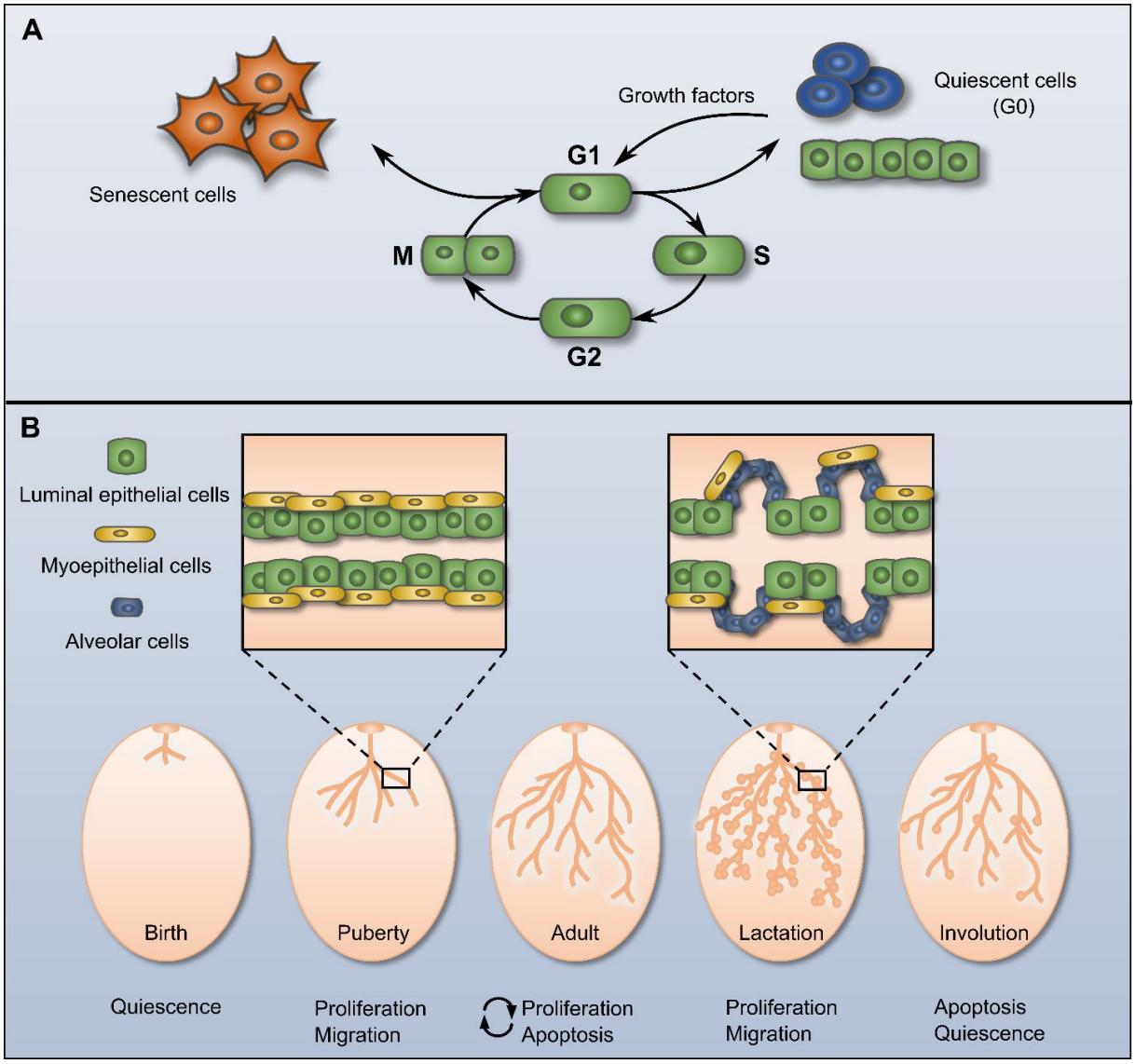

Figure 1: Schematic representation of proliferation states and the development of the mammary gland.

(A) Cells are shown that enter a reversible (quiescent) or irreversible (senescent) proliferation state from the G1-phase of the cell cycle. Quiescent cells usually require appropriate extrinsic signals to resume proliferation. **(B)** The development of the mammary gland from birth to involution is shown. During puberty and adulthood, the epithelial ductal cells expand into the mammary fat pad until it is filled out and the branching process stops. The ducts of the branching structures contain an inner layer of luminal epithelial cells and an outer layer of myoepithelial cells. During pregnancy and lactation, hormonal changes remodel the mammary gland to form secretory alveoli. Upon weaning, the gland is restructured once again by involution, which causes the mammary gland to return to its quiescent state. Each cycle of pregnancy, lactation and involution is accompanied by an interplay of cellular responses such as proliferation, migration and apoptosis. The schematic representation of the mammary gland development **(B)** is based on Inman et al., 2015.

1.2 CELL CYCLE PROGRESSION THROUGH PRO-MITOTIC SIGNALING

As indicated above, proliferation is crucial for many biological processes such as the development of the mammary gland or regeneration of the liver. For a cell to divide, it needs to enter the cell cycle, a complex process in which various regulatory proteins are required to guide a cell through a specific sequence of events. In these events, cells increase in size (G1-phase), duplicate their DNA (S-phase), prepare to divide (G2-phase) and finally split into two daughter cells (mitosis or M-phase). To prevent uncontrolled cell divisions, transitions between consecutive phases need to be strictly regulated by different molecular regulators.

1.2.1 CDK-CYCLIN NETWORK

Two key protein families that determine this progression through the cell cycle are cyclins and cyclin-dependent kinases (CDKs). While cyclin levels increase or decrease over the course of the cell cycle, CDK protein levels remain stable. CDKs are serine/threonine kinases that are inactive in the absence of partner cyclins. Upon formation of a heterodimer, CDKs are activated and able to mediate the phosphorylation of downstream targets to coordinate the transitions of cell cycle phases. Each transition is regulated by different cyclin-CDK combinations (Figure 2A) (Schafer, 1998; Vermeulen et al., 2003; Suryadinata et al., 2010). In order to facilitate cell cycle entry and the transition from G0 to G1, CDK3-cyclin C complexes are required. These complexes initiate the phosphorylation of the retinoblastoma protein (RB) at S807/811 and thereby inactivate it. In its active from, RB binds and represses the E2F family of transcription factors. Upon phosphorylation of RB, E2F proteins can dissociate and induce the expression of genes necessary for G0 exit. Interestingly, S807/811 is also a substrate for CDK4-cyclin D complexes, and cells lacking CDK3 but possessing functional CDK4 can still undergo the transition from G0 to G1 (Ren and Rollins, 2004; Sage, 2004). Furthermore, a study in T-lymphocytes showed that CDK4/6-cyclin D activity is necessary for G0 exit (Lea et al., 2003). After a cell enters the G1-phase, it requires continuous mitogenic signals and a steady rate of protein synthesis to progress through G1 and prevent it from reverting to a quiescent state. If both conditions are met, cells pass a restriction point at which they will continue to progress into S-phase even if growth factors are removed (Zetterberg et al., 1995). At the beginning of the G1-phase, and before the restriction point, mainly CDK4/6-cyclin D complexes mediate the phosphorylation of RB. Upon phosphorylation, E2F transcription factors are activated, which induces the accumulation of cyclin E in later stages of G1 in cells that have passed the restriction point (Ohtani et al., 1995; Ekholm et al., 2001). Cyclin E then forms an active complex with CDK2 that further phosphorylates pRB together with CDK4/6-cyclin D.

Throughout the remainder of the cell cycle, pRB stays hyperphosphorylated and thus in an inactive state (Schafer, 1998). The phosphorylation of RB at multiple sites leads to a complete activation of E2F and thereby to an even stronger transcriptional activation of the cyclin E gene (Suryadinata et al., 2010). The CDK2-cyclin E complexes then regulate the progression from G1- to S-phase (Ohtsubo et al., 1995). As cells pass into S-phase, cyclin A accumulates and associates with CDK2 while cyclin E is degraded by the ubiquitin-proteasome pathway (Clurman et al., 1996; Ekholm et al., 2001). Interestingly, cyclin A activates two distinct CDKs and therefore plays an important role not only in regulating S-phase, but also in controlling the transition from G2- to M-phase. While the activation of CDK2 leads to S-phase progression, the binding to CDK1 promotes the transition from G2- to M-phase (Bendris et al., 2011). To precisely time the mitotic entry, the activated CDK1-cyclin A dimers regulate the activation and stabilization of CDK1-cyclin B complexes (Boer et al., 2008). Once cyclin B has bound CDK1, cyclin A is degraded by ubiquitin-mediated proteolysis (Elzen and Pines, 2001). Depending on CDK1-cyclin B, cells progress through mitosis and ultimately exit this cell cycle phase upon proteasomal degradation of cyclin B (Hershko, 1999; Suryadinata et al., 2010). Besides mitogenic stimuli that induce cyclins and CDKs, there are also anti-mitogenic signals that prevent the progression of the cell cycle, for example by inducing cyclin-dependent kinase inhibitors (CKIs) such as p15 and p21 (Quereda et al., 2016).

1.2.2 MAPK SIGNALING

The MAPK pathway is crucial for cell cycle entry and progression as it regulates cyclins and CKIs. To activate the MAPK pathway, cells rely on mitogenic stimuli, such as EGF and their respective receptors. When EGF binds and activates the EGF receptor (EGFR), the small GTPase RAS induces phosphorylation and activation of the kinase rapidly accelerated fibrosarcoma (RAF), which induces a cascade of phosphorylation events that include consecutive activation of MAPK/ERK kinase (MEK) and extracellular signal-regulated kinase (ERK). Upon phosphorylation, ERK translocates to the nucleus and activates transcription of target genes (Figure 2B). Among the first target genes expressed is the transcription factor *FOS*, which is crucial for cellular processes such as proliferation. Thus, *FOS* is usually not expressed in quiescent cells, but its transcription is induced within minutes after stimulation. Once the transcription factor is produced, it is rapidly degraded. However, the FOS protein can be stabilized through C-terminal phosphorylation which is mediated by nuclear ERK. Therefore, ERK not only activates mRNA transcription of *FOS*, but also prevents the degradation of the corresponding protein. Moreover, target genes of the FOS transcription factor, such as *FRA1/FOSL1*, are stabilized by ERK phosphorylation as well. For this reason, a prolonged ERK activity is required to induce FOS and subsequent FRA/FOSL1 production (Marshall, 1995; Plotnikov et al., 2011; Gillies et al., 2017). In

addition to this temporal encoding, information in the MAPK pathway may be encoded by the amplitude and duration of ERK signaling (Heinrich et al., 2002). Other features like frequency and amplitude of cytoplasmic to nuclear ERK oscillation may further affect cellular responses (Shankaran et al., 2009). Besides modulating *FOS* expression, ERK promotes proliferation by inducing expression of cyclin D and repression of CKIs (Zhang and Liu, 2002; Rubinfeld and Seger, 2005). As mentioned above, activated CDKs phosphorylate RB, which marks the transition from G1- to S-phase of the cell cycle. Other signaling-induced processes, such as expression and stabilization of *MYC*, contribute to regulating the G1- to S-phase transition (Leung et al., 2008).

1.2.3 PI3K/AKT SIGNALING

In addition to the MAPK pathway, EGFR also activates the PI3K/AKT pathway through direct or indirect recruitment and activation of the PI3K subunits p85 and p110. In quiescent cells, the regulatory subunit p85 maintains the catalytic subunit p110 in a low-activity state. Through interaction with activated growth factor receptors, the basal inhibition of p110 by p85 is disrupted and the subunits are recruited to their substrate phosphatidylinositol-4,5-bisphosphate (PIP2) at the plasma membrane. PI3K activity then leads to generation of phosphatidylinositol-3,4,5-triphosphate (PIP3), which in turn recruits the kinases AKT and phosphoinositide-dependent kinase 1 (PDK1) to the membrane. This brings the proteins into proximity and enables phosphorylation and thus activation of AKT by PDK1 (Figure 2B). Through activation of mechanistic target of rapamycin kinase (mTOR), AKT influences translation and contributes to cyclin D accumulation during cell cycle entry (Cantley, 2002; Hay and Sonenberg, 2004; Engelman et al., 2006). In addition, AKT also mediates inhibitory phosphorylation of the cyclin D repressor forkhead box O (FOXO) and the kinase glycogen synthase kinase 3 beta (GSK3beta), which induces cyclin D degradation (Schmidt et al., 2002; Dong et al., 2005). Furthermore, AKT signaling may contribute not only to the transition from G1- to S-phase, but also to other cell cycle transitions by affecting the activity and localization of regulatory proteins and by controlling metabolism (Ward and Thompson, 2012).

The PI3K and MAPK pathways interact closely upon mitogenic stimulation (Moelling et al., 2002; Chen et al., 2012). It has been suggested that both pathways are compensatory through co-regulated proteins (Zwang et al., 2011). Other reports indicate that AKT negatively regulates MAPK activity through inactivation of RAF, whereas MEK suppresses PI3K signaling by promoting membrane localization of the phosphatase and tensin homologue (PTEN) (Zimmermann and Moelling, 1999; Zmajkovicova et al., 2013). PTEN dephosphorylates PIP3 and thus terminates PI3K/AKT signaling (Engelman et al., 2006).

Taken together, the importance and synergy of ERK and AKT in initiating the cell cycle from G0- to S-phase has been well researched, such as the mechanisms by which these pathways interact in controlling cyclin D. In contrast, the relative roles of AKT and ERK in controlling later stages of the cell cycle are less clear and therefore require further detailed investigations.

In addition to pro-mitotic signals mediated by the MEK/ERK and PI3K/AKT pathways, there are also anti-proliferative signals that prevent uncontrolled cell division. One of the most important signaling pathway to transmit such anti-mitotic signals is the mothers against decapentaplegic homologue (SMAD) network.

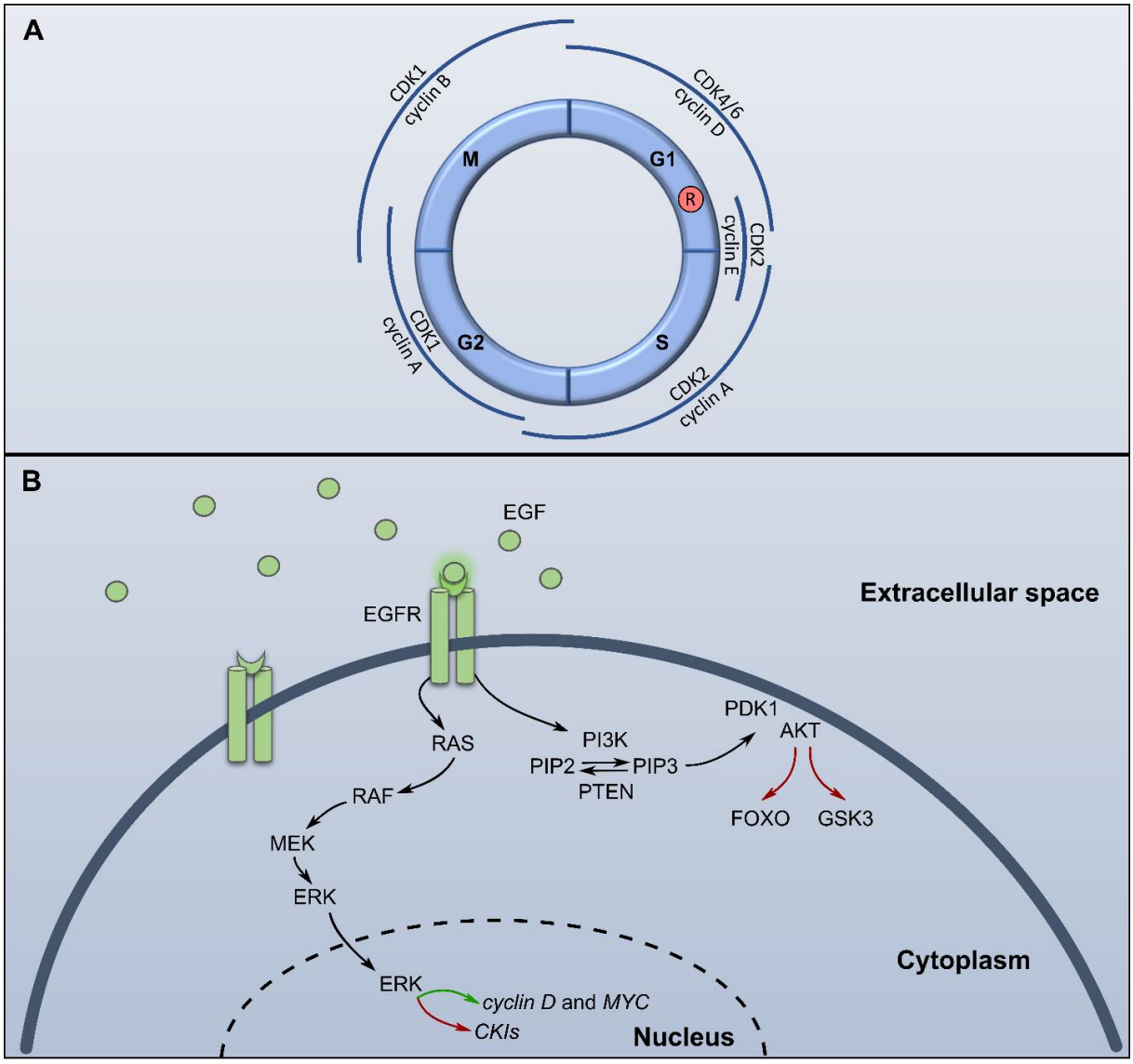

Figure 2: Schematic representation of CDKs, cyclins and signaling pathways that control the cell cycle.

(A) Various CDK-cyclin combinations that regulate cell cycle progression are shown. CDK4/6-cyclin D and CDK2-cyclin E complexes regulate G1-phase progression and S-phase entry, respectively. To control S-phase progression, cyclin A activates CDK2. Afterwards, CDK2 is replaced by CDK1 to mediate the transition from G2- to M-phase through activation and stabilization of CDK1-cyclin B complexes. Finally, CDK1 and cyclin B regulate M-phase progression until cyclin B is degraded and cells exit the corresponding cell cycle phase. Additionally, the restriction point (R) is marked in the cell cycle. Once cells reach the R-point, they are committed to enter S-phase despite a lack of growth factors. **(B)** The MEK/ERK and PI3K/AKT signaling pathways are shown. EGFR stimulation triggers the activation of RAS, RAF, MEK, ERK, PI3K and AKT. Upon activation, ERK translocates into the nucleus and regulates expression and stabilization of numerous targets, while activated AKT inhibits different kinases and transcription factors such as GSK3 and FOXO, respectively. Green arrows indicate a positive and red arrows a negative regulation. The schematic representation of the cell cycle **(A)** is based on Suryadinata et al., 2010.

1.3 SMAD SIGNALING AND ITS PLETHORA OF CELLULAR FUNCTIONS

The SMAD pathway is a crucial signaling network during embryonic development and in the adult organism as it controls many cellular processes including cell growth, proliferation, differentiation, migration, adhesion and cell death (Schmierer and Hill, 2007; Heldin et al., 2009). Cytokines of the TGFb superfamily are inducers of the signaling pathway and regulate this plethora of cellular functions. This group of cytokines is comprised of over 30 different ligands, including bone morphogenetic proteins (BMPs), growth differentiation factors (GDFs), anti-Muellerian hormones (AMH), activins, nodal and TGFbs (Shi and Massagué, 2003). To initiate signaling events, ligands bind to two pairs of type I and type II receptor serine/threonine kinases on the cell surface. Upon ligand binding, the receptors form a heterotetrameric complex that allows the type II receptors to phosphorylate the type I receptors. Activated signaling complexes then mediate phosphorylation of intracellular SMAD proteins at their C-terminal domains (Shi and Massagué, 2003; David and Massagué, 2018). This phosphorylation process is enhanced or inhibited by the internalization of receptor complexes. While endocytosis mediated by clathrin promotes SMAD activation, endocytosis mediated by lipid rafts facilitates degradation of ligand-receptor complexes. Internalized receptors that are not degraded can be recycled to the cell surface or continue to phosphorylate SMAD proteins from the endosome (Chen, 2009).

The SMAD family consists of eight members, which can be classified in three categories: receptor-regulated SMADs (R-SMADs; isoforms 1, 2, 3, 5, 8), the common-mediator SMAD (Co-SMAD; isoform 4) and inhibitory SMADs (I-SMADs; isoforms 6 and 7) (Massagué et al., 2005). Depending on the type of ligand, either SMAD2/3 or SMAD1/5/8 are activated. After phosphorylation, R-SMADs heterotrimerize with SMAD4, translocate to the nucleus and interact with transcription factors to regulate the expression of SMAD target genes (Feng and Derynck, 2005). Within the nucleus, SMAD-specific phosphatases such as protein phosphatase 1A (PPM1A) and pyruvate dehydrogenase phosphatase (PDP) dephosphorylate R-SMADs and enable their nuclear export (Chen et al., 2006; Lin et al., 2006; Bruce and Sapkota, 2012). Back in the cytoplasm, R-SMADs can be phosphorylated again. The cycle of SMAD import and export continues for as long as active receptors are present (Inman et al., 2002). Ultimately, SMAD signaling is terminated by a variety of control mechanisms. Besides SMAD dephosphorylation in the nucleus, negative feedback regulators of the pathway such as SMAD6 and 7, can inhibit and terminate signal transduction through various mechanisms (Schmierer and Hill, 2007). For example, I-SMADs interfere with oligomerization or phosphorylation of SMAD molecules. While SMAD6 impairs the receptor-mediated phosphorylation of SMAD2 and prevents subsequent

heterotrimerization with SMAD4, SMAD7 recruits the E3 ubiquitin ligase SMURF2 for degradation of TGFb receptors (Imamura et al., 1997; Kavsak et al., 2000; David and Massagué, 2018).

In general, SMAD signaling is a simple and straightforward pathway comprising two signaling branches (SMAD2/3 and SMAD1/5/8) as well as a small set of type I and type II receptors. Ligands that signal via SMAD2/3 utilize either TGFb receptor 2 (TGFBR2), activin A receptor 2A (ACVR2A), activin A receptor 2B (ACVR2B) or BMP receptor 2 (BMPR2) as type II receptors and TGFb receptor 1 (TGFBR1), activin A receptor 1B (ACVR1B) or activin A receptor 1C (ACVR1C) as type I receptors. To increase signaling efficiency, some ligands require a specific co-receptor such as TGFb receptor 3 (TGFBR3), that facilitates the binding to their corresponding type I/II receptor complexes. The wide range of cytokines and limited selection of receptors lead to multiple ligands sharing the same serine/threonine kinase receptors. For instance, activin A and GDF11 both bind to ACVR2A and ACVR2B and mediate the phosphorylation of SMAD2/3 through ACVR1B. However, GDF11 can also signal through TGFBR1, the type I receptor for TGFb ligands (David and Massagué, 2018). Therefore, activin A, TGFb and GDF11 not only utilize the same signaling branch, but also partially identical receptors. A schematic representation of SMAD signaling after activin A, TGFb and GDF11 treatment is shown below (Figure 3). Interestingly, many *in vitro* and *in vivo* studies have shown that the different members of the TGFb superfamily exert quite distinct biological functions. For example, knockout experiments revealed that 50 % of TGFb deficient mice died during embryogenesis and survivors developed inflammatory disorders, whereas mice with activin A deficiency either died during the perinatal period or showed craniofacial defects. Furthermore, knockout of GDF11 induces completely different phenotypes, since mice deficient for this growth factor are viable and exhibit posterior displacement of hindlimbs. Although the common SMAD2/3 pathway is functional, compensation by other ligands is not possible, indicating a divergence of ligand-mediated effects (Chang et al., 2002; Matsuo et al., 2006). Strikingly, even strongly related ligands such as myostatin (GDF8) and GDF11 mediate distinct biological functions. While GDF8 is best known for inhibiting muscle growth and limiting bone mass, GDF11 regulates skeletal patterning during embryogenesis and has been proposed as a rejuvenating factor. A more recent study even showed that GDF11 counteracts the functions of GDF8 by promoting osteogenesis (Katsimpardi et al., 2014; Sinha et al., 2014; Suh et al., 2020). However, the postnatal functions of GDF11 are controversially discussed, possibly due to its diverse functionality (Simoni-Nieves et al., 2019). Taken together, ligands of the TGFb superfamily can exhibit diverse and sometimes contradicting effects on cellular responses, even though they utilize the same signaling branch and similar receptor complexes. The molecular mechanisms controlling these biological functions are poorly understood and the question how the SMAD pathway can distinguish between a

multitude of ligands remains unanswered. The converging signaling pathway and the limited number of receptors suggest that the distinction is made on the ligand/receptor level. For example, agonists and antagonist of SMAD signaling that control ligand availability and ligand-receptor interactions specify signaling input on an extracellular level. Follistatin (FST), a GDF8/11 and activin A inhibitor or decorin, a TGFb and GDF8 antagonist, are two of many ligand regulators that add complexity to the straightforward signaling pathway (Chang, 2016). Furthermore, co-receptors like TGFBR3, cripto and cryptic can promote ligand-specific responses. Besides these additional components influencing downstream signaling in a ligand-dependent manner, signals mediated by members of the TGFb superfamily might also be spatially and temporally interpreted by the pathway. Thus, ligand-specific functions would be encoded by distinct activation patterns (dynamics) of R-SMADs shaped by intrinsic properties of ligands and receptors, such as binding affinities, binding kinetics and geometry of ligand-receptor complexes (Nickel and Mueller, 2019). As it has been reported that dynamic features like amplitude, duration or frequency of pathway activation are able to control cellular responses (Purvis and Lahav, 2013; Johnson and Toettcher, 2019), the idea of a quantitative SMAD pathway seems to be a possibility.

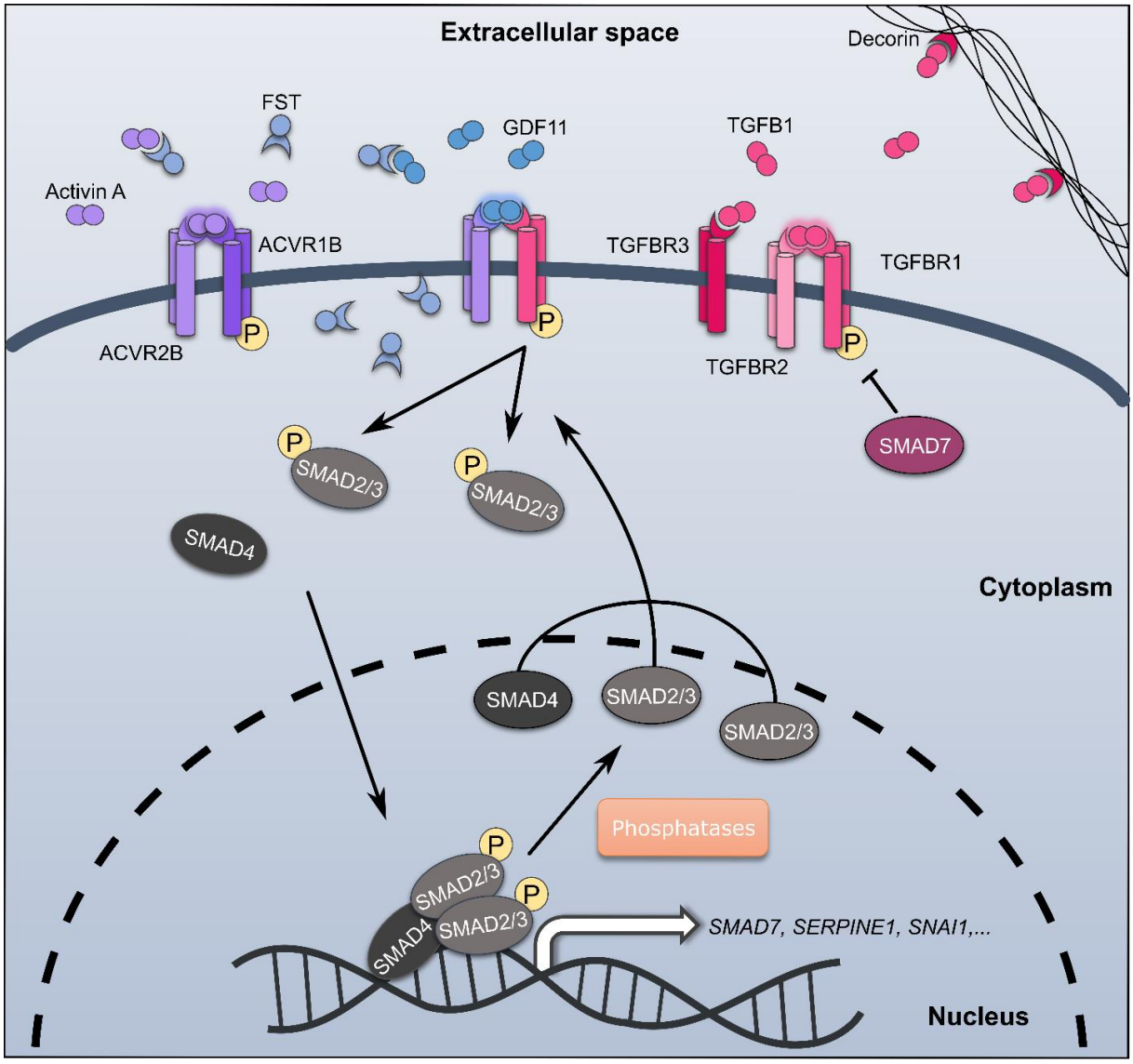

Figure 3: Schematic representation of the SMAD signaling pathway after stimulation with different ligands.

In the extracellular space, activin A, GDF11 and TGFB1 dimers initiate the signaling events by binding to a pair of their corresponding type II receptors. Upon ligand binding, type II receptors form a complex with two type I receptors. Type II receptors phosphorylate and thus activate type I receptors, which subsequently activate intracellular SMAD2/3 by phosphorylation. Afterwards, activated SMAD2/3 proteins form a heterotetrameric complex with SMAD4 and enter the nucleus to regulate gene expression. One of many target genes of the SMAD pathway is SMAD7, which negatively regulates the signaling process by engaging E3 ubiquitin ligase and thus initiating receptor degradation. Besides SMAD7, there are also ligand-specific antagonists that inhibit SMAD signaling, such as FST and decorin. Both proteins can bind ligands and prevent their interaction with corresponding receptors. Within the nucleus, SMAD-specific phosphatases, like PPM1A, dephosphorylate SMAD2/3 and initiate the separation of the SMAD complex. Ultimately, SMAD2/3 and SMAD4 split up and re-enter the cytoplasm.

1.4 MEASUREMENT OF PROTEIN DYNAMICS IN SINGLE CELLS

Cellular signaling is often investigated with experiments based on populations of cells. While these studies provide a useful overview, essential information about the heterogeneity of individual cells is usually lost in the average response of the population (Loewer and Lahav, 2011). This was for example demonstrated for the p53 tumor suppressor pathway. In response to DNA damage, p53 dynamics were described as damped oscillations (Lev Bar-Or et al., 2000). Single-cell experiments, however, revealed that individual cells show varying numbers of undamped p53 pulses of fixed amplitude and duration (Lahav et al., 2004). In case of SMAD signaling, studies based on individual cells revealed that R-SMADs-SMAD4 complex formation and nuclear translocation upon TGFb stimulation occur with considerable cell-to-cell variability (Warmflash et al., 2012; Zieba et al., 2012). Thus, when studying signaling networks, it is important to investigate not only the population average but also the single-cell level. Furthermore, since cell signaling events can occur within seconds, minutes or hours after stimulation and often involve translocation of signaling molecules, analyses with high temporal and spatial resolution are essential in order to fully understand dynamic behavior of biological responses. While techniques such as immunofluorescence microscopy or flow-cytometry enable investigations of single cells, they are limited by their inability to analyze the same cell over time. In contrast, live-cell time-lapse microscopy provides unmatched temporal resolution and allows to follow signaling processes of thousands of individual cells (Figure 4). To utilize this approach, reporter cell lines need to be generated, containing fluorescently labeled proteins of interest. Thereby, quantitative measurements of protein levels and subcellular localization are facilitated (Ankers et al., 2008). As shown in previous studies, cells can encode information in dynamic patterns of signaling molecules. For example, while p53 pulses following γ-irradiation are associated with cell cycle arrest, a single sustained p53 response upon UV radiation leads to apoptosis (Purvis et al., 2012). Another example is the activation of the ERK pathway by nerve growth factors (NGF) and EGF. While NGF mediates a rather sustained ERK response that leads to differentiation of rat neuronal precursors, EGF causes a transient activation that leads to cell proliferation (Gotoh et al., 1990; Traverse et al., 1992; Nguyen et al., 1993; Purvis and Lahav, 2013). Therefore, it is important to examine dynamical patterns of signaling molecules.

Since a key step in SMAD signaling is the rapid translocation of SMAD proteins from the cytoplasm to the nucleus upon ligand stimulation, a technique such as live-cell imaging is crucial to gain a better understanding of the corresponding pathway. For this reason, we used SMAD2/SMAD4 reporter cell lines, time-lapse imaging and automated image analyses in a recent study to quantitatively characterize dynamics of TGFb signaling in individual cells (Strasen et al., 2018). With this approach,

strongly heterogeneous SMAD2 dynamics were observed in TGFb-treated cell populations. By utilizing dynamic time-warping, thousands of SMAD2 time courses were clustered to identify six cellular sub-populations with qualitatively distinct signaling behavior. For example, cells that do not respond to stimulation (non-responders) and cells that show a strong and sustained response were divided in different sub-populations. The distribution of the signaling classes were dependent on extracellular stimuli. While the fraction of non-responders decreased with increasing TGFb concentrations, the fraction of cells showing stronger SMAD2 activation increased. Interestingly, a correlation between the sub-populations and cellular responses was observed. In general, SMAD2 activation resulted in increased motility and reduced cell division rate in all signaling classes except for non-responders. However, cells exhibiting a sustained response, showed more pronounced phenotypic changes compared to transiently responding cells. These results emphasize that the cell-specific temporal dynamics of SMAD signaling are an important determinant of the broad range of cell fates induced by SMAD signaling.

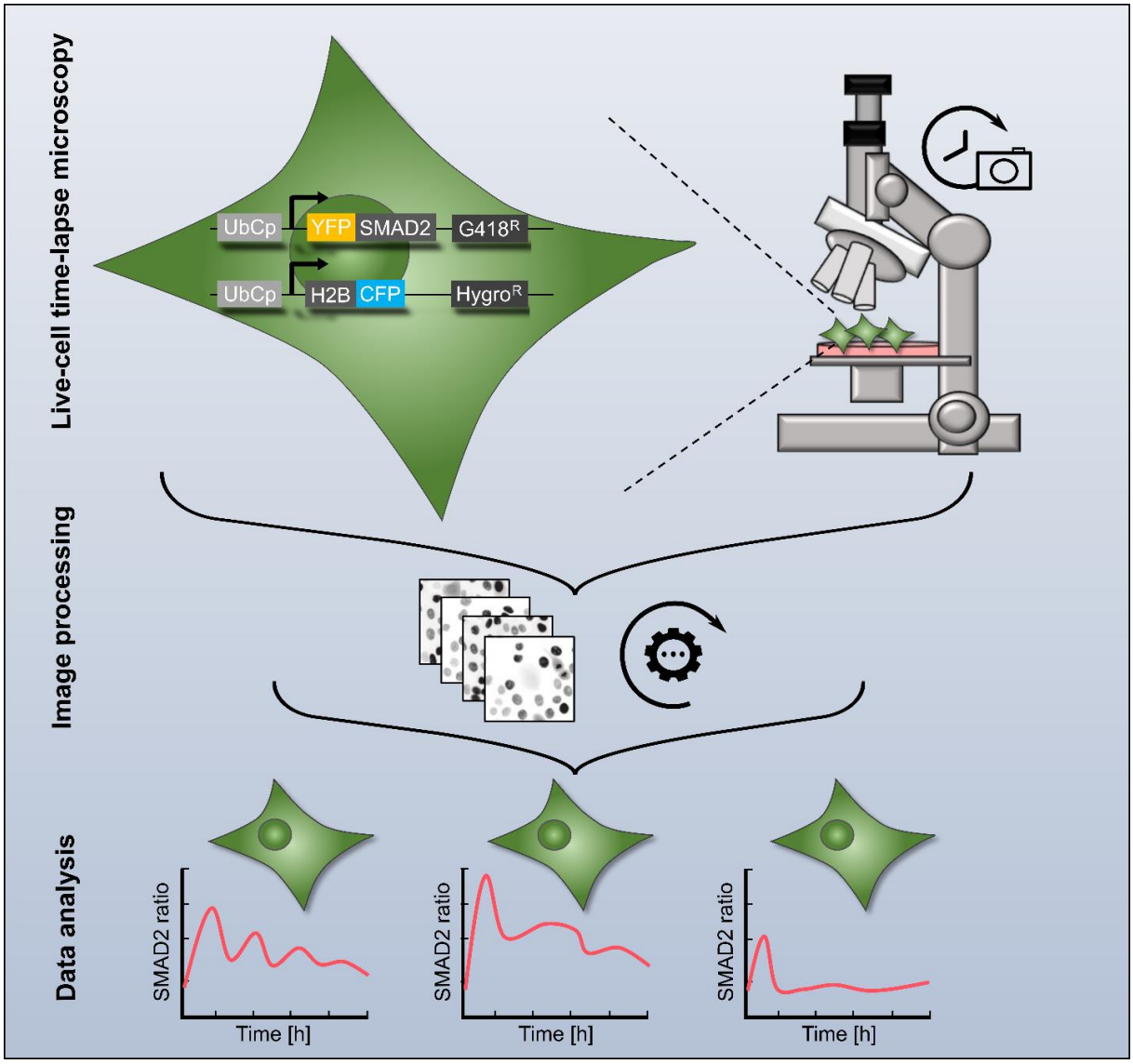

Figure 4: Schematic representation of live-cell time-lapse microscopy and single-cell analysis.

To utilize time-lapse microscopy, a reporter cell line that contains fluorescently labeled proteins of interest is required. For the present study, a transgenic MCF10A SMAD2 reporter cell line was used that expresses a SMAD2 coding sequence fused to a yellow fluorescent protein (YFP-SMAD2) and a histone 2B coding sequence fused to a cyan fluorescent protein (H2B-CFP). Both transgenes are under control of a constitutive human Ubiquitin C promoter (UbCp). The fluorescently labeled proteins can then be measured over several hours with a high temporal and spatial resolution. As a result, large data sets of time series images are generated, which are evaluated using automated image analysis. With this approach, hundreds of individual cells are tracked over time and protein dynamics of each cell are measured. To study SMAD2 translocation, the ratio between nuclear and cytoplasmic protein can be determined.

1.5 GENE EXPRESSION AND ASSOCIATED CELL FATES OF SMAD SIGNALING

1.5.1 TRANSCRIPTIONAL CONTROL BY SMAD SIGNALING

As mentioned in the previous sections, the SMAD pathway regulates a diverse array of cellular processes including proliferation, migration and cell death. To elicit such a variety of biological functions, members of the TGFb superfamily initiate different programs of gene expression. The signal transducers for these cytokines are SMAD proteins, which accumulate in the nucleus upon stimulation and bind DNA directly or indirectly (Figure 5). By binding to enhancer/promoter sequences in the regulatory regions of target genes, activated SMAD complexes can act as transcription factors and regulate gene expression positively or negatively (Massagué, 2012; Hill, 2016). The common mediator SMAD4 as well as all R-SMADs except for SMAD2 can bind DNA directly. In general, SMADs consist of highly conserved N-terminal and C-terminal domains known as mad homology 1 (MH1) and mad homology 2 (MH2), respectively (Hill, 2016). The two domains are separated by a flexible linker region that contains sites for regulatory phosphorylation by kinases such as MAPKs and CDKs (David and Massagué, 2018). While the MH1 domain in R-SMADs can bind DNA, the MH2 domain mediates protein-protein interactions with TGFb receptors, SMAD proteins and DNA-binding co-factors (Shi et al., 1998; Macias et al., 2015). The MH1 domain of SMAD1, SMAD3, SMAD4 and SMAD5 recognize common 5 bp, GC-rich sites (GGCGC and GGCCG), which are considerably enriched in promotor and enhancer elements of SMAD target genes. Therefore, at first sight, SMAD complexes seem to be limited in their DNA-binding specificity, since most SMADs bind to the same DNA motifs. Yet, ligand-activated SMAD2/3 and SMAD1/5/8 can regulate different sets of target genes (David and Massagué, 2018). This specificity is usually achieved by SMAD proteins cooperating with other DNA-binding transcription factors. Depending on the DNA-binding partner, these interactions occur either via the MH1 or MH2 domain. One of the first transcription factors reported to interact with SMADs was the forkhead box protein H1 (FOXH1). In case of activin stimulations, activated SMAD2-SMAD4 complexes translocate into the nucleus, where FOXH1 binds the MH2 domain of SMAD2 and recruits the complexes to an activin-response element to provide ligand-dependent transcription (Chen et al., 1997; Zhou et al., 1998; Feng and Derynck, 2005). Further examples are the FOXO transcription factors, a subgroup of the forkhead family, which form complexes with TGFb-activated SMAD proteins and mediate cytostasis by inducing *CDKN1A* expression (Seoane et al., 2004). Interestingly, this process is negatively regulated by the PI3K pathway and thus shows a good example of an interplay between proliferative and anti-proliferative signals. In essence, SMAD signaling provides a simple signal transduction mechanism but TGFb superfamily ligands mediate

complex cellular responses such as EMT and apoptosis. Therefore, SMAD proteins cooperate with a remarkable diversity of transcription factors to initiate different programs of gene expression.

1.5.2 EMT, CYTOSTASIS AND APOPTOSIS

During EMT, tightly connected adherent cells lose their cell polarity and cell-cell interactions to acquire a motile and migratory phenotype. While the transition from epithelial to mesenchymal cells is an essential event during embryonic development and tissue remodeling, it can also lead to aggressive tumor progression in cancers (Arima et al., 2008). To facilitate this transition, this process drives cells through a progressive adoption of gene expression changes. In brief, upon SMAD activation, cells upregulate the expression of transcription factors such as *SNAI1* and *ZEB1*. While SNAI1 initiates EMT by decreasing E cadherin (*CDH1*) expression, ZEB1 downregulates *CDH1* expression further to maintain the mesenchymal phenotype (Figure 5). Furthermore, markers of mesenchymal cells like N-cadherin (*CDH2*) and vimentin (*VIM*) are upregulated through this process (Zhang et al., 2014). Besides EMT, ligands of the TGFb superfamily mediate anti-proliferative and pro-apoptotic signals. As mentioned above, activated SMAD proteins can initiate cytostatic effects by inducing *CDKN1A* expression. Moreover, MYC, a potent regulator of cell cycle progression, has been shown to be a downstream target of the SMAD pathway (Yagi et al., 2002). To repress *MYC* transcription, the MH2 domain of SMAD3 forms a complex with the transcription factors E2F4/5 and DP1 as well as the co-repressor p107. In response to TGFb stimulation, this complex relocates from the cytoplasm to the nucleus and binds the inhibitory element of the *MYC* promotor to facilitate repression of the corresponding gene (Chang et al., 2002). Additionally, it has been shown that TGFb upregulates cell cycle inhibitors such as *CDKN1B* and *CDKN2B* (Robson et al., 1999). Not only the cytostatic activity, but also the ability to induce apoptosis, makes SMAD signaling an important tumor suppressor pathway. The apoptotic response to TGFb is well documented in various cell lines and many SMAD-associated events have been identified to mediate apoptosis (Schuster and Krieglstein, 2002). One downstream effector of TGFb signaling that was repeatedly reported to initiate apoptosis is the zinc-finger transcription factor krueppel-like factor 10 (KLF10). Overexpression of this protein has been demonstrated to induce apoptosis in hepatocytes and epithelial cells (Chalaux et al., 1999; Ribeiro et al., 1999). Another crucial determinant of TGFb-mediated apoptosis is the *BIM* gene (Wildey et al., 2003; Yu et al., 2008). This pro-apoptotic regulator is expressed by SMAD3-induced runt-related transcription factor 1 (*Runx1*), which binds to FOXO3 to upregulate the corresponding gene (Ramesh et al., 2009). A more recent publication connected TGFb-initiated apoptosis with an altered regulation of SRY-box transcription factor 4 (*SOX4*) and *KLF5* in pancreatic cancer cells (David et al., 2016). Both proteins, SOX4 and KLF5,

have also been associated with apoptosis in other studies (Zhao et al., 2008; Hur et al., 2010; Cheng et al., 2018).

Taken together, SMAD proteins modify gene expression by directly binding to the regulatory region of target genes or by interacting with various activators and repressors. Due to that, ligands of the TGFb superfamily can elicit complex gene expression changes and a variety of biological responses.

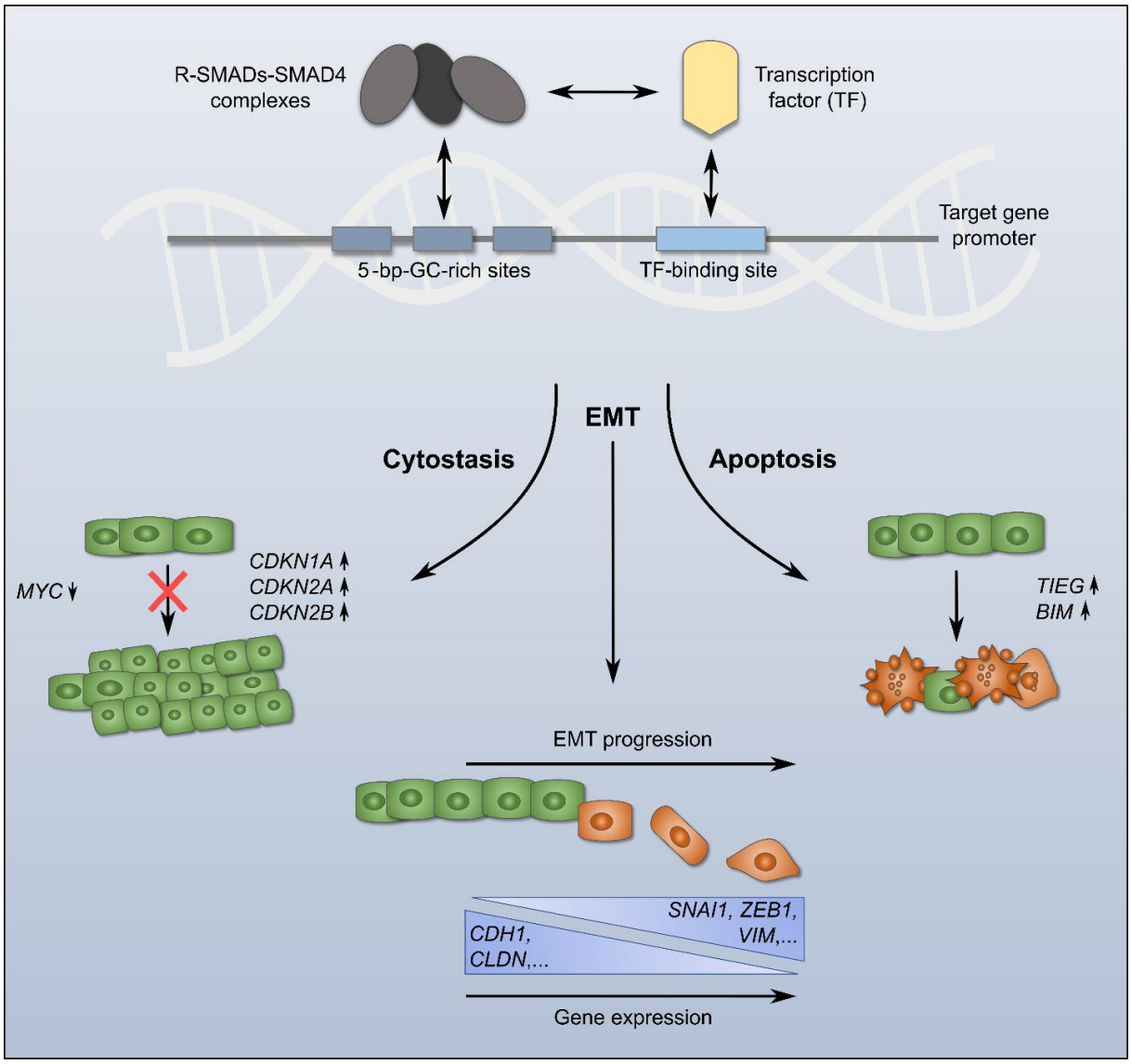

Figure 5: Schematic representation of SMAD-mediated gene expression and associated cellular responses.

Ligand-activated SMAD complexes regulate gene expression by either binding promotor sequences of target genes directly or by interacting with specific transcription factors. By initiating different programs of gene expression, stimulus-dependent SMAD signaling mediates cell fates, such as cytostasis, EMT and apoptosis. For example, the signaling pathway can induce EMT by upregulating the expression of mesenchymal markers like *SNAI* and *VIM* and downregulating the expression of epithelial markers like *CDH1*.

1.6 AIM OF THIS THESIS

This study aims to evaluate the interplay of different signaling pathways in regulating cell fate decisions. As described above, the physiology of the mammary gland is a prime example for a tissue whose development is orchestrated by an interplay of signaling pathways. Cell fate decisions such as proliferation, quiescence, migration and apoptosis need to be precisely balanced to ensure a successful progression of the mammary gland from birth to involution. As disturbances of the corresponding pathways can lead to severe diseases such as cancer, it is of utmost importance to gain a deeper understanding of the signaling processes determining these cellular outcomes. Therefore, to approach this task, I investigate how signaling networks in individual breast epithelial cells influence each other to ultimately control cellular outcomes. To this end, I combined time-resolved single-cell measurements of signaling dynamics with pharmacological or genetic perturbations and RNA sequencing.

In the first chapter, the objective is to investigate how the MEK/ERK and PI3K/AKT pathways synergize upon EGF stimulation to regulate cell cycle entry and progression. As the importance of ERK and AKT in initiating the progression from G0- to S-phase has been researched before, the focus lies on examining the relative roles of the corresponding pathways in controlling different stages of the cell cycle.

The objective of the second chapter is to examine how the cell cycle and mitogenic pathways, such as those mentioned above, influence stimulus-dependent SMAD signaling in individual cells. Moreover, I aim to study gene expression changes and SMAD-associated cell fates such as apoptosis and EMT in quiescent and proliferating cells and correlate them to SMAD2 dynamics. Thereby, I intent to answer the question whether the corresponding cellular responses are ligand specific or whether the dynamics of SMAD2 nuclear accumulation mediate a multitude of functions regardless of the type of ligand.

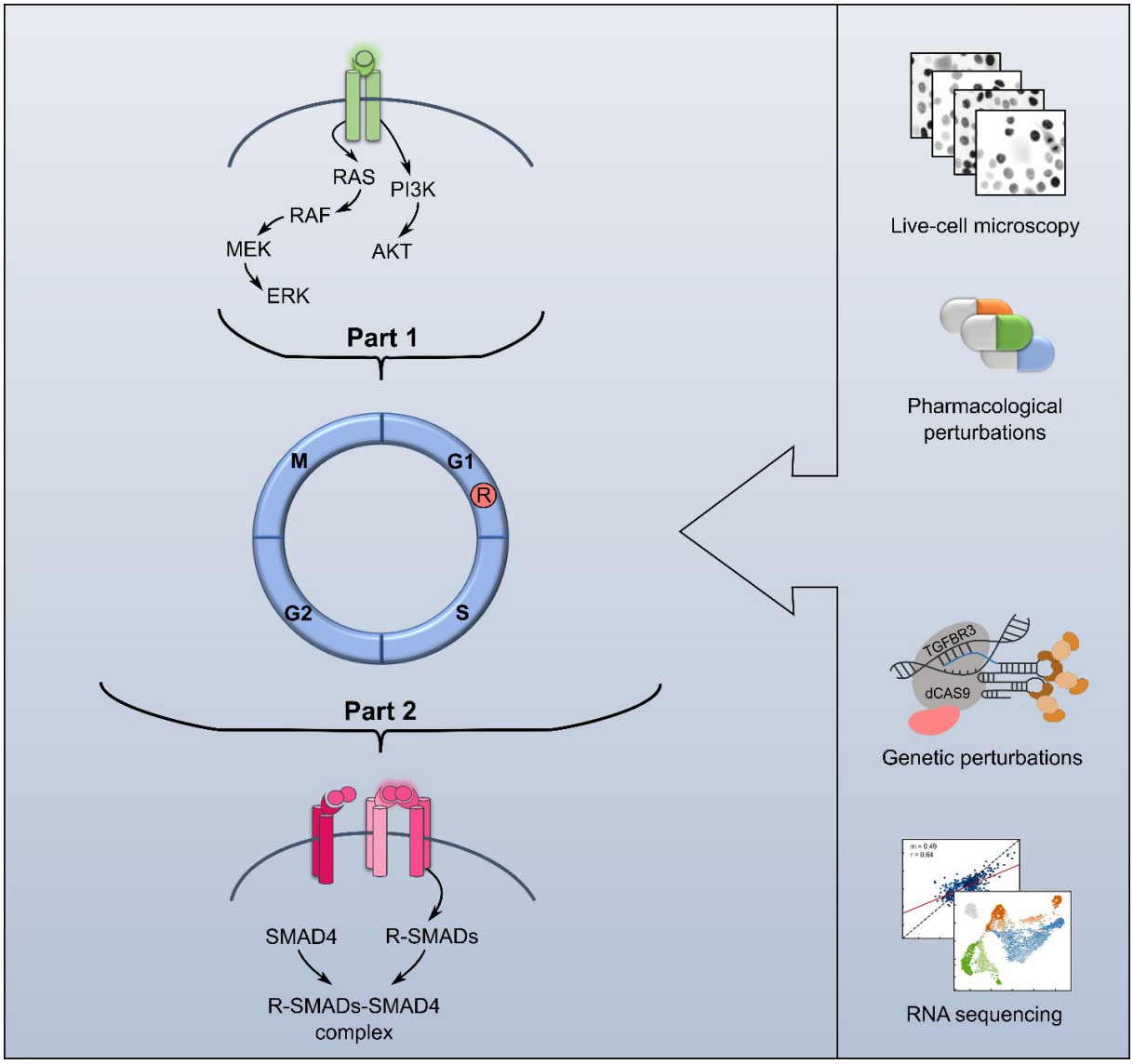

Figure 6: Graphical abstract of this thesis.

The overall aim of the present study is to investigate the effects of mitogenic signaling pathways on cell cycle entry and progression (Part 1) as well as to elucidate the impact of the cell cycle and mitogenic signals on SMAD2 dynamics (Part 2). To achieve this objective, I combine live-cell time-lapse imaging of specific reporter cell lines on a single-cell level with pharmacological or genetic perturbations and RNA sequencing.

2 DISENTANGLING PRO-MITOTIC SIGNALING

Part 1 of this work is based on a study that was recently published in Cell Reports (Benary*, M.**, Bohn*, S.**, Lüthen, M., Nolis, I.K., Blüthgen, N., and Loewer, A. (2020). Disentangling Pro-mitotic Signaling during Cell Cycle Progression using Time-Resolved Single-Cell Imaging. Cell Reports *31*, 107514. https://doi.org/10.1016/j.celrep.2020.03.078). All the following experiments, except for rehydration and library preparation for single-cell sequencing, were performed by me. Data analysis was carried out by Manuela Benary (Charité-Universitätsmedizin Berlin) and the manuscript was written with contributions from all authors. Figures and text have been adapted for this thesis.

*These authors contributed equally

2.1 RESULTS OF PART 1

The rate and timing of cell divisions need to be precisely coordinated by intracellular signaling pathways and extracellular stimuli to maintain the balance between quiescence and proliferation and enable proper cellular homeostasis. To study the influence of signaling pathways on cell cycle entry and progression, I quantified EGF-induced mitogenic signaling in quiescent cells and decoded the dynamic contributions of downstream signaling pathways by combining time-resolved single-cell measurements of ERK activity in an untransformed human breast epithelial cell line with targeted pharmacological perturbations, single-cell RNA sequencing (scRNA-seq) and statistical analyses.

2.1.1 QUANTITATIVE LIVE-CELL IMAGING REVEALS CELL-SPECIFIC ACTIVATION PATTERNS OF THE EGFR/ERK PATHWAY

To analyze EGF-induced signaling in living cells, I used a previously established MCF10A reporter cell line termed FIRE (Fra-1-based integrative reporter of ERK). This reporter is based on the fluorescent protein mVenus fused to a nuclear localization signal (NLS) and the PEST domain of FRA1, a transcription factor stabilized by ERK phosphorylation (Albeck et al., 2013) (Figure 7A and B). In the absence of mitogenic stimuli activating the EGFR/ERK pathway, the constitutively expressed reporter is rapidly degraded. When cells are treated with the growth factor EGF, FIRE is stabilized through ERK-dependent phosphorylation and accumulates in the nucleus (Figure 7C). It therefore provides a specific linear measure of the integrated activity of the EGFR/ERK pathway over long, physiologically relevant time scales (Gillies et al., 2017). By withdrawing mitogenic growth factors and serum for 48 h (2.3.2) before stimulating reporter cells with defined EGF doses (from 0.5 ng/ml to 50 ng/ml) I was able to investigate the progression of quiescent cells from G0-phase of the cell cycle to mitosis. I then measured the nuclear fluorescence intensity of FIRE for 48 h and generated time-resolved trajectories of FIRE intensity, representing more than 850 individual cells per condition by using automated image analysis followed by data processing and normalization (Figure 7D and E) (2.3.5).

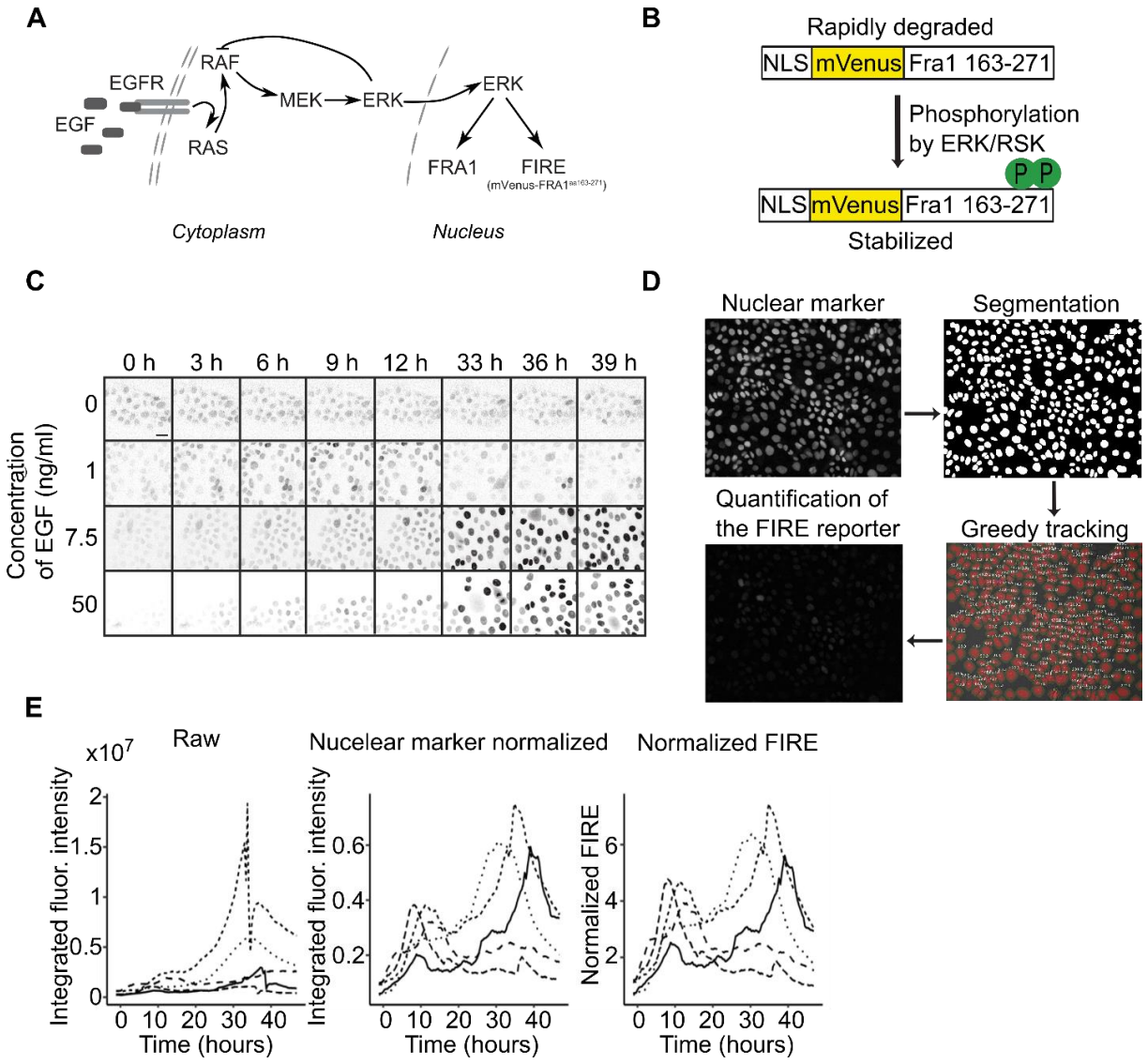

Figure 7: Analyzing ERK activity in living cells.

(A) Scheme of the EGF pathway, where EGFR stimulation triggers the activation of RAF, MEK and ERK by phosphorylation. ERK translocates to the nucleus, where it phosphorylates numerous targets, including the transcription factor FRA1. Phosphorylation of the PEST domain of FRA1 by ERK leads to stabilization of the protein. I used a fluorescent reporter that contains the PEST domain of FRA1 and is stabilized by ERK phosphorylation (FIRE). See also Albeck et al., 2013. **(B)** Scheme of the FIRE activity is shown. The reporter consists of the PEST domain of FRA1 fused to mVenus, a yellow fluorescent protein, and a nuclear localization sequence. The reporter is constitutively expressed by the murine stem cell virus long terminal repeat (MSCV LTR) and then rapidly degraded. ERK phosphorylates the FRA1 domain at multiple sites and thereby stabilizes the reporter. **(C)** Example images of the FIRE reporter at indicated time points and EGF concentrations. Scale bar: 24 µm. **(D)** Workflow for segmenting and tracking single cells. Cells stably expressed NLS-CFP as a nuclear marker (panel 1), which was used to segment the nucleus (panel 2). For tracking single cells, a customized greedy algorithm was used; in panel 3 tracked cells are labeled with their corresponding identifier. For each tracked cell, the total fluorescence intensity of the FIRE reporter was quantified (panel 4). **(E)** Time courses of five cells are shown (different dashed lines) to exemplify the normalization procedure. The raw integrated fluorescence intensities for the FIRE reporter in each cell are depicted over time (panel 1). The integrated fluorescence intensity of the FIRE reporter in each cell was normalized by the corresponding

fluorescence intensity of the NLS-CFP nuclear marker to remove spurious spikes in single-cell trajectories (panel 2). Subsequently, time courses were further normalized by the mean nuclear marker normalized FIRE level of cells in the absence of EGF stimulation leading to a measure of FIRE induction upon EGF treatment.

If cells were not stimulated with EGF, they showed no detectable changes in reporter activity, indicating that there was no residual input to the MAPK pathway under my experimental conditions (Figure 7C and Figure 8A). By treating the cells with low EGF doses (0.5 ng/ml and 1 ng/ml EGF), I observed a transient FIRE accumulation during the first 10-15 h (first phase). When stimulated with concentrations above 2.5 ng/ml, cells showed a second phase of FIRE activity with increasing amplitude and duration after approximately 15 h (second phase) (Figure 8A and B). On the single-cell level, most cells showed a first FIRE response at EGF concentrations of as low as 0.5 ng/ml, while the fraction of cells showing a second phase of FIRE signals saturated at EGF concentrations of 5 ng/ml or higher (Figure 8C). Additionally, the two phases were analyzed separately by looking at different features like amplitude (Amp), fold change (FC), timing of the maximum (Time), duration and area under the curve (AUC) (Figure 8D). Again, the results showed that low EGF concentrations did not induce a second phase of FIRE activation. Noticeable increases in FC, AUC and Amp of the second phase were only achieved by EGF concentrations from 2.5 ng/ml to 50 ng/ml (Figure 8F). In contrast, at early time points (first phase) the values of these three features increased regardless of EGF concentrations (Figure 8E). Therefore, the features of the first phase allow me to discriminate if the cells were stimulated or not and the features of the second phase to discriminate between high and low doses. Taken together, using quantitative live-cell imaging I was able to show a bi-phasic ERK activity profile with an early and late response at high EGF concentrations.

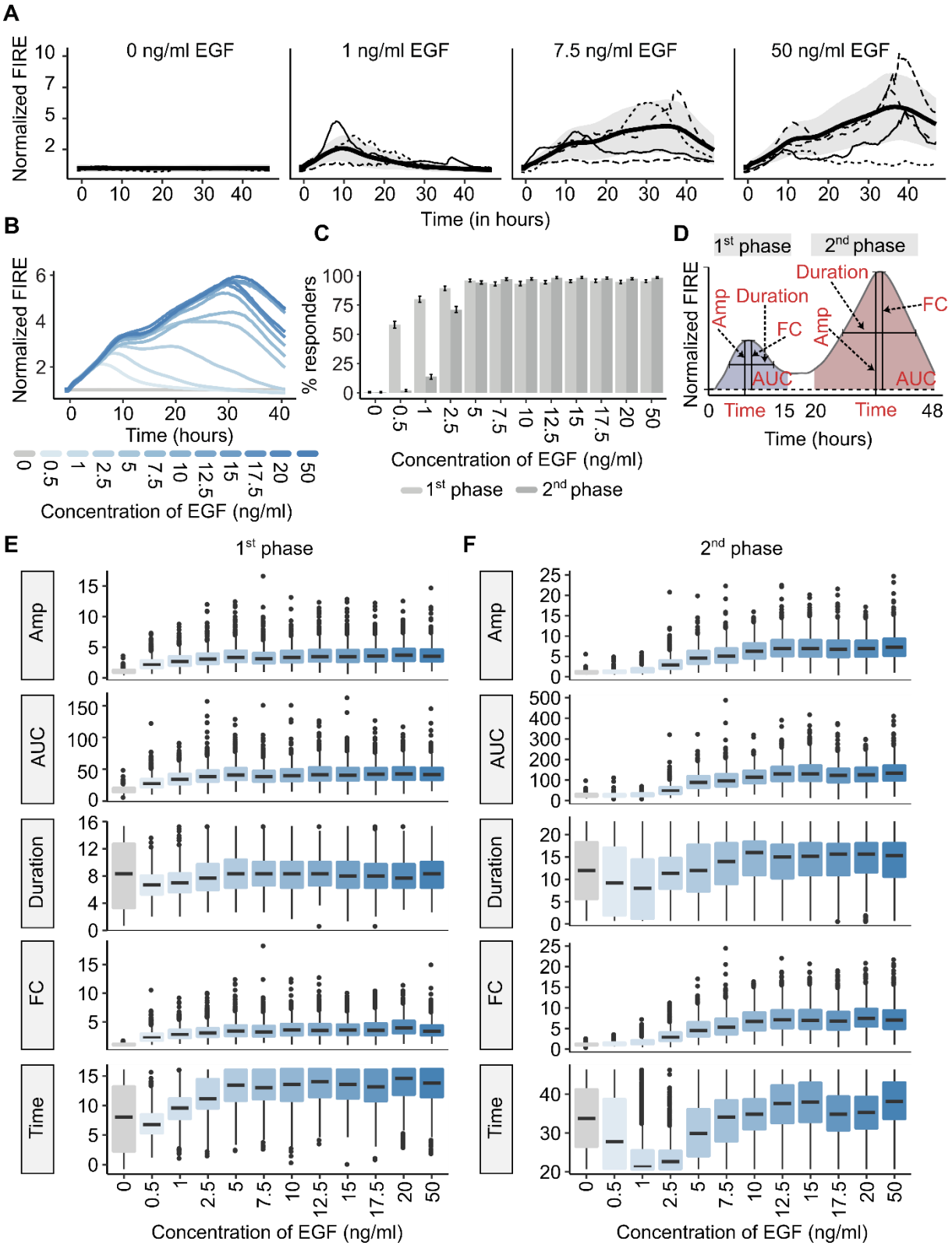

Figure 8: Dynamic features of the bi-phasic ERK activity profile.

(A) Examples of single-cell FIRE reporter time series for randomly selected single cells treated with indicated EGF concentrations. Mean time courses (bold lines) and standard deviations (gray ribbons) of all measured cells are indicated. Growth factor- and serum-deprived cells were treated with the indicated doses of EGF. Images were acquired every 20 min for 46 h. The number of cells analyzed is indicated in 6.3 (Appendix) for each live-cell microscopy experiment. **(B)** Average

FIRE reporter time series for concentrations from 0 ng/ml EGF to 50 ng/ml EGF. Color indicates EGF concentration. **(C)** Percentage of cells showing a response within 16 h (light gray) after stimulation and between 20 h after stimulation and the end of measurement (gray). Cells with amplitudes greater than three standard deviations from the average of unstimulated cells were considered responders. Error bars indicate 95 % confidence interval based on bootstrapping (n = 1,000). **(D)** Scheme of features describing the FIRE response after EGF treatment. The FIRE response is separated into early and late responses, and each phase is characterized by the following features: amplitude (Amp), time of the maximum (Time), fold change of the amplitude (FC), duration of the response and area under the curve (AUC). **(E)** Shown are box plots comparing the features of first response, namely amplitude (in arbitrary unit (au)), time of the maximum (in hours), fold change of the amplitude (in au), duration of the response (in hours) and area under the curve (in au). The amplitude was defined as the mean of the three highest FIRE responses after normalization. The fold change is taken with respect to the mean response of FIRE in the same cell before stimulation. The area under the curve has been estimated using a spline interpolation and the duration is an estimation of full width at half maximum (2.3.6). Boxes include data between the 25th and 75th percentiles. Black lines indicate the median, whiskers extend to maximum values within 1.5× the interquartile range and dots represent outliers. The same applies to all following box plots. **(F)** Corresponding box plots comparing the features of the second response (as in **(E)**).

2.1.2 ERK ACTIVITY IS NECESSARY BUT NOT SUFFICIENT FOR CELL CYCLE ENTRY AND PROGRESSION

To characterize how EGF signaling controls the phenotypic response of individual cells, I determined if and when cells entered S-phase using a fusion of a red fluorescent protein mCherry (RFP) with the first 110 amino acids of geminin (Albeck et al., 2013) (Figure 9A). As geminin is degraded by APC^{Cdh1} during G1-phase and only accumulates during S- and G2-phase (Sakaue-Sawano et al., 2008; Clijsters et al., 2013), I defined an increase of more than 2× the standard deviation of the basal RFP level as the time of S-phase entry (Figure 9B). This method to determine S-phase entry correlated well with measurements of actively replicating cells marked by EdU incorporation, even at low stimulation levels (Figure 9C-E). At the transition between meta- and anaphase of mitosis, geminin is degraded by APC^{Cdc20}, which resulted in a sharp decline in the intensity of the geminin reporter (Figure 9B). I will refer to the duration of geminin accumulation as the duration of S/G2-phases, whereas the beginning of geminin accumulation will be termed S-phase entry. The timing of the meta- to anaphase transition will be called cell division.

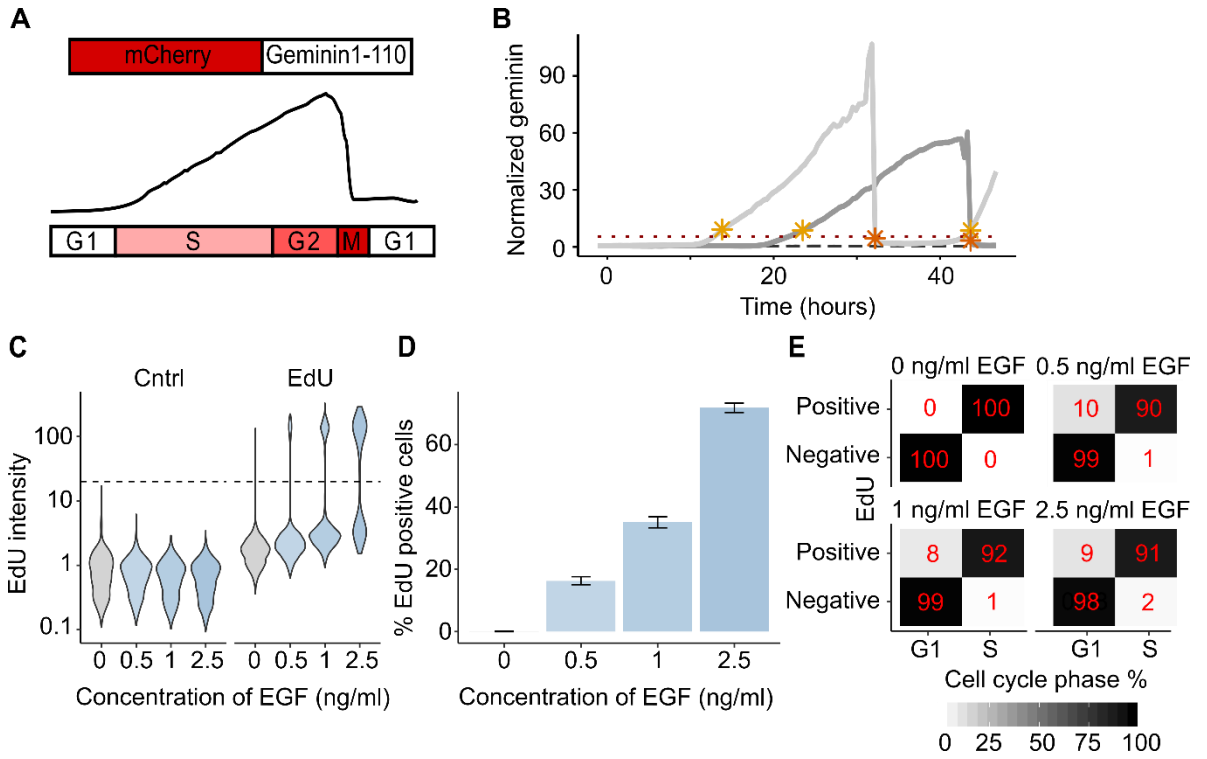

Figure 9: Following cell cycle progression in individual cells.

(A) Scheme of the geminin-based cell cycle reporter. The reporter consists of the first 110 amino acids of geminin fused to a red fluorescent protein. The reporter is kept at low levels during G1-phase, accumulates over S/G2/M-phase and is rapidly degraded at the transition between meta- and anaphase of mitosis (Clijsters et al., 2013). **(B)** Time courses of the normalized geminin reporter for three cells are shown to exemplify the detection of cell cycle phases (light gray, dark gray and dashed lines). The red dotted line indicates the threshold for detecting cell cycle phases. Light orange asterisks show the time points for cells entering S-phase and dark orange asterisk show the time points immediately after division. **(C)** Violin plots showing the EdU intensity (log_{10}-normalized) distribution. Cells were stained with EdU 20 h after stimulation with different concentration of EGF. Suggested threshold to separate EdU positive from EdU negative cells is indicated as black dashed line. **(D)** Percent of EdU positive cells at indicated concentrations of EGF. Error bars indicate 95 % confidence interval based on bootstrapping (n = 1,000). **(E)** Comparing EdU negative or positive cells with cells in G1- or S-phase, respectively, according to geminin levels. Red numbers indicate the percentage of cells in the corresponding cell cycle phase.

Without EGF stimulation, cells showed neither S-phase entry nor cell division, emphasizing that there was no residual mitogenic activity under my experimental conditions and all observed cell cycle progression was dependent on EGF-induced signaling. I observed that increasing the EGF concentrations resulted in more and more cells entering S-phase, reaching a maximum of roughly 90 % of the cells at concentrations of 7.5-10 ng/ml EGF (Figure 10A). I observed a similar increase of cells dividing at least once within 48 h. However, the fraction of dividing cells remained considerably lower at approximately 70 % (Figure 10A) as the duration of S/G2-phases extended beyond the observation period in cells with late S-phase entry. Accordingly, the time of S-phase entry was heterogeneously distributed around 20 h post stimulation in individual cells, mostly independent of the strength of the

mitogenic stimulus (Figure 10B). Cells responding to low EGF concentrations, however, only entered S-phase at earlier time points. This can be explained by the rapid decay of EGF under these conditions and thereby a lack of mitogenic signaling at later times. The duration of S/G2-phases was similarly distributed with a median around 18 h (Figure 10C). Interestingly, there was no clear correlation between time of S-phase entry and duration of S/G2-phases (Figure 10D).

Only about half of the cells entered S-phase when stimulated with low EGF concentrations (Figure 10A). For this reason, I wanted to see if cells that entered S-phase differed in their integrated ERK activity profile compared to cells that remained in a quiescent state. When analyzing cells that have been treated with 1 ng/ml EGF, a concentration at which about 50 % of the cells entered the cell cycle, the median FIRE signal during the first response was only slightly higher in cells entering S-phase than those that remained in G0/G1, indicating that the FIRE signal has low predictive power for the cell cycle fate of a cell (Figure 10F). Additionally, actively replicating cells marked by EdU incorporation showed only minor increases in FIRE levels at various time points (Figure 10E). Cells treated with higher EGF concentrations displayed no noticeable differences in the shape and amplitude between cells entering S-phase and those which did not (Figure 10F). Even when I align the single-cell FIRE trajectories to the time of S-phase entry to correct for asynchronies in the response and compared these trajectories to FIRE trajectories of quiescent cells aligned to a matched time distribution, I again detected only marginal differences (Figure 10F).

As I could not observe a strong correlation between the FIRE signal and S-phase entry, I analyzed if cell divisions were affected by integrated ERK activity. Comparing the fold change in FIRE levels during the first response in dividing and non-dividing cells, I observed a similar trend as for S-phase entry (Figure 10G). Interestingly, a more pronounced difference between cycling and quiescent cells was only observed when FIRE levels in the 16 h prior to cell division were analyzed. However, as this difference was only visible in cells treated with high doses of EGF, the measurements did not provide support for a decisive influence of ERK signaling in the completion of the cell cycle. Another interesting observation was that integrated ERK activity was not increased at low doses of EGF in the hours before cell division. This suggested that ERK activity might occur at late S-phase when EGF is present but may not be necessary to complete the cell cycle. Generally, my findings corroborated that ERK activity is required for quiescent cells to re-enter the cell cycle as previously reported (Zhang and Liu, 2002; Sharrocks, 2006), but since the variability of cellular responses cannot be explained, it is likely that additional mitogenic inputs are transmitted upon ligand stimulation.

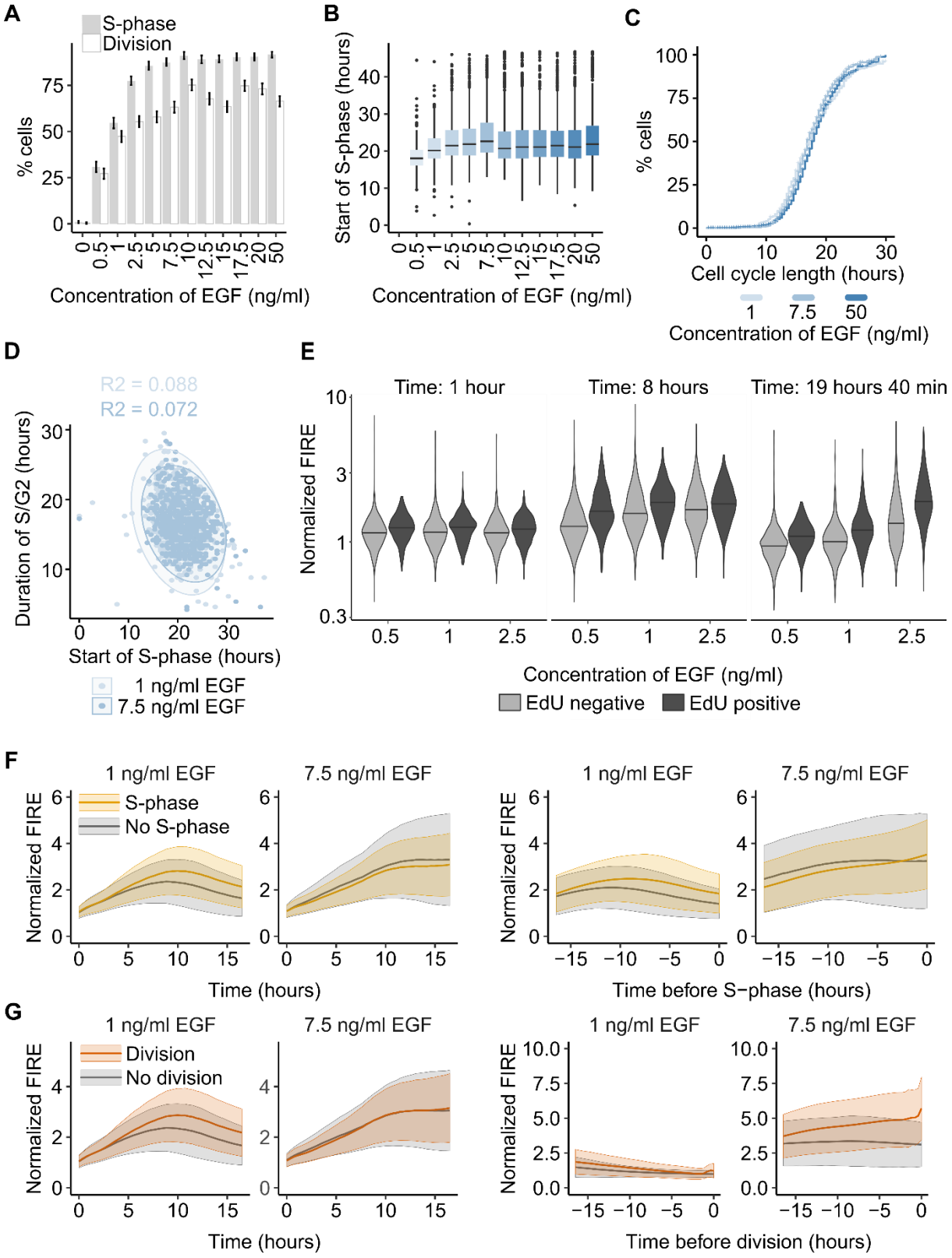

Figure 10: The role of ERK activity for cell cycle entry and progression.

(A) Percentage of cells entering S-phase (light gray) and dividing (white) at indicated concentrations of EGF. Error bars indicate 95 % confidence interval estimated with bootstrapping (n = 1,000). **(B)** Distribution of the time at which S-phase starts after stimulation with indicated concentrations of EGF. **(C)** Estimates of the length of S/G2-phase distribution (time from beginning

of S-phase to division) for three different concentrations of EGF (1 ng/ml, 7.5 ng/ml, and 50 ng/ml) using Kaplan-Meier analysis (2.3.7). **(D)** Scatterplot comparing the time at which S-phase starts after stimulation and length of S/G2-phase for two different concentrations of EGF (1 ng/ml and 7.5 ng/ml). Ellipses indicate area that include 95 % of the cells. **(E)** Normalized FIRE intensity at different time points (1 h, 8 h and 19 h 40 min) before EdU staining. Cells were labeled with EdU (for 40 min) 20 h after EGF treatment. Violin plots with EdU positive cells are dark gray and populations with EdU negative cells are light gray. Horizontal lines indicate the median FIRE intensity. **(F-G)** Average (bold line) and standard deviation (ribbon) of reporter time series (normalized to unstimulated control) of cells entering S-phase (yellow) and cells that do not enter S-phase (gray) stimulated with indicated concentrations of EGF. Left graphs show the first 16.5 h after stimulation; right graphs show 16.5 h before the onset of S-phase or equivalently sampled time series for non-responding cells **(F)**. Comparison of dividing cells (orange) and non-dividing cells (gray) for the first 16.5 h after stimulation or before division **(G)**.

2.1.3 PI3K SIGNALING CONTRIBUTES A NECESSARY MITOGENIC STIMULUS UPON EGF TREATMENT

Next, I systematically perturbed components of the MAPK signaling pathway (2.3.3) while monitoring integrated ERK activity, time of S-phase entry and duration of the S/G2-phase to determine the extent to which the ERK/MAPK pathway transmits pro-mitotic signals from EGFR activation (Figure 11A). By using the small molecule inhibitor gefitinib, the activity of EGFR was blocked, which abrogated all ERK signaling activity as well as cell cycle entry and progression (Figure 11B and C). This re-emphasized that in this model, EGFR signaling is essential for cell cycle entry. Although MEK inhibition prevented FIRE activation to a similar extent as the EGFR inhibitor (Figure 11B), about 10 % of cells started cycling in this condition (Figure 11C). Interestingly, the duration of S/G2-phases of those cells that entered the cell cycle was unaffected by MEK inhibition (Figure 11D). Although MEK appeared to be an important factor in cell cycle progression, inhibition of the kinase did not completely block cell cycle entry as it was observed with EGFR inhibition. This suggested that parallel pathways contribute significantly to mitogenic signaling. Therefore, I pharmacologically inhibited kinases from interacting pathways like p38 (SB203580), c-Jun N-terminal kinase (JNK) (JNK inhibitor VI) and GSK3 (SB216763). JNK and GSK3 inhibition had no effect on ERK activity and only led to minor changes in the cellular response (Figure 11B-D). However, I observed an increased FIRE signaling upon p38 inhibition (Figure 11B). Interestingly, this did not lead to an increase in the fraction of cells entering S-phase or dividing (Figure 11C). In contrast, I observed a longer duration of S/G2-phases as well as a concomitant decrease in the number of cells dividing (Figure 11C and D). This again indicated that ERK activity is not limiting for cell cycle regulation. Finally, I inhibited the PI3K pathway using a pharmacological inhibitor (LY29402). As the PI3K pathway is activated in parallel to MAPK signaling through the EGF receptor, it is an obvious candidate for transmitting additional mitogenic input. Indeed, inhibiting the kinase led to almost a complete block of cell cycle entry and progression. Interestingly, those few cells that entered the cell cycle had prolonged S/G2-phases (Figure 11C and D). When assayed with the FIRE

reporter, ERK was still as active as in control cells (Figure 11B). The effect of inhibiting the downstream kinase AKT with the small molecule MK-2206 led to similar effects on the cell cycle as PI3K inhibition (Figure 11B-D).

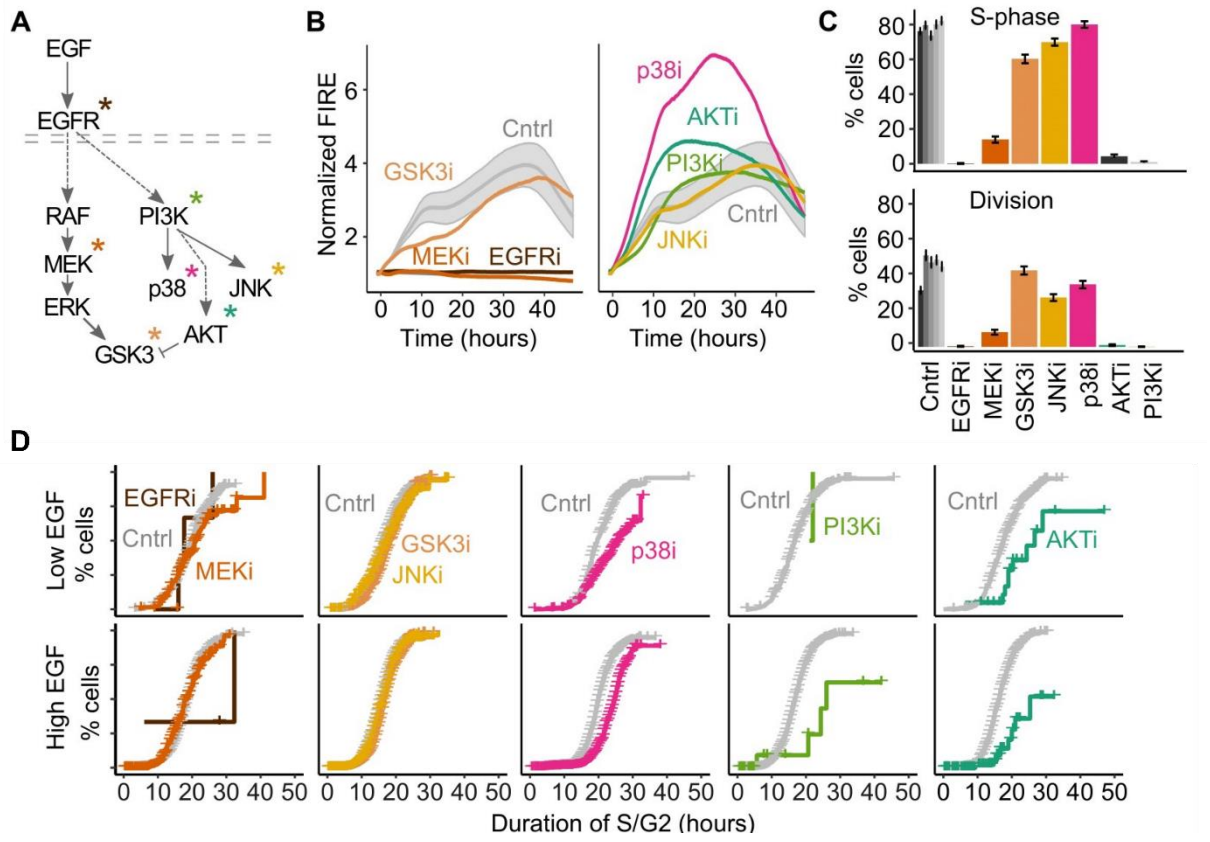

Figure 11: Pharmacological perturbation reveals relative contributions of MEK/ERK and PI3K/AKT pathways during mitogenic signaling.

(A) Scheme of the EGF pathway indicating the targets (colored asterisks) of pharmacological inhibitors used in this study. Dashed lines indicate indirect activation. **(B)** Average time courses of the FIRE reporter after stimulation with EGF for controls (gray) and after pre-incubation with the indicated inhibitors. For controls, the standard deviation around the mean of five experiments is shown (gray ribbon) (6.3). **(C)** Effect of inhibitors on the percentage of cells entering S-phase (top panel) or dividing (bottom panel) at the indicated concentration of EGF. Error bars indicate 95 % confidence interval based on bootstrapping (n = 1,000). **(D)** Effect of inhibitors on the duration of S/G2-phases for two different EGF (1 ng/ml and 7.5 ng/ml) concentrations by using Kaplan-Meier analysis.

Strikingly, I observed strong FIRE levels upon p38, PI3K and AKT inhibition. As blockage of these three kinases led to less cell cycle entry and increased FIRE activity, it was plausible that inhibited cell cycle progression might affect ERK activity. To test this hypothesis, I inhibited cell cycle progression using the CDK4/6 inhibitor palbociclib and CDK1 inhibitor RO3306. While CDK4/6 inhibition completely prevented S-phase entry and cell division, CDK1 inactivation only reduced the number of cells dividing. Nevertheless, as FIRE levels were not amplified in both conditions, a direct influence of cell cycle blockage on ERK activity seemed unlikely (Figure 12A-D).

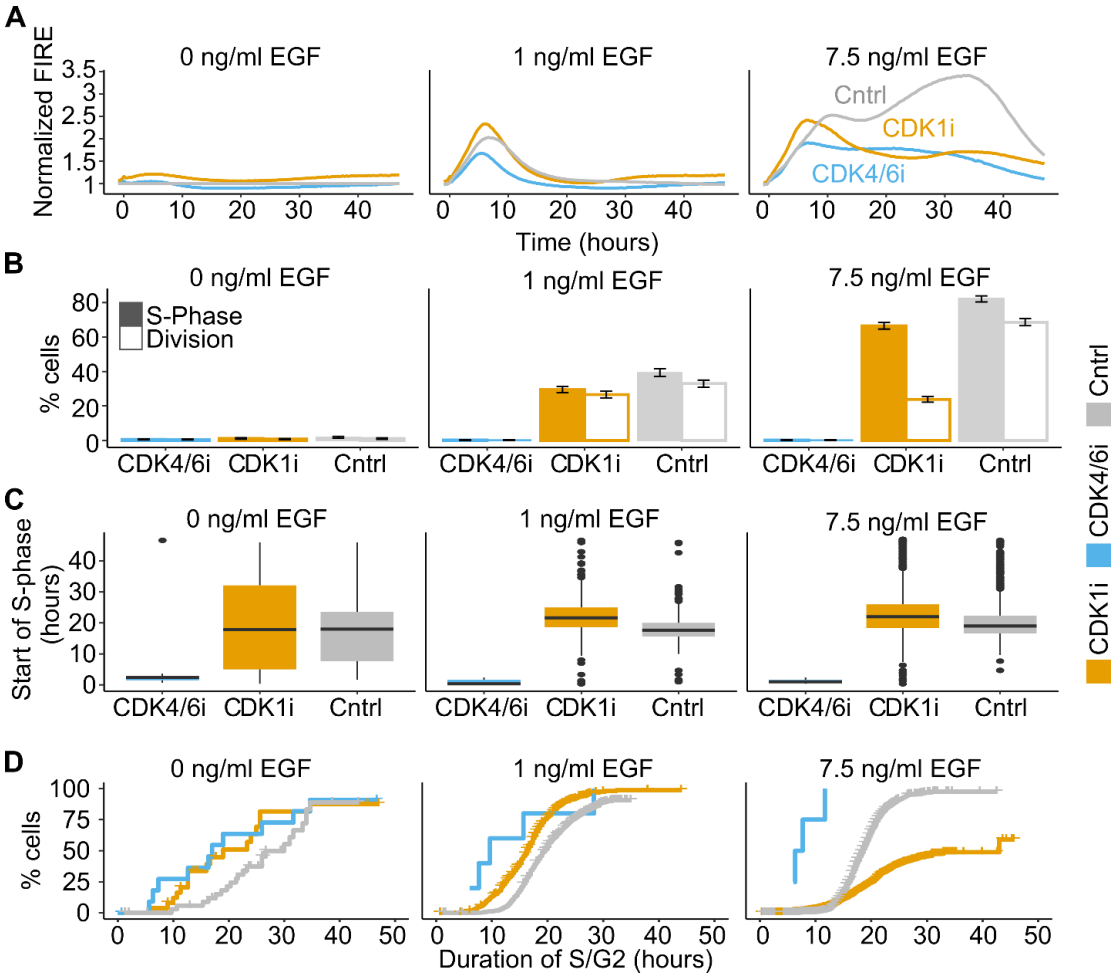

Figure 12: Inhibited cell cycle progression does not affect ERK activity.

(A) Average time courses of the FIRE reporter after stimulation with different concentrations of EGF and preincubation with CDK inhibitors. **(B)** Effect of CDK inhibitors on the percent of cells entering S-phase (solid bars) or undergoing division (open bars). Error bars indicate 95 % confidence interval based on bootstrapping (n = 1,000). **(C)** Start of S-phase within 47 h after stimulation with different concentrations of EGF and CDK inhibition. **(D)** Effect of CDK inhibition on the duration of S/G2-phases upon stimulation with different concentrations of EGF using Kaplan-Meier analysis.

2.1.4 CELL CYCLE ENTRY AND PROGRESSION HAVE DIVERGING TEMPORAL REQUIREMENTS FOR MAPK AND PI3K SIGNALING

The next step was to better understand the contribution of MAPK and PI3K signaling for regulating cell cycle entry and progression. To this end, I inhibited the corresponding pathways as well as EGFR activity at different time points after EGF stimulation (Figure 13A). When EGFR-dependent signaling was blocked entirely 10 h after EGF treatment by gefitinib treatment, FIRE signals rapidly decreased, and cell cycle entry was prevented in nearly all cells (Figure 13B-E). Sustaining EGFR activity for 15 or 20 h led to an increasing fraction of cells entering and progressing through the cell cycle. As expected, the duration of ERK activity was extended as well. When I inhibited MEK at different time points after EGF

stimulation, a similar decay of the FIRE response was observed (Figure 13B). However, more cells entered S-phase when the MEK inhibitor was added at 10 h compared to gefitinib. Even more striking was the relative increase in cells dividing compared with EGFR inhibition at all time points tested (Figure 13C). In contrast, PI3K inhibition at 10 h, 15 h or 20 h post EGF treatment showed a comparable suppression of S-phase entry and cell division as EGFR inhibition despite only temporarily attenuating ERK activity (Figure 13B and C). Blocking EGFR, MEK or PI3K signaling for different periods at the beginning of the experiment led to delayed FIRE accumulation and S-phase entry as expected (Figure 13F-I). However, cells still entered S-phase in comparable numbers after inhibitors were washed away (Figure 13J and K). A decrease in dividing cells was only observed when inhibitors were present for 15 h due to the limited observation period. These results corroborate that both ERK and PI3K activity are necessary for S-Phase entry (Jones and Kazlauskas, 2001).

A close look at the cells that progressed into S-phase upon PI3K inhibition revealed higher geminin levels at the time of treatment, indicating that they already passed the restriction point and initiated the transition from G1- to S-phase prior to the loss of PI3K activity (Figure 13D). Importantly, the duration of S/G2-phases in cycling cells was strongly increased when PI3K signaling was blocked 10-20 h after EGF treatment (Figure 13E). The same decreased rate of cell cycle progression was observed upon EGFR inactivation. However, preventing ERK activation through MEK inhibition had no effect once cells entered the cell cycle (Figure 13E).

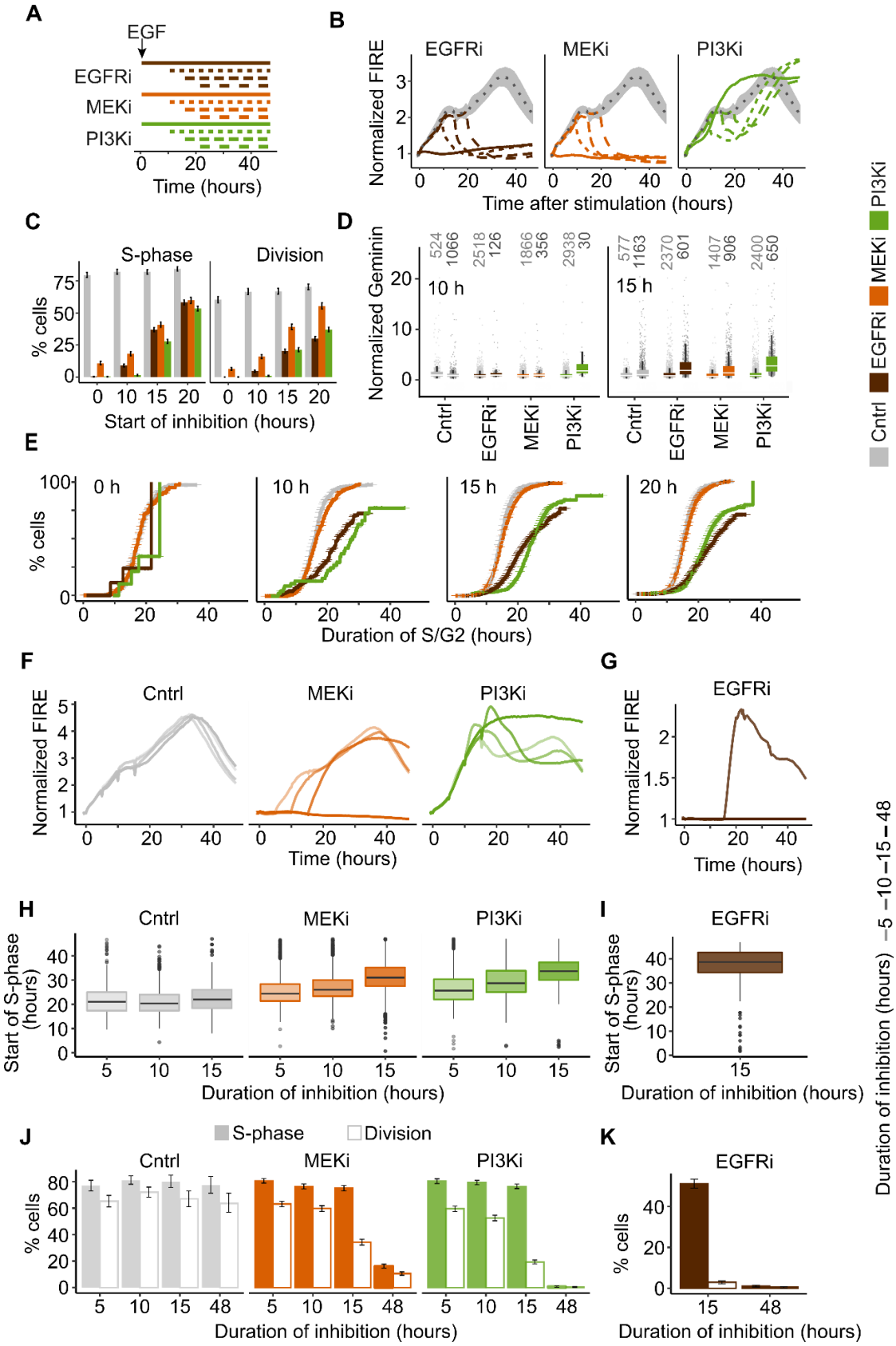

Figure 13: Temporal requirements for ERK and AKT activity differ during cell cycle progression.

(A) Scheme of experiment. EGFR, MEK, and PI3K inhibitors were added either at time of stimulation or 10 h, 15 h, or 20 h after stimulation. **(B)** Average time courses of the FIRE reporter after stimulation with 7.5 ng/ml EGF and incubation with the

indicated pharmacological inhibitors at different time points or controls (gray). For controls, the standard deviation around the mean of three experiments is shown (gray ribbon). **(C)** Effect of inhibitors on the percentage of cells entering S-phase (left) or dividing (right) for the indicated time of inhibition after stimulation. Error bars indicate 95 % confidence interval based on bootstrapping (n = 1,000). **(D)** Comparison of geminin levels at time of inhibitor treatment (as indicated) between cells entering S-phase (right, dark gray) and cells that do not enter S-phase (left, light gray) within the time of measurement. Numbers of cells for each condition are indicated. **(E)** Effect of the time of inhibitor treatment (as indicated) on the duration of S/G2-phases after stimulation with 7.5 ng/ml EGF compared to controls using Kaplan-Meier analysis. **(F)** Average time courses of the normalized FIRE reporter after stimulation with 7.5 ng/ml EGF alone or in combination with a MEK inhibitor or PI3K inhibitor. The inhibitors were washed from the medium 5 h, 10 h or 15 h later. **(G)** Average time course of the normalized FIRE reporter stimulation with 7.5 ng/ml EGF in combination with an EGFR inhibitor. The inhibitor was either kept during the complete experiment (dark) or washed off after 15 h (light). **(H)** Comparing the effect of pulsed inhibition using a MEK or a PI3K inhibitor on the timing of S-phase entry. **(I)** Comparing the effect of pulsed inhibition using an EGFR inhibitor on the timing of S-phase entry. **(J)** Effect of pulsed inhibition on the percent of cells entering S-phase (solid bars) or dividing (open bars). Error bars indicate 95 % confidence interval based on bootstrapping (n = 1,000). **(K)** Same approach as in **(J)**, but the EGFR inhibitor was used instead.

To further investigate the role of PI3K signaling for S- and G2-phase progression, I aimed to initiate ERK activation for a short period of time and then additionally activate PI3K by additional ligands. To do so, I used EGF at a low dose (0.5 ng/ml) that, due to ligand degradation, is expected to induce only transient signaling. I additionally stimulated cells with insulin-like growth factor (IGF) (2.5 µg/ml), which is expected to preferentially initiate the phosphorylation and thus activation of AKT (Zheng and Quirion, 2006; Ma and Bai, 2012) (Figure 14A). By using the FIRE reporter, transient ERK activation at low doses of EGF that was unaffected by the addition of IGF was confirmed (Figure 14B). Moreover, IGF treatment alone did not induce FIRE accumulation (Figure 14C). Although the transient ERK activation was sufficient to induce cell cycle entry in approximately 25 % of cells (Figure 14D), these cells needed longer to complete S/G2-phase than cells with high EGF inputs (Figure 14E). However, when I combined low EGF input with IGF stimulation, which predominantly activates the PI3K pathway, it rescued the phenotype and resulted in cell cycle progression rates comparable to high EGF stimuli (Figure 14E). Importantly, IGF treatment alone did not result in appreciable cell cycle entry (Figure 14F), whereas a combination of low EGF and strong IGF inputs led to a modest increase in the fraction of cells entering S-phase and dividing (Figure 14D). Consistently, actively replicating cells incorporating EdU showed slightly increased levels of phosphorylated AKT compared to cells remaining in G1 upon treatment with both EGF alone and EGF together with IGF (Figure 14G and H). Similar results were obtained when combining low doses of EGF with insulin (5 µg/ml), which also activates the PI3K pathway (Engelman et al., 2006) (Figure 14I-K).

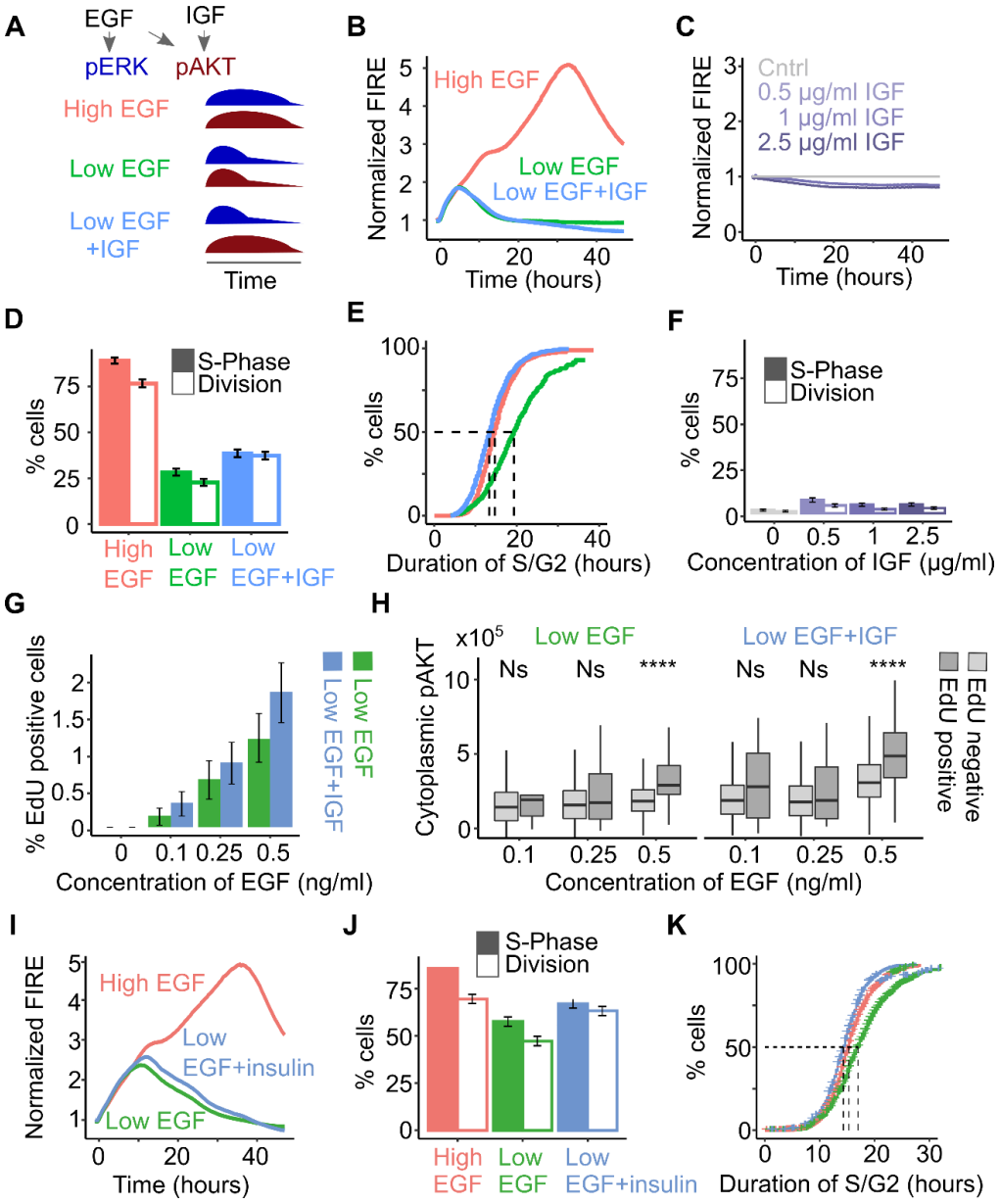

Figure 14: AKT activation rescued delayed cell cycle progression at low EGF concentrations.

(A) Scheme of the EGF and IGF pathways and the rescue approach. **(B)** Average time courses of the FIRE reporter after stimulation with different concentrations of EGF as well as co-stimulation with IGF (2.5 µg/ml). **(C)** Average time courses of the FIRE reporter after stimulation with different concentrations of IGF alone. **(D)** Percentage of cells entering S-phase (solid bars) or dividing (open bars) after stimulation. Error bars indicate 95 % confidence interval based on bootstrapping (n = 1,000). **(E)** Comparing the effect of IGF stimulation on the duration of S/G2-phases using Kaplan-Meier analysis. **(F)** Effect of IGF stimulations alone on the percent of cells entering S-phase (solid bars) or undergoing division (open bars). Error bars indicate 95 % confidence interval based on bootstrapping (n = 1,000). **(G)** Percentage of EdU positive cells. Cells were first stimulated with different concentrations of EGF (green bars) alone or in combination with 2.5 µg/ml IGF (blue bar) and after 20 h stained with EdU. Error bars indicate 95 % confidence interval based on bootstrapping (n = 1,000). **(H)** Comparing the distribution of cytoplasmic pAKT levels between EdU negative (light gray) and EdU positive cells (dark gray) using immunofluorescence (2.3.8). P-values based on a t-test are indicated with asterisk (ns: p > 0.05, *: p <= 0.05, **: p <= 0.01, ***: p <= 0.001, ****: p <= 0.0001). **(I)** Average time courses of the FIRE reporter after stimulation with different concentrations of EGF in

comparison to a rescue experiment with additional insulin. **(J)** Effect of insulin stimulation on the percent of cells entering S-phase (solid bars) or dividing (open bars). Error bars indicate 95 % confidence interval based on bootstrapping (n = 1,000). **(K)** Comparing the effect of insulin stimulation on the duration of S/G2-phases using Kaplan-Meier analysis.

To strengthen the understanding of PI3K signaling and its role during S- and G2-phase, I stimulated cells with EGF and inhibited MEK and PI3K activity 15 h later. I then employed scRNA-seq to determine expression profiles of individual cells 20 h and 30 h after addition of the growth factor (Figure 15A, 2.3.9-2.3.11). Visualization of the resulting data by dimensionality reduction using uniform manifold approximation and projection (UMAP) showed clear separation of quiescent and EGF-stimulated cells (Figure 15B, gray and blue dots). Blocking PI3K and MEK signaling led to distinct expression profiles that clustered separately from cells treated with EGF only (Figure 15B, green and red dots). Interestingly, expression profiles of inhibitor-treated cells differed at the 20 h and 30 h time points. Similar results were obtained in a replicate experiment and by using a different dimensionality reduction method (principal component analysis, (Figure 15D and E)). To correlate expression profiles of individual cells with cell cycle progression, the cell cycle state of each cell was mapped by using characterized marker genes (Stuart et al., 2019) (2.3.11). With this approach I was able to determine cell cycle distributions for each condition and time point that were comparable to previous analyses using time-lapse microscopy (Figure 15F). Combining the UMAP projection with cell cycle information revealed a clear progression of EGF-stimulated cells from G1- to S- and G2/M-phase (compare Figure 15B and C). Importantly, cells progressing into S- and G2/M-phase in the presence of PI3K and MEK inhibitors showed clearly distinguishable expression profiles. Using the pathway activity scores calculated by the PROGENy method (Schubert et al., 2018), I validated that inhibitor treatment led to the expected changes in MAPK and PI3K signaling (Figure 15G).

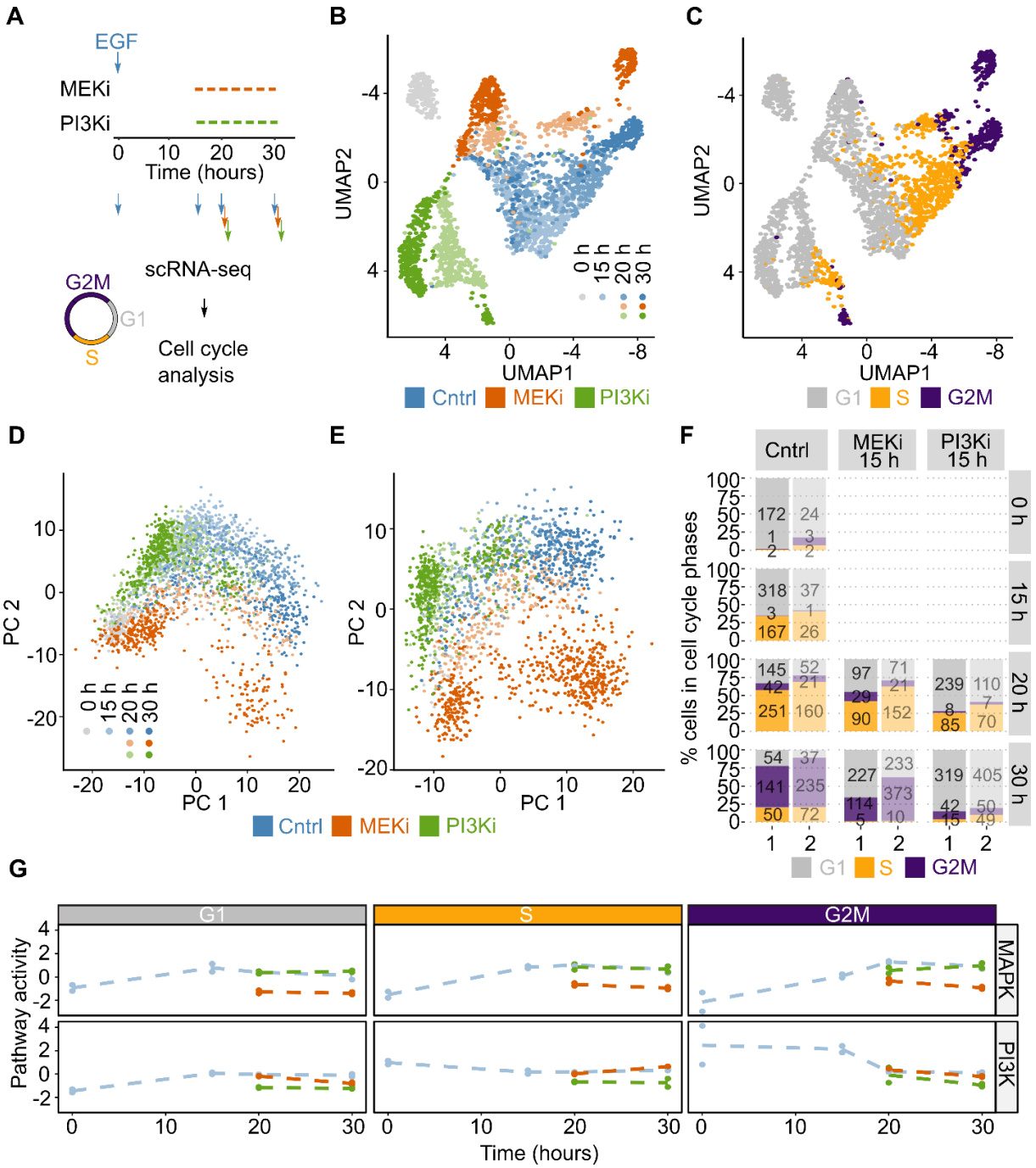

Figure 15: Cell cycle resolved expression analysis of single cells upon mitogenic stimulation.

(A) Scheme of scRNA-seq experiments. Cells were stimulated with 7.5 ng/ml EGF. MEK or PI3K inhibitors were added after 15 h and cells were sampled for scRNA-seq at the indicated time points. **(B)** UMAP for one experiment. Cells are barcoded for experimental condition. **(C)** UMAP as in **(B)** with cells barcoded for cell cycle phases. **(D)** Principal component analysis (PCA) of highly variable genes based on scRNA-seq from the first replicate. The first two principal components (PC) are plotted; dots indicate individual cells; colors correspond to stimulation with EGF (blue), additional inhibition with MEK (orange) or PI3K (green) inhibitor. As indicated, cells were sampled at different time points. **(E)** PCA of highly variable genes based on scRNA-seq from a replicate experiment. **(F)** Stacked bar plot indicating the number and fractions of cells in G1-phase (gray), S-phase (yellow) and G2/M-phase (purple) for different conditions and for two replicates. **(G)** PROGENy pathway activity

scores for MAPK pathway (upper panel) and PI3K pathway (lower panel) over time and for the different conditions. Each dot indicates one replicate and dashed lines connect the corresponding mean values as guidance.

As a next step, differentially expressed genes upon inhibitor treatment depending on cell cycle state and time point were determined and the corresponding molecular pathways using gene ontology (GO) term analysis were resolved (Figure 16). In G1-phase cells, I mainly observed changes in the expected molecular pathways, such as response to growth factors. In S-phase cells, only PI3Ki-treated cells showed significant changes, which mainly affected pathways involved in metabolic processes, such as mitochondrial respiration, translation and ribonucleotide synthesis. In G2/M-phase cells at 30 h post EGF stimulation, MEK and PI3K inhibition induced distinct alterations in pathway activity. For PI3K inhibition, changes in G2/M-phase cells partially overlapped with those observed during S-phase (Figure 16).

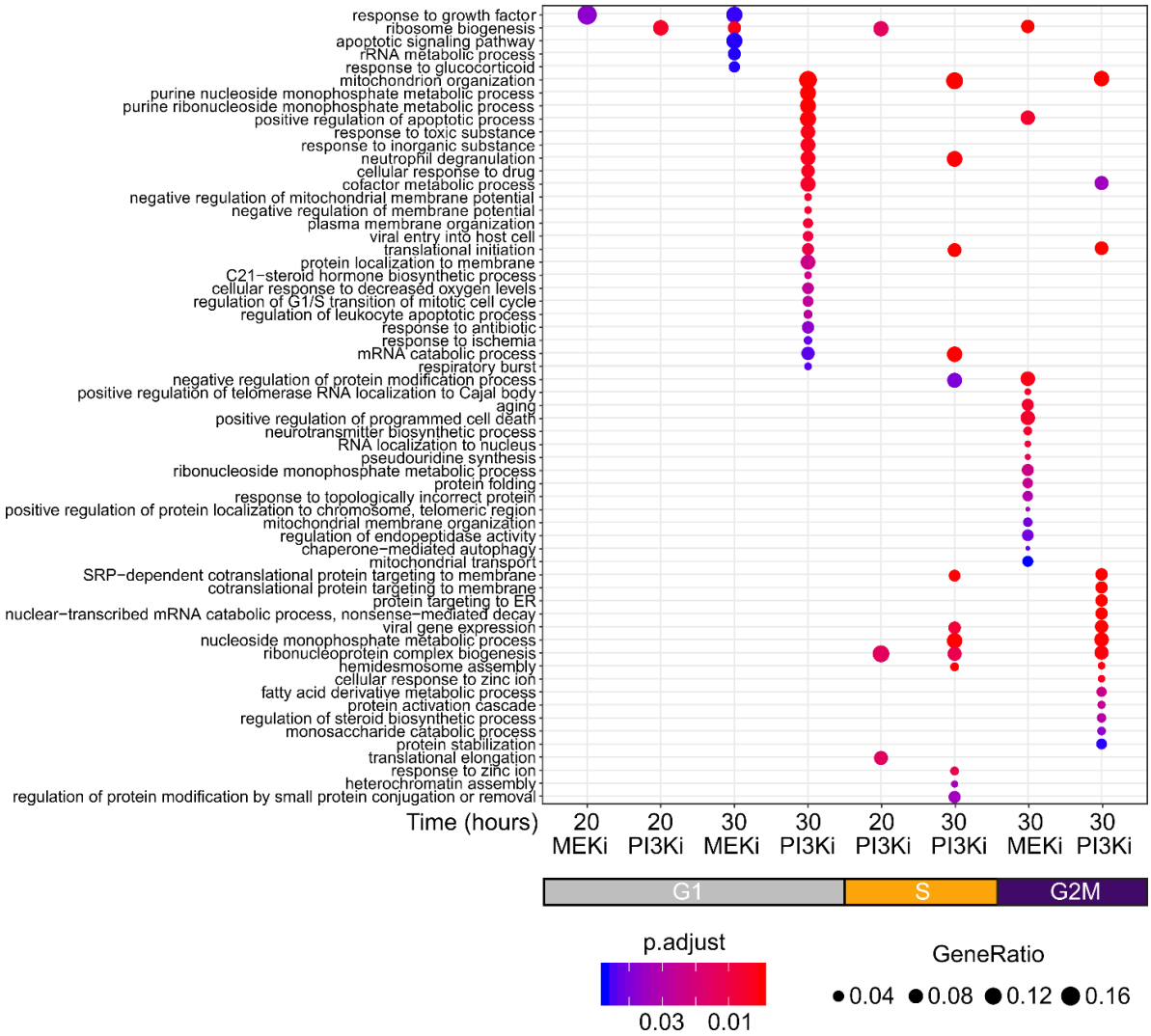

Figure 16: Pathway enrichment analysis upon pharmacological inhibition of MEK and PI3K.

Pathway enrichment using differential gene expression for samples treated with MEK or PI3K inhibitor in comparison to EGF stimulation at the indicated time points and cell cycle phases.

I further analyzed cell cycle distributions to determine if the observed delay in cell cycle progression upon PI3Ki treatment was due to an increased duration of S- or G2/M-phase. As expected, I observed a decreased fraction of cells in S-, G2- or M-phase 20 h after EGF treatment when MEK or PI3K activity was inhibited 15 h post stimulation (Figure 17A). The fraction of S/G2M-phase cells further decreased at the 30 h time point, as no additional cells could enter S-phase in the absence of MAPK or PI3K signaling, whereas others successfully completed cell division. By analyzing the ratio between S- and G2/M-phase cells under both conditions, I observed that most cells without active MEK completed S-phase between the 20 h and 30 h time point (Figure 17B). However, upon PI3Ki treatment, a noticeable fraction of cells remained in S-phase at the 30 h time point, suggesting a delay in S-phase progression. To further validate these findings, I imaged FIRE reporter cells upon EGF treatment by time-lapse microscopy, inhibited MEK and PI3K activity after 15 h and labeled the cells with EdU (2.3.4) at 22.5 h and 32.5 h post stimulation, respectively (Figure 17C). Consistent with the scRNA-seq analysis, most geminin-positive cells were EdU positive and thereby actively replicating at the 22.5 h time point (Figure 17D). After 32.5 h, most MEKi treated cells completed S-phase and entered G2-phase. As expected, control conditions showed active replicating cells at 32.5 h as cells were still able to enter S- from G1-phase. However, although no additional cells were able to enter S-phase upon PI3K inhibition, I observed that most of the treated cells were still EdU positive at the later time point. To estimate the corresponding time of S-phase progression, cells were binned according to the time of S-phase entry, as indicated by geminin accumulation relative to the time of metabolic labeling, and the corresponding fraction of EdU-positive cells was determined (Figure 17E). Nearly all control and MEKi-treated cells completed S-phase within 16 h, whereas most cells without active PI3K remained in S-phase for over 20 h. This severe delay in S-phase progression was further supported by a slower rate of EdU incorporation in PI3Ki- than in MEKi-treated cells (Figure 17F).

Taken together, quantitative time-resolved analysis at the single-cell level uncovered that the mitogenic EGF signal is transmitted both via the MAPK and PI3K signaling pathway. Activation of both pathways together is necessary for cell cycle entry. However, timely progression through S-Phase is mainly dependent on a sustained PI3K signaling to adjust to the metabolic needs of the cells during replication.

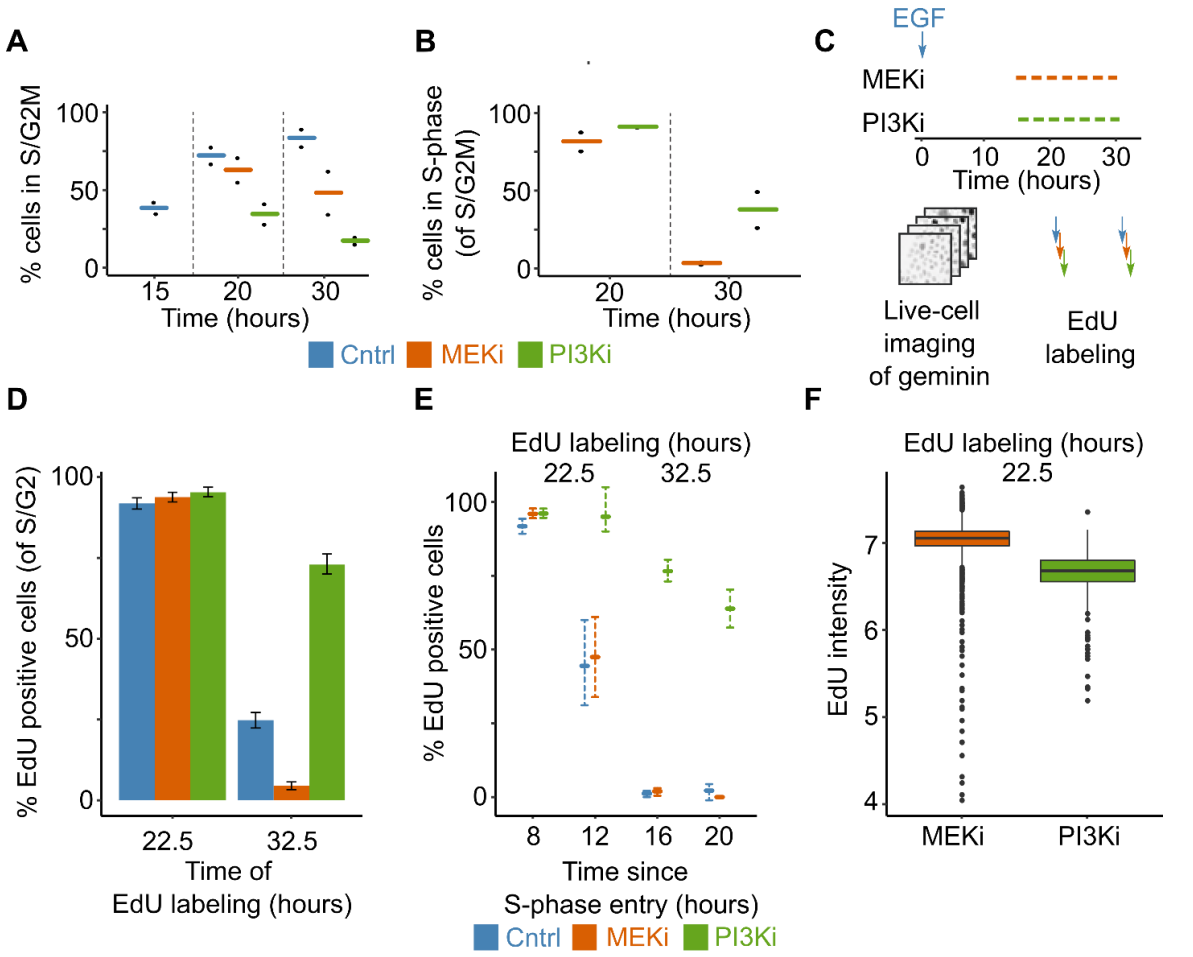

Figure 17: PI3K signaling is required for timely progression through S-Phase.

(A) Percentage of cells in S/G2M-phase based on cell cycle markers (dots, replicates; lines, mean). **(B)** Effect of MEK or PI3K inhibitors, respectively, on percentage of cells in S-phase. **(C)** Scheme of live-cell imaging experiments with EdU stainings at different time points. **(D)** Percent of EdU-positive cells that started S-phase before EdU staining based on analysis of geminin levels. Error bars indicate 95 % confidence interval based on bootstrapping (n = 1,000). **(E)** Effect of MEK or PI3K inhibitor on the number of EdU-positive cells labeled at indicated time points. Cells were binned according to the time since entering S-phase (based on geminin). Error bars indicate 95 % confidence interval based on bootstrapping (n = 1,000). **(F)** Effect of MEK (orange) and PI3K inhibitor (green) on the extent of EdU incorporation.

2.2 DISCUSSION OF PART 1

Mitogenic signaling gives multicellular organisms the opportunity to regulate the rate and timing of cell division. To ensure precise control over cell cycle entry and progression, the information flow through multiple signaling pathways needs to be integrated dynamically to coordinate the different components of the cell cycle machinery (Chambard et al., 2007). By combining live-cell microscopy, scRNA-seq, pharmacological perturbations and computer-aided data analysis, I was able to disentangle the contributions of the MAPK and PI3K/AKT pathways to mitogenic signaling during different cell cycle phases. By using a specific fluorescent reporter cell line, I measured signaling activity in single cells. In addition to unrivaled temporal resolution, live-cell microscopy allows resolving non-genetic heterogeneity that can strongly influence the outcome of signaling events (Spiller et al., 2010). Several strategies have been developed to monitor MAPK pathway activity in living cells: fluorescence resonance energy transfer (FRET)-based reporters allow direct measurements of substrate phosphorylation but are limited by a low signal-to-noise ratio and are prone to saturation (Komatsu et al., 2011; Selimkhanov et al., 2014; Ryu et al., 2015; Gillies et al., 2017). Translocation-based reporters provide a similar, but more robust ratio-metric measure (Regot et al., 2014). However, their sensitivity is also restricted to certain segments of the ERK dynamic range (Gillies et al., 2017). Nuclear localization of an ERK-YFP fusion correlates with its activity on short time scales but can be affected by other cellular processes (Cohen-Saidon et al., 2009). Finally, as I was interested in understanding how and when total ERK activity affects cell cycle progression, I decided to employ the FIRE reporter that linearly reflects integrated ERK activity (Albeck et al., 2013; Gillies et al., 2017). When my results are compared to previously reported data from Albeck et al., 2013, it is important to note that different experimental conditions were used. I primarily focused on the response of quiescent cells to acute growth factor stimulation, whereas previous studies focused on steady-state EGF signaling under sustained stimulations. Additionally, only signaling effects of the MAPK-pathway in the nucleus were considered, since the FIRE reporter is not able to capture cytoplasmic activity (Murphy et al., 2002). This might explain why under some conditions, such as PI3K and AKT inhibition, FIRE response and phosphorylation diverge.

Using computer-aided data analysis, I extracted time series of ERK activity over two days for thousands of cells treated with varying concentrations of EGF. Thereby, I was able to show a bi-phasic ERK activity profile with an early and late response at high EGF concentrations. The continuous measurements from unperturbed individual cells, thus, confirmed previous observations from biochemical studies of cell populations (Meloche et al., 1992). From this data, it was proposed that initial ERK activity is necessary to mediate the transition from the G0 state of the cell cycle to G1. During G1-phase, reduced

nuclear ERK activity promotes cell cycle progression, as the transcription factor FOS is degraded and replaced by FRA1 (Burch et al., 2004). Sufficiently strong activation of ERK during late G1-phase is finally necessary to induce transcription factors such as early growth response protein 1 (EGR1), which mediate the all-or-none decision to enter S-phase and divide (Zwang et al., 2011). I could confirm that ERK signaling is required for S-phase entry by using pharmacological inhibitors to artificially abbreviate ERK activity (Figure 13). However, I did not detect a clear correlation between ERK activity and S-phase entry at low EGF doses in simultaneous measurements of FIRE and cell cycle reporters (Figure 10F). Consistently, there was no direct correlation between S-phase entry and the occurrence of a second signaling phase (Figure 8C and Figure 10A). One possible explanation could be that entering S-phase is similar to a stochastic decision that requires sustained ERK activity. Depending on the duration of G1-phase, transient ERK signaling may be sufficient in one cell to enter S-phase, while in other cells both phases of ERK signaling may be required. Another explanation for the observed heterogeneity in S-phase entry might be varying levels of cell cycle inhibitors such as p21. In previous single-cell experiments, it was shown that the decision between proliferation and quiescence in cycling MCF10A cells is controlled by a bifurcation in CDK2 activity due to varying levels of p21 as a consequence of endogenous DNA damage during replication (Spencer et al., 2013; Arora et al., 2017; Barr et al., 2017). It will now be interesting to investigate if p21 heterogeneity persists during growth factor deprivation-induced quiescence or if other molecular mechanisms are responsible for the heterogeneous responses to low EGF concentrations. For example, it could be possible that heterogeneous expression of inhibitors of the PI3K pathway, which I showed to be required for cell cycle entry as well, contributes to the proliferation–quiescence decision.

In addition to quantifying the decision to enter the cell cycle, the frequency and timing of cell division were determined by following the phenotypic response of each cell. Using pharmacological perturbations, I showed that ERK signaling is dispensable after the restriction point has been exceeded, while PI3K/AKT activity was required both for entering S-phase and for timely progression to mitosis. However, it was not possible to induce cell cycle entry by activation of AKT through IGF or insulin alone. During G1, it is known that ERK and AKT signaling interact at the level of cell cycle inhibitors, although the precise effects may depend on the cell line studied (Zwang et al., 2011; Worster et al., 2012). My experiments using inhibitors at different time points after EGF stimulation revealed that PI3K inhibition completely blocked S-phase entry, whereas with MEK inhibition some cells still entered S-phase. These results are consistent with previous studies, which showed that G1 progression requires PI3K/AKT and ERK signaling, whereas S-phase entry itself is mainly dependent of PI3K/AKT (Jones and Kazlauskas, 2001). As AKT activity can suppress anti-proliferative gene products induced during early G1-phase, it

may render cells permissive for ERK-driven S-phase entry (Zwang et al., 2011). However, the role of AKT in controlling S/G2 progression is less well documented. It was shown that blocking PI3K/AKT signaling prolongs progression through S/G2-phase, but it remained unclear which of the two phases is prolonged (Dangi et al., 2003). Employing scRNA-seq and life-cell imaging combined with metabolic labeling showed that inhibition of AKT signaling strongly prolongs S-phase (Figure 15 and Figure 17). One proposed mechanism is that AKT phosphorylates CDK2 and regulates its subcellular localization during S-phase (Maddika et al., 2008). The resulting nucleo-cytoplasmic shuttling of CDK2 may be important for cell cycle progression. Therefore, in further studies it could be interesting to research AKT activity and CDK2 localization simultaneously in living cells. Additionally, high metabolic demands of S-phase may require strong AKT signaling. The AKT signaling pathway is crucial for cellular metabolism, including glycolysis and nucleotide biosynthesis (Ward and Thompson, 2012). Analysis of the differentially expressed genes in the scRNA-seq data showed that, indeed, PI3K inhibition deregulates genes involved in metabolic processes during S-phase (Figure 16). This provides evidence that high metabolic demands are not fulfilled in the absence of AKT activity, which contributes to prolonged S-phase progression. Additionally, AKT signaling also influences cell growth via mTOR signaling (Ward and Thompson, 2012), and cell size, in turn, might influence the length of S-phase (Lloyd, 2013). However, it is currently unknown if and how cell size and cell cycle are coupled (Lloyd, 2013).

One of the most important cell fate decisions is the control of proliferation and perturbation of this process can be involved in severe pathologies. For instance, amplification of EGF receptors in breast cancer cells or mutations in the PI3K pathway, such as PTEN deletion, can lead to increased mitogenic signaling. While single perturbations will not lead to changes in cell proliferation in most cases, the accumulation of alterations observed during tumorigenesis can cause hypersensitivity to growth factors. A detailed understanding of temporal requirements and synergies between major mitogenic mechanisms could be advantageous in developing therapeutic interventions that prevent altered cell signaling. Instead of treatments with single agents such as gefitinib, a thoughtful schedule of combination therapies might be more efficient in targeting both proliferating and quiescent cells. Additional studies utilizing quantitative experimental data and computer-aided analysis will provide the necessary molecular insights for such next-generation therapies.

2.3 MATERIAL AND METHODS OF PART 1

2.3.1 CELL LINES

MCF10A cells were grown in Dulbecco's Modified Eagle Medium (DMEM/F12, Thermo Fisher Scientific) supplemented with 5 % horse serum (Thermo Fisher Scientific), 20 ng/ml EGF (PeptroTech), 0.5 µg/ml hydrocortisone (Sigma Aldrich), 100 ng/ml cholera toxin (Sigma Aldrich), 10 µg/ml insulin (Sigma Aldrich), 2 mM glutamax (Thermo Fisher Scientific), 100 U/ml penicillin and 100 µg/ml streptomycin (Thermo Fisher Scientific). From now on this medium is referred to as growth-medium. The FIRE reporter has been previously described (Albeck et al., 2013). In brief, it is an indirect reporter of ERK activity, which consists of the PEST domain of FRA1 fused to YFP. Expression is driven by the MSCV LTR. The reporter cell line also stably expresses NLS-CFP (mCerulian) as a nuclear marker to facilitate automatically tracking and segmenting cells. In addition, the reporter cell line also expresses geminin as a marker for the transition from G1- into S-phase and for division.

2.3.2 GROWTH FACTOR DEPRIVATION AND LIVE-CELL TIME-LAPSE IMAGING

For live-cell imaging experiments, I used 24-well imaging plates (ibidi). I seeded 3.75×10^4 cells per well and incubated them in growth-medium for 36 h before the medium was exchanged to DMEM/F12 containing 0.3 % tissue culture grade BSA (Sigma Aldrich), 0.5 µg/ml hydrocortisone, 100 ng/ml cholera toxin, 100 U/ml penicillin and 100 µg/ml streptomycin. From now on this medium is referred to as deprivation-medium. Cells were incubated for 48 h in the serum- and growth factor-free medium to ensure that cells go into a quiescent state. At least 2 h before the experiment, I changed medium to phenol red-free FluoroBrite medium (Thermo Fisher) containing 0.3 % tissue culture grade BSA, 0.5 µg/ml hydrocortisone, 100 ng/ml cholera toxin, 2 mM glutamax, 10 mM HEPES (Thermo Fisher scientific), 100 U/ml penicillin and 100 µg/ml streptomycin (from now on referred to as deprivation-microscopy-medium). Cells were imaged with a Nikon Eclipse Ti-E inverted microscope with perfect focus system. All experiments were performed using a 20 × CFI Plan Fluor objective and a Nikon DS-Qi2 digital camera. Fluorescent proteins were excited with a X-Cite 120 LED illumination system (Lumen Dynamics) at 540 nm for YFP and 485 nm for CFP. The used filter sets were: 500/20 nm excitation, 515 nm beam splitter and 480/40 nm emission filter for YFP and 436/20 nm excitation, 455 nm beam splitter and 480/40 nm emission filter for CFP. Over 48 h images were taken every 20 min. The monitoring and acquisition of the images was controlled by Nikon NIS Elements AR

software. To ensure a stable environment, the microscope was enclosed with an incubation chamber controlling temperature, atmosphere (5 % CO_2) and humidity (Okolab).

2.3.3 LIGAND AND INHIBITOR TREATMENT

Inhibitor and ligand treatments were performed in the appropriate deprivation-(microscopy)-medium. In stimulation experiments, cells were imaged for 1 h prior to growth factor stimulation. If not marked differently, inhibitors were diluted in DMSO and used as indicated below. Control cells were treated with medium only or medium containing DMSO.

Inhibitors and ligands	**Used concentration**
CHIR-98014 GSK3b inhibitor (Selleckchem)	1 µM
Gefitinib EGFR inhibitor (Cayman Chemical)	10 µM
IKK2 inhibitor (Calbiochem)	5 µM
JNK inhibitor VIII (Cayman Chemical)	10 µM
Ly294002 PI3K inhibitor (Alexis Biochemicals)	50 µM
MK-2206 AKT1/2/3 inhibitor (Selleckchem)	5 µM
Palbociclib CDK4/6 inhibitor in Sodium DL-Lactate (MedchemExpress)	10 µM
RO-3306 CDK1 inhibitor (Axon Medchem	10 µM
SB203580 p38 inhibitor (Selleckchem)	10 µM
SB216763 GSK-3 inhibitor (Sigma Aldrich)	1 µM
Selumetinib (AZD6244) MEK1/2 inhibitor (Selleckchem)	1 µM
Sorafenib RAF kinases inhibitor (Selleckchem)	10 µM
U0126 MEK1/2 inhibitor (Selleckchem)	10 µM
EGF (Peprotech)	various concentrations
IGF (Peprotech)	various concentrations
Insulin (Peprotech)	10 µg/ml

2.3.4 EDU STAINING

For EdU staining in live-cell imaging, cells were incubated with 10 mM EdU (EdU Click-647, Thermo Fisher Scientific) at defined time points. After 40 min, EdU was washed off with deprivation-microscopy-medium and the supernatant of a backup plate, which was treated equally, was utilized to ensure appropriate EGF concentrations. Immediately after the experiment, cells were fixed with 2 % paraformaldehyde (Sigma-Aldrich) in PBS. Afterwards, cells were washed with PBS, permeabilized with 0.1 % Triton X-100 (Carl Roth) in PBS and blocked with 10 % goat serum (PAN-Biotech GmbH) in PBS. For EdU detection, a reaction cocktail was prepared according to the manufacturer's instructions and added to the cells. After 30 min incubation at room temperature, cells were washed with 0.1 % Triton X-100 in PBS and counterstained with 2 mg/ml Hoechst (Invitrogen) in

0.1 % Triton X-100/PBS. Using the same positions, cells were imaged for one additional loop in the microscope and correlated with the previous captured images.

2.3.5 DATA ANALYSIS OF LIVE-CELL MICROSCOPY EXPERIMENTS

Cells were tracked throughout the duration of the experiment using custom-written MATLAB (MathWorks, Natick, MA) scripts based on code developed by the Alon lab (Cohen et al., 2008) and the Cell Profiler project (Carpenter et al., 2006) as previously described (Strasen et al., 2018). In brief, I applied flat-field correction and background subtraction to raw images before segmenting individual nuclei from images of the NLS-CFP reporter using adaptive thresholding and seeded watershed algorithms. Segmented cells were assigned to corresponding cells in subsequent images using a greedy match algorithm based on a cost function, which included the velocity and direction of movement for a cell. Only cells tracked from the first to last time point were considered. Additionally, the fluorescence intensity of the nuclear marker was used to ensure consistency. I then quantified the nuclear fluorescence intensity of the FIRE reporter for each cell over time and normalized the resulting single-cell trajectories by dividing with the nuclear fluorescence of the NLS-CFP reporter to account for changes in nuclear shape. This normalization eliminated spurious peaks and disturbances by cell division. The measurements of unstimulated control cells included in each experiment were used for further normalization resulting in a fold change of FIRE levels compared to unstimulated means (Figure 7E). Specifically, for each cell the FIRE levels at each time point were divided by the mean FIRE level of the unstimulated control at that time point. Cells with an amplitude greater than three standard deviations (sd) from the average amplitude of unstimulated cells were considered to be responders. To identify cell cycle states using geminin, the time courses were first normalized by the mean of the unstimulated control. Time points with a geminin response smaller than a threshold (mean + 2*sd of unstimulated control) were defined as part of the G1-phase, when geminin is not expressed (Figure 9B). Using run-length encoding, the duration of S/G2-phase and the time point of division could be identified. To avoid false positive detection of cell cycle phases, only cells were included in the analysis in which the time between beginning of S-phase and division was at least 4 h. Percent of dividing cells was used to compare effects between different concentrations of EGF or different types of inhibitors. The standard error was calculated with bootstrapping (n = 1,000, R package: boot).

2.3.6 FEATURE ANALYSIS

The time courses were separated into early (less than 16 h after stimulation) and late response (more than 20 h after stimulation). For each signaling phase, the amplitude was defined as the mean of the

three highest FIRE responses after normalization and the time of response as the mean time for the three highest FIRE responses. The fold change was taken with respect to the mean response of FIRE in the same cell before stimulation. The duration was measured as full width at half maximum, limited to the maximum possible observation period. The area under the curve was estimated using a spline interpolation (R package: MESS). To identify responding cells, the amplitude of the first response and the second response was compared to the distribution of the respective amplitude in the control experiment (without EGF).

2.3.7 KAPLAN-MEIER ANALYSIS

The analysis of duration of the S/G2-phase might be affected as cells are not monitored indefinitely and thus, the data was incomplete. This shortcoming was overcome by calculating Kaplan-Meier curves. Kaplan-Meier curves are a way to analyze times-to-event with incomplete data. This type of analysis is commonly used in clinical studies (Bewick et al., 2004) to account for patient drop-outs. In the analysis of S/G2-phase duration, cells which passed into S-phase were characterized in terms of whether they underwent division (event occurrence) in the measured time course or not (censored data). The cumulative events (completion of division) over time were shown (R package: survival, survminer).

2.3.8 IMMUNOFLUORESCENCE

Cells were seeded and treated equally to live-cell microscopy experiments. After a 48-h growth factor and serum deprivation, cells were stimulated with EGF at specific time points to fix all conditions with 2 % paraformaldehyde in PBS simultaneously. After cells were fixed for 10 min at room temperature, the paraformaldehyde was washed away with PBS. Next, cells were permeabilized with 0.1 % Triton X-100 in PBS for 20 min, blocked with 10 % goat serum in PBS for 30 min and incubated with primary antibodies (listed below) in 1 % BSA/PBS for 1 h. Afterwards, cells were washed using 0.1 % Triton X-100 in PBS and incubated with a secondary antibody (listed below) in 1 % BSA/PBS. After further washing steps, cells were stained with 2 mg/ml Hoechst in 0.1 % Triton X-100 in PBS. Cells were washed and subsequently stored in PBS. Images were acquired with the same objective and filter sets as described in 2.3.2. Again, automated segmentation was performed in MATLAB with algorithms from CellProfiler (Carpenter et al., 2006).

Antibody	Dilution
Mouse monoclonal anti-pAKT (Thermo Fisher Scientific)	1:250
Rabbit monoclonal anti-pRB (Cell Signaling Technology)	1:1,600
Goat polyclonal anti-mouse AlexaFluor™ 488 (Thermo Fisher Scientific)	1:1,000
Goat polyclonal anti-rabbit AlexaFluor™ 647 (Thermo Fisher Scientific)	1:1,000

2.3.9 CELL PREPARATION FOR SINGLE-CELL RNA SEQUENCING

For scRNA-seq, 6-cm plates were used with 4.3×10^5 cells per plate and treated equally to the live-cell microscopy experiments. After a 48-h growth factor and serum deprivation, cells were stimulated with EGF at specific time points to trypsinize them simultaneously and adjust the cell number to 5×10^5 cells per condition. Each sample was resuspended in 50 µl BD Stain Buffer and labeled with a specific Sample Tag (10 µl) (both from BD Single-Cell Multiplexing Kit - Human) for 20 min at room temperature. After adding 100 µl BD Stain Buffer, cells were mixed, centrifuged and washed with 500 µl BD Stain Buffer. Using 500 µl RNase free PBS, all cells were pooled in a single tube and counted to ensure a sufficient cell number. After centrifugation and resuspension in 800 µl RNase free PBS, 3.2 ml pre-chilled methanol was added dropwise to the sample while mildly vortexing. Cells were kept on ice for 15 min, mixed, divided into 1 mL aliquots and stored at -80 °C.

2.3.10 REHYDRATION AND LIBRARY PREPARATION FOR SINGLE-CELL RNA SEQUENCING

Rehydration was done at 4 °C; cells were pelleted and washed twice in rehydration buffer (DPBS, 10 % BSA, 0.5 U/ml RNase Inhibitor), then filtered and counted. The 3’ RNA library was prepared according to the Chromium Single Cell 3’ Reagent Kits v3-protocol (CG000183 Rev A) with a targeted cell recovery of 10,000 cells. At step 2.3.d of cDNA cleanup, the supernatant was removed and used for sample tag library preparation according to the BD Single-Cell Multiplexing Kit-Human protocol (Reagent Kit v2). The cDNA library was complemented with 5 % of its corresponding sample tag library to be run in the same sequencing run. Samples were sequenced on an HiSeq 4000 sequencer (Illumina).

Commercial kits used for rehydration and library preparation
Chromium Single Cell 3’ GEM, Library & Gel Bead Kit v3 (10x Genomics)
Chromium Single Cell B Chip Kit (10x Genomics)
Chromium i7 Multiplex Kit (10x Genomics)

2.3.11 SINGLE-CELL RNA SEQUENCING ANALYSIS

Read mapping and counting was done using Cell Ranger version 3.0.2 (10x Genomics) and a dual genome reference consisting of the human genome GRCh38 as supplied by Cell Ranger. Additionally,

an artificial genome containing the BD sequence tags was utilized. Demultiplexing was done using a custom script that reads the BAM file and counts sequences that map to the artificial BD sequence tags genome and removes duplicate UMIs per cell. Subsequently, cells were assigned to samples (or duplets) using the HTODemux() function of Seurat (Stuart et al., 2019) after normalization (as described in the Seurat manual). Transcriptome analysis of the scRNA-seq samples was done using Seurat. In brief, low quality cells were removed based on mitochondrial contamination and number of unique genes. Each gene was normalized by the total expression in the cell, scaled by 10,000 and log-transformed. Cell cycle status was defined using a list of cell cycle markers from Tirosh et al., 2016, as provided by Seurat. For the analysis of the differential gene expression, cells were grouped by experiment, condition and cell cycle phase to generate pseudo-bulk samples. This analysis was done using DESeq2 (Love et al., 2014). To identify the effect of inhibitors on pathway activity, variance-stabilized data as provided by DESeq2 and applied PROGENy were used (Schubert et al., 2018). The differentially expressed genes in the pseudo-bulk samples were further analyzed using GO enrichment (R package: clusterProfiler; (Yu et al., 2012)). The identified GO terms were simplified using a semantic similarity measure, which depends on the frequencies of two GO terms involved and that of their closest common ancestor term (R package: GOSemSim; (Yu et al., 2010)).

3 THE CELL STATE AND SMAD SIGNALING

3.1 RESULTS OF PART 2

After investigating the interplay between the MAPK and PI3K/AKT pathways and their relative contributions to cell cycle entry and progression, I examined how such mitogenic signals affect the SMAD pathway. In general, these networks interact to precisely regulate the switch between dividing and non-dividing cells, thereby enabling tissue repair and regeneration. As SMAD signaling opposes the effects of mitogenic signaling and thus prevents uncontrolled cell divisions, it plays a major role in this regulatory process. To study the crosstalk between the different signaling pathways, I quantified ligand-induced SMAD signaling in quiescent and proliferating MCF10A SMAD2 reporter (S2-R) cells by combining time-resolved single-cell measurements with targeted genetic and pharmacological perturbation as well as computer-aided analyses.

3.1.1 SMAD SIGNALING IN QUIESCENT AND PROLIFERATING CELLS

3.1.1.1 TGFB-MEDIATED SMAD SIGNALING IS ATTENUATED IN QUIESCENT CELLS

To investigate how SMAD signaling is affected by the cell state, I stimulated proliferating and quiescent cells with high doses of TGFB1 (from now on referred to as TGFb) and monitored the translocation of SMAD transcription factor complexes from the cytoplasm to the nucleus by time-lapse microscopy (3.3.12). To follow this translocation in single cells with high temporal and spatial resolution, an established S2-R cell line expressing a YFP-SMAD2 fusion protein as well as histone H2B-CFP as a nuclear marker was used (Strasen et al., 2018). To force the reporter cells into a quiescent state, I withdrew serum and growth factors from the growth-medium for 48 h. Afterwards, the number of cell divisions was determined (3.3.14.1). While cycling cells were dividing approximately once in 24 h, quiescent cells showed nearly no division at all (Figure 18A). By measuring the cell cycle distribution (3.3.16), a clear G0/1 arrest was observed, indicating that a 48-h growth factor deprivation was sufficient to put the reporter cells into quiescence (Figure 18B). After validating the proliferation state, SMAD2 responses were measured using live-cell microscopy and automated image analysis (3.3.14). Over 24 h, images were acquired at regular intervals (6 min) to provide a high temporal resolution. This approach allowed to follow hundreds of cells and measure the H2B-CFP and SMAD2-YFP fluorescence throughout the entire experiment. With the acquired data, median trajectories, reflecting the ratio between nuclear and cytoplasmic SMAD2 (nuc/cyt SMAD2 ratio), were generated. The results revealed that SMAD2 in proliferating cells was predominantly located in the cytoplasm in absence of TGFb and strongly accumulated in the nucleus 1-2 h post stimulation. After the first response, SMAD2 relocalized to the cytoplasm until the nuc/cyt SMAD2 ratio adapted to a lower signaling plateau and

stayed above initial values throughout the experiment (second/sustained response). Interestingly, if quiescent cells were stimulated with the cytokine TGFb, less SMAD2 translocated from the cytoplasm into the nucleus compared to cycling cells (Figure 18C-E). Not only the first response but also the sustained signaling seemed to be strongly attenuated (Figure 18G and H). This effect was validated for endogenous SMAD2 in wild-type MCF10A cells using immunofluorescence (3.3.15) (Figure 18F). Additionally, levels of phosphorylated SMAD2 in wild-type and reporter cells confirmed this phenomenon (3.3.17) (Figure 18I). In essence, the dynamic behavior of SMAD2 switched from a strong and sustained to a weak and transient signaling response by growth factor and serum deprivation.

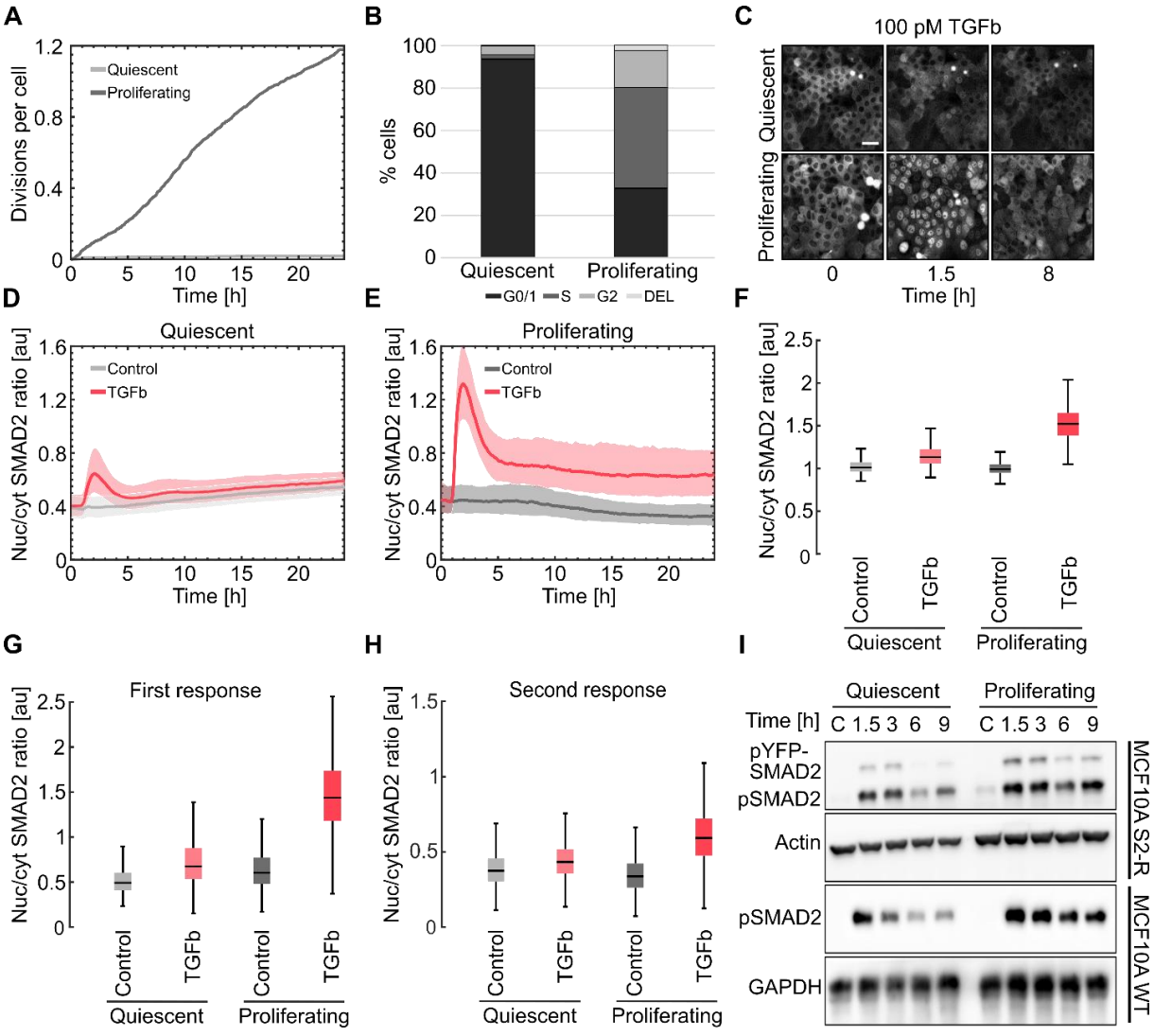

Figure 18: TGFb-mediated SMAD signaling is strongly influenced by the cell state.

(A) Cell proliferation of the S2-R cell line shown as number of cell divisions per cell within 24 h after a 48-h growth factor deprivation (quiescent). To identify mitosis, cells were imaged in live-cell microscopy and the integrated H2B-CFP fluorescence intensity was analyzed. A decrease of ~50 % in intensity indicated a successful cell division. Cells cultured in normal growth-medium (proliferating) served as control. **(B)** Distribution of cell cycle phases of growth factor-deprived and dividing cells. To determine the number of cells in G0/1-, S-, and G2-phase, the cell cycle distribution generated by MetaCyte

was used. DEL represents cells that could not be assigned to a cell cycle phase. **(C)** Live-cell time-lapse images of quiescent and proliferating S2-R cells treated with 100 pM TGFb (3.3.13). Pictures were taken before treatment (0 h) and 1.5 h or 8 h after treatment. Scale: 24 µM. **(D-E)** Analysis of the nuc/cyt SMAD2 ratio upon stimulation with 100 pM TGFb in proliferating **(D)** and quiescent **(E)** cells. Cells were imaged 1 h prior to TGFb stimulation. Solid lines represent median trajectories and shaded areas indicate 25th and 75th percentiles. The number of cells analyzed in time-lapse microscopy experiments is indicated in 6.7 (Appendix). **(F)** Quantification of nuc/cyt SMAD2 ratio 3 h after treatment with 100 pM TGFb in proliferating and quiescent wild-type MCF10A cells using immunofluorescence. The generated boxes include data between the 25th and 75th percentiles. The black line indicates the median and whiskers extend to maximum values within 1.5× the interquartile range. **(G-H)** Single-cell analysis of quiescent and proliferating S2-R cells. The generated boxes include data between the 25th and 75th percentiles. The black line indicates the median and whiskers extend to maximum values within 1.5× the interquartile range. **(G)** Quantification of the highest nuc/cyt SMAD2 ratio within the first 5 h after stimulation with 100 pM TGFb (first response). **(H)** Quantification of the lowest nuc/cyt SMAD2 ratio within 6 h after the first peak (second response). **(I)** Western blot analysis of SMAD2 activation in quiescent and proliferating S2-R or wild-type (WT) MCF10A cells. Cells were stimulated with 100 pM TGFb and SMAD2 phosphorylation was analyzed at indicated time points. Endogenous pSMAD2 with a molecular weight of ~60 kDa and transgenic pYFP-SMAD2 with a molecular weight of ~75 kDa were observed. Actin and glyceraldehyde 3-phosphate dehydrogenase (GAPDH) were used as loading controls.

As several factors like EGF, insulin and horse serum were missing from the quiescence-inducing medium, the question arose which extracellular signals were necessary to form a strong sustained SMAD2 response upon TGFb stimulation. Since EGF is a potent mitogen and capable of re-introducing quiescent cells into the cell cycle (Part 1 of this study), I first added EGF back to the medium and incubated the cells for different periods of time. As shown in Figure 19A, a 6-8 h preincubation with EGF was sufficient to rescue the first response of the TGFb-induced SMAD2 translocation. To test if the attenuation of the signaling response was caused by an altered cell cycle state or changes in mitogenic signaling itself, quiescent cells were treated with the CDK4/6 inhibitor palbociclib to keep cells in a non-dividing state despite the stimulation with EGF (Figure 19B). Interestingly, 8 h of EGF preincubation was still sufficient to rescue SMAD2 dynamics even though cells could not progress through the cell cycle, indicating that rather a loss of mitogenic signaling was responsible for SMAD2 attenuation instead of progression through the cell cycle (Figure 19C). To further validate this observation, I mimicked growth factor deprivation by pharmacologically inhibiting MEK/ERK and PI3K/AKT signaling in proliferating cells for 48 h. Indeed, as shown in Figure 19D, a sustained MEK/ERK, but not PI3K/AKT activity was required for a strong SMAD2 response. These findings suggested a crosstalk of MAPK signaling and the SMAD pathway. Since the rescue of SMAD2 dynamics by EGF took several hours, these interactions might rather be mediated by MEK/ERK target genes instead of a post-translational modification (PTM)-based direct crosstalk of SMAD and MAPK signaling.

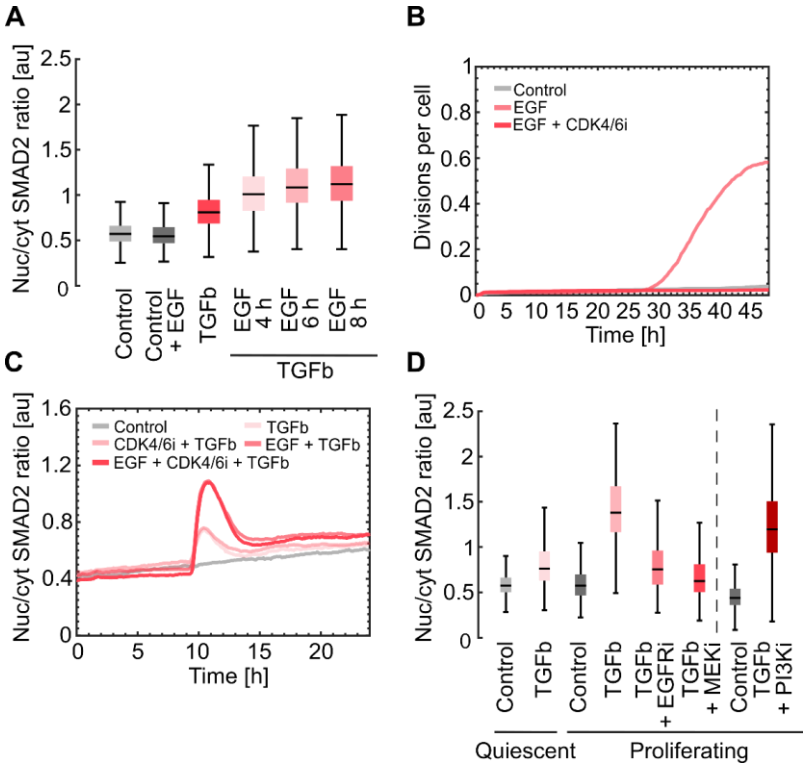

Figure 19: TGFb-mediated SMAD signaling is attenuated if MAPK activity is switched off.

(A) Single-cell analysis of quiescent S2-R cells. Quantification of the highest nuc/cyt SMAD2 ratio after treatment with 50 ng/ml EGF for the indicated duration followed by a stimulation with 100 pM TGFb. The generated boxes include data between the 25th and 75th percentiles. The black line indicates the median and whiskers extend to maximum values within 1.5× the interquartile range. **(B)** Cell proliferation of quiescent MCF10A FIRE reporter cells shown as number of cell divisions per cell within 48 h. Cells were either treated with a CDK4/6 inhibitor (t = 0 h) and 50 ng/ml EGF (t = 1 h) or DMSO (t = 0 h) and EGF (t = 1 h). CDK4/6 inhibitor was used to prevent cell cycle progression despite EGF stimulation. **(C)** Analysis of the nuc/cyt SMAD2 ratio in quiescent cells after modulation by various treatments. Cells were stimulated with EGF and CDK4/6 inhibitor as described in **(B)** followed by a 100 pM TGFb treatment at t = 9 h. Despite the lack of CDK4/6 activity EGF preincubation still rescued the SMAD2 dynamics. **(D)** Single-cell analysis of S2-R cells treated with different inhibitors. Quantification of the highest nuc/cyt SMAD2 ratio within the first 5 h after stimulation with 100 pM TGFb. Proliferating cells were treated with EGFR, MEK or PI3K inhibitors (same inhibitors as in Part 1 of this study) 48 h before treatment with TGFb and compared to quiescent cells. The generated boxes include data between the 25th and 75th percentiles. The black line indicates the median and whiskers extend to maximum values within 1.5× the interquartile range.

3.1.1.2 GDF11-MEDIATED SMAD SIGNALING IS INCREASED IN QUIESCENT CELLS

After uncovering that TGFb-mediated SMAD signaling is attenuated in quiescent cells, I performed a small-scale ligand screening in S2-R cells to determine if the response to other ligands of the TGFb superfamily was dampened as well. Proliferating and quiescent cells were stimulated with different ligands (activin A, GDF3, GDF8 and GDF11) which are known for their activation of SMAD2/3 via the use of alternative receptor complexes. Despite activating the same signaling molecules, the strength

of the first response differed greatly. While TGFb and activin A mediated a strong SMAD2 translocation in proliferating cells, the other ligands, GDF3, GDF8 and GDF11 barely initiated SMAD signaling. Interestingly, GDF8 and GDF11 induced an amplified first response in quiescent cells and thereby showed the opposite effect previously observed for TGFb (Figure 20A). Therefore, the tested ligands could be categorized in three groups: Attenuated in quiescent cells (TGFb), amplified in quiescent cells (GDF8 and GDF11) and unaffected by the cell state (activin A). Since GDF11 revealed a contrasting effect to TGFb and induced the strongest response after growth factor deprivation, I chose GDF11 for further experiments in this study. To compare GDF11- and TGFb-mediated SMAD2 dynamics in more detail, an experiment with different ligand concentrations was performed and the median trajectories of nuc/cyt SMAD2 ratios were determined. Both ligands showed a dose-dependent effect in quiescent and proliferating cells (Figure 20B-E). Interestingly, the first response of GDF11-mediated SMAD signaling was increased upon growth factor deprivation. However, a sustained response as seen in proliferating cells treated with high doses of TGFb could not be detected (Figure 20C and D). While I saw a different dynamical pattern in these two experimental conditions, SMAD2 dynamics in quiescent cells treated with TGFb and proliferating cells stimulated with GDF11 behaved very similarly (Figure 20B and E). After discovering that cells switched from a high sensitivity for TGFb ligands to increased sensitivity for GDF11 ligands upon growth factor deprivation, this phenomenon was verified for endogenous SMAD2 utilizing western blot analysis and immunofluorescence. Again, increased GDF11-mediated SMAD2 activation in quiescent cells was observed (Figure 20F and G). Like in previous experiments (Figure 19D), I investigated if a sustained loss of MAPK activity is responsible for this effect. Indeed, pharmacologically inhibiting MEK and EGFR for 48 h perfectly replicated the effect of the growth factor deprivation on SMAD signaling (Figure 20H). Taken together, quiescent and proliferating cells reacted with differing degrees of sensitivity to ligand stimulations due to an interaction with the MAPK pathway.

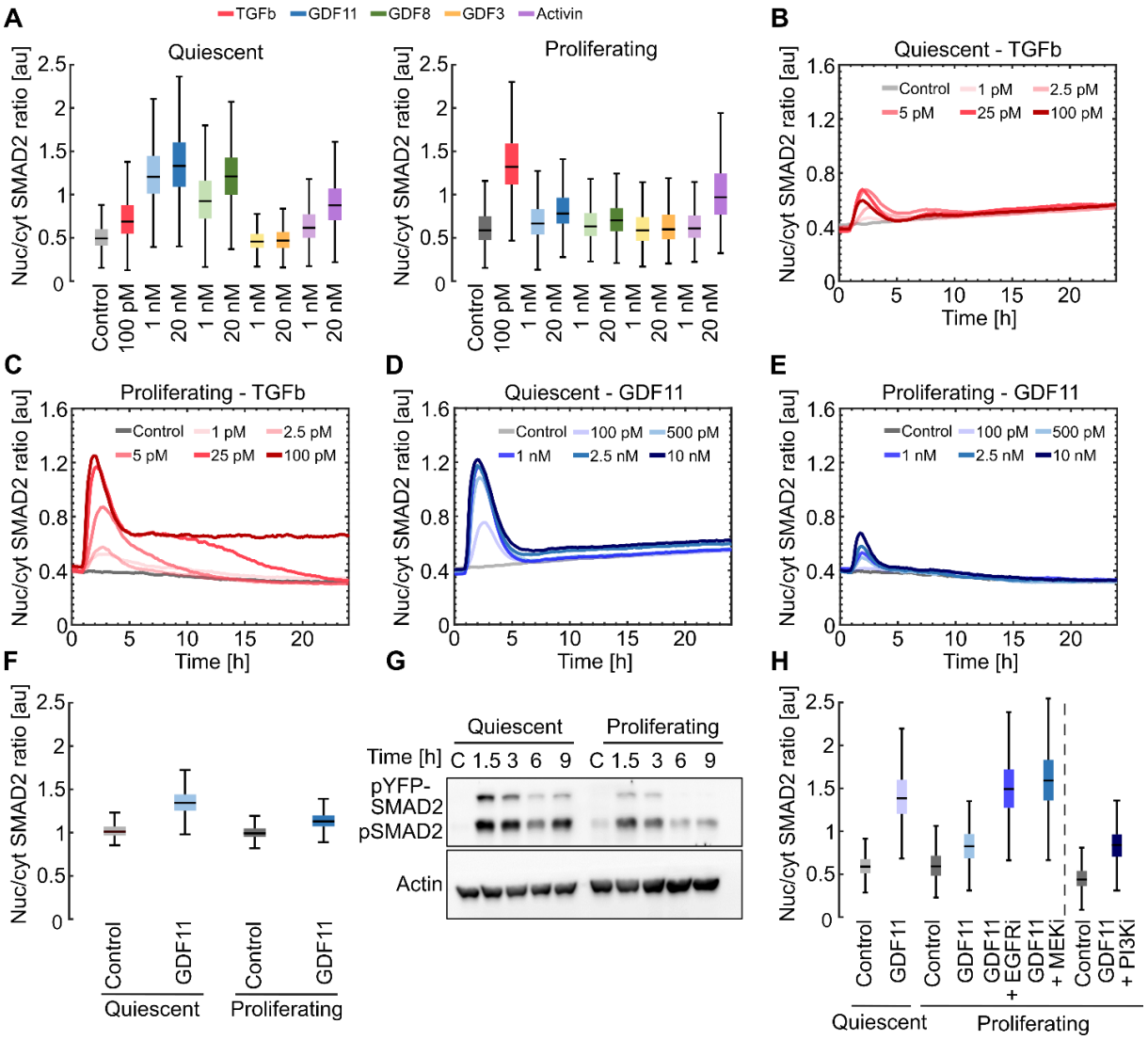

Figure 20: GDF11-mediated SMAD signaling is amplified if MAPK activity is switched off.

(A) Single-cell analysis of S2-R cells stimulated with different ligands of the TGFb superfamily. Quantification of the highest nuc/cyt SMAD2 ratio in quiescent and proliferating cells within the first 5 h. Ligands other than TGFb were used with a concentration of 1 nM and 20 nM. The generated boxes include data between the 25th and 75th percentiles. The black line indicates the median and whiskers extend to maximum values within 1.5× the interquartile range. **(B-C)** Median nuc/cyt SMAD2 ratio of quiescent **(B)** and proliferating **(C)** cells stimulated with varying concentrations of TGFb over 24 h. Cells were imaged 1 h prior to TGFb stimulation. **(D-E)** Median nuc/cyt SMAD2 ratio of quiescent **(D)** and proliferating **(E)** cells stimulated with varying concentrations of GDF11 over 24 h. Cells were imaged 1 h prior to GDF11 stimulation. **(F)** Quantification of nuc/cyt SMAD2 ratio 3 h after treatment with 10 nM GDF11 in proliferating and quiescent wild-type MCF10A cells using immunofluorescence. The generated boxes include data between the 25th and 75th percentiles. The black line indicates the median and whiskers extend to maximum values within 1.5× the interquartile range. **(G)** Western blot analysis of SMAD2 activation in quiescent and proliferating S2-R cells. Cells were stimulated with 10 nM GDF11 and SMAD2 phosphorylation was analyzed at indicated time points. Endogenous pSMAD2 with a molecular weight of ~60 kDa and transgenic pYFP-SMAD2 with a molecular weight of ~75 kDa were observed. Actin was used as a loading control. **(H)** Single-cell analysis of S2-R cells treated with different inhibitors. Quantification of the highest nuc/cyt SMAD2 ratio within the first 5 h after stimulation with 5 nM GDF11. Proliferating cells were treated with EGFR, MEK or PI3K inhibitors 48 h before treatment with GDF11 and

compared to quiescent cells. The generated boxes include data between the 25th and 75th percentiles. The black line indicates the median and whiskers extend to maximum values within 1.5× the interquartile range.

3.1.1.3 LACK OF MAPK ACTIVITY INDUCES REWIRING OF THE SMAD NETWORK

The obtained results showed that, depending on the activity of MAPK, ligands from the TGFb superfamily can signal very differently in quiescent and proliferating cells. A long-term MEK/ERK activity was required for strong and sustained SMAD signaling induced by TGFb, whereas for GDF11 it was the reverse effect, as a sustained lack of MEK/ERK activity substantially increased the strength of the signaling. A comprehensive understanding of the crosstalk between the two signaling networks would be necessary to decode possible interaction points. As previous experiments suggested that the SMAD network was rewired on a slow time scale of several hours to switch ligand sensitivity a direct interaction of MEK/ERK with the SMAD pathway seemed unlikely. Instead, I assumed that the rewiring was mediated through changes of target genes. Therefore, gene expression in proliferating and quiescent cells was analyzed at a genome-wide level by RNA sequencing (3.3.20). Since growth factor deprivation changes the physiological condition of a given cell, the expression of a great number of genes is expected to change with the cell state. To narrow down potential key players of this rewiring, I used all information gathered from previous experiments. For example, it was shown that a 48-h MEK inhibition had the same effect on SMAD signaling as a 48-h growth factor deprivation and that restimulation of quiescent cells with EGF was sufficient to rescue TGFb-mediated SMAD2 activation. Thus, not only mRNAs from proliferating and quiescent cells were sequenced but also multiple control conditions like proliferating cells treated with a MEK inhibitor for 48 h, quiescent cells stimulated with EGF for 8 h or quiescent cells treated with a MEK inhibitor and EGF for 8 h. This limited the number of potential candidates responsible for the ligand sensitivity switch, as now the genes had to fulfill the following criteria: upregulated expression in non-dividing conditions (quiescent cells, MEK inhibitor-treated cells and MEK inhibitor- and EGF-treated cells) and downregulated expression in dividing conditions (proliferating cells and EGF rescue cells) or vice versa. To apply this approach to all analyzed genes, first the RPKM values for each condition were calculated (3.3.20). Then, a two-step filter system was applied. First, the gene had to exhibit a fold change of at least 1.5 between proliferating and quiescent cells. Second, if growth factor deprivation negatively regulated the gene, the lowest RPKM value of the dividing conditions and the highest RPKM value of the non-dividing conditions were compared and had to exhibit a fold change of at least 1.5. If the gene was positively regulated in growth factor-deprived cells, the highest RPKM value of the dividing conditions was compared to the lowest RPKM value of the non-dividing conditions (Figure 21A). With this approach, the list of 13,251 differentially expressed genes was narrowed down to 1,900 genes that fulfilled all

criteria. To further limit the number of possible candidates, a list of SMAD pathway-associated genes was composed using different database resources (6.6) and compared with the filtered genes of the RNA sequencing (Figure 21B). Finally, a set of 63 genes was identified, which were differentially regulated and associated with SMAD signaling (Figure 21C). From this list, ten examples were selected and illustrated. As can be seen in Figure 21D, even after a rigorous selection procedure, there were still many genes that fitted perfectly in the filtering pattern. The multitude of suitable candidates suggested that a pathway-rewiring, in which many SMAD-associated genes were modulated, could be responsible for switching the ligand sensitivity. Thus, instead of modifying one key player, it might require orchestrated gene expression changes. Nonetheless, the genes of the final list were researched, and interesting candidates were determined.

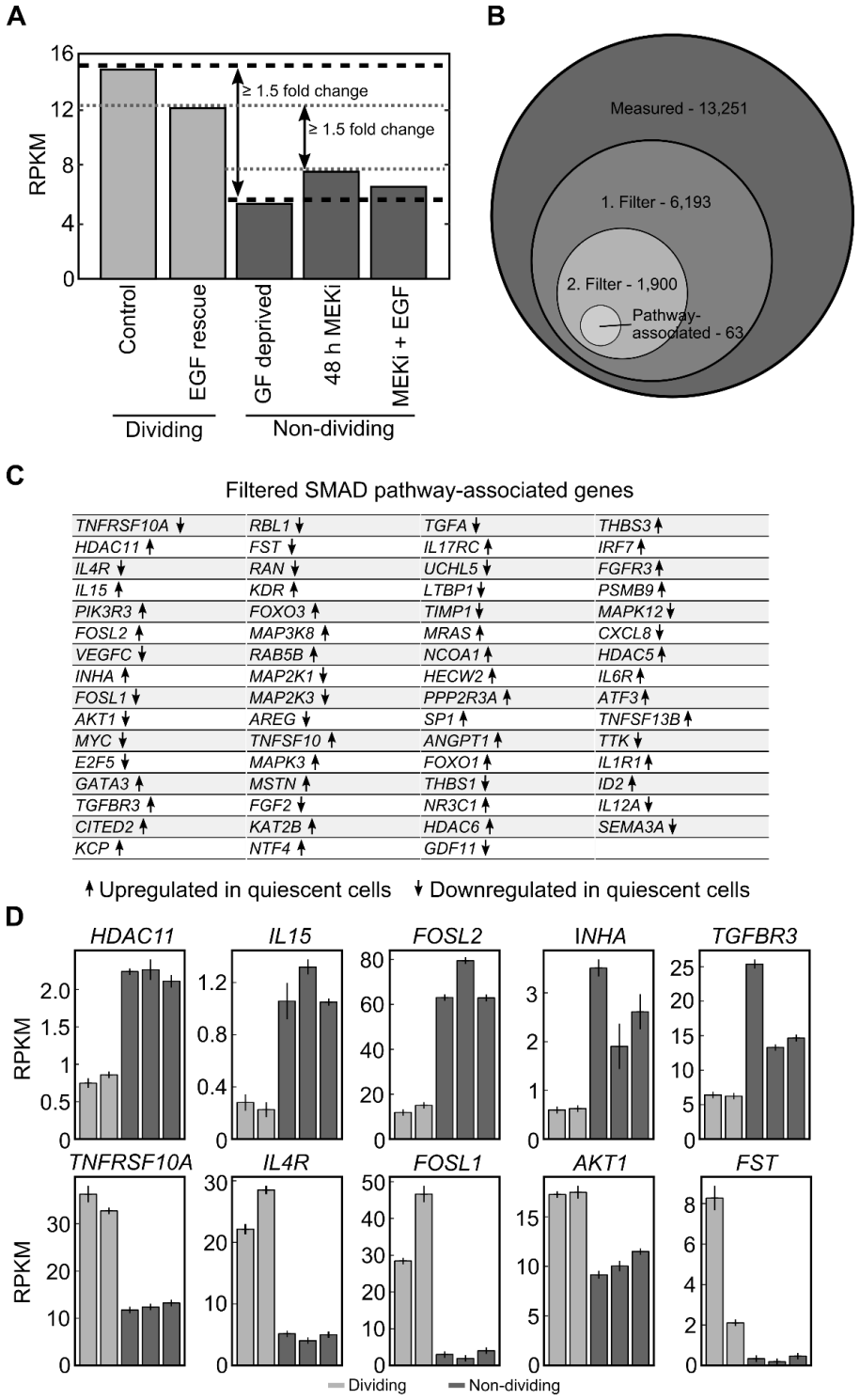

Figure 21: Global gene expression analysis identified potential key regulators of SMAD signaling.

The analysis was performed in close collaboration with Lorenz Ripka (IMB Mainz). **(A)** Schematic representation of how gene filtering was applied to identify key players. First, proliferating (control) cells were compared to growth factor-deprived cells to determine if the gene is up- or downregulated. The fold change had to be at least 1.5. Next, if the gene was downregulated, the lowest RPKM value of the dividing conditions and the highest RPKM value of the non-dividing conditions were compared. Again, the fold change had to be at least 1.5. If the gene was upregulated in growth factor-deprived cells, the highest RPKM value of the dividing conditions was compared to the lowest RPKM value of the non-dividing conditions.

(B) Scaled Venn diagram showing the number of genes after each filtering step. **(C)** List of filtered genes which could be associated with the SMAD pathway. Arrows indicating if the gene was up- or downregulated upon growth factor deprivation. **(D)** Examples of genes listed in **(C)** shown as bar graphs. Order of the conditions (x-axis) as shown in **(A)**.

3.1.1.4 GENERATING A *FST* KNOCKOUT AND *TGFBR3* OVEREXPRESSION CELL LINE

Literature research uncovered that FST is a known antagonist of GDF11 (Gamer et al., 1999) but not TGFb signaling. Thereby, the downregulation of *FST* in quiescent cells (Figure 21D) could potentially explain the increase in GDF11-mediated SMAD signaling as previously observed. Additionally, references were found, which showed that TGFBR3 negatively influences TGFb-mediated signaling through ectodomain shedding. In short, cells can release soluble TGFBR3 which binds and sequesters ligands to inhibit TGFb signaling (Elderbroom et al., 2014). Furthermore, *TGFBR3* is reported to co-vary with *GDF11* (Wang et al., 2014) and enhance GDF11-mediated SMAD2 activation (Bajikar et al., 2017). Taken together, both proteins might have the potential to change SMAD signaling and explain the observed differences in quiescent and proliferating cells.

To further validate the hypothesis of FST as a key player, I investigated GDF11 signaling in proliferating U-2 OS and HEK293T cells by western blot analysis. These cell lines were chosen because both express the corresponding receptors but only U-2 OS cells produce FST. Therefore, it was expected that GDF11-mediated SMAD signaling is stronger in HEK293T cells. Indeed, HEK293T cells showed comparatively high quantities of phosphorylated SMAD2 upon treatment with 4 nM GDF11 (Figure 22A). To ensure that FST is responsible for the observed differences, the next step was to introduce FST into HEK293T cells. To this end, cells were transfected with a plasmid expressing *FST* under the control of the constitutive CMV promotor as well as a hygromycin B resistance gene (pCMV3-FST). After cells were selected for two weeks, RT-qPCR was performed to quantify *FST* mRNA levels (3.3.19). As shown in Figure 22B, the transfection was successful and HEK293T cells were expressing the GDF11 antagonist. Again, western blot analysis of pSMAD2 was carried out and revealed that *FST* overexpression almost completely abolished GDF11 signaling, which further strengthened my hypothesis (Figure 22C). However, it should be kept in mind that different cell lines were compared that vary from one another in many ways.

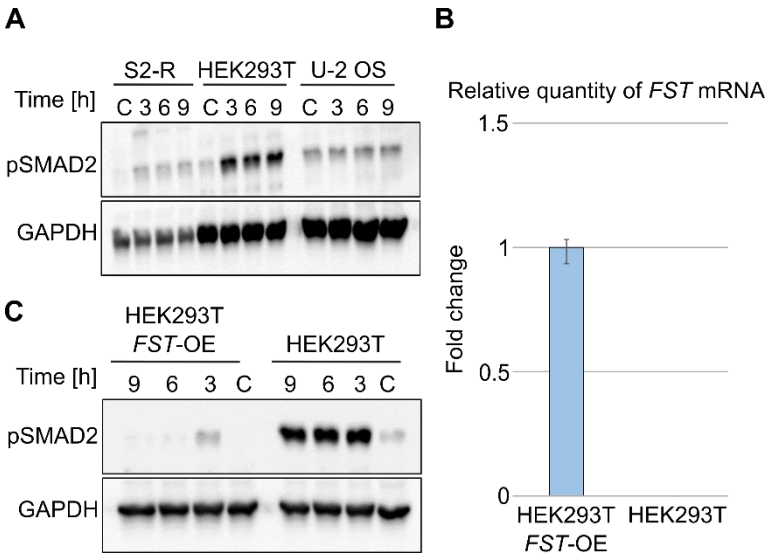

Figure 22: GDF11-mediated SMAD signaling could be attenuated by *FST* overexpression in HEK293T cells.

(A) Western blot analysis of SMAD2 activation in proliferating S2-R, U-2 OS and HEK293T cells. Cells were stimulated with 4 nM GDF11 and SMAD2 phosphorylation was analyzed at indicated time points. Endogenous pSMAD2 with a molecular weight of ~60 kDa was observed. GAPDH was used as a loading control. **(B)** Quantification of *FST* mRNA in HEK293T cells stably expressing transgenic *FST* (HEK293T *FST*-OE) by RT-qPCR. Wild-type HEK293T cells served as a control. Actin was used as an internal control. Error bars indicate standard deviation of technical triplicates. **(C)** Western blot analysis of SMAD2 activation in wild-type HEK293T and *FST* overexpression cells. Cells were stimulated with 4 nM GDF11 and SMAD2 phosphorylation was analyzed at indicated time points. Endogenous pSMAD2 with a molecular weight of ~60 kDa was observed. GAPDH was used as a loading control.

To investigate the role of FST in MCF10A cells, a stable *FST* knockout in the S2-R cell line was created utilizing the clustered regularly interspaced short palindromic repeats (CRISPR)/CRISPR-associated 9 (Cas9) system (3.3.2). The knockout of *FST* has to affect both alleles of the gene to ensure a complete loss of the corresponding protein. To this end, a template DNA, for inserting a blasticidin resistance with a constitutive simian virus 40 (SV40) promoter (SV40-Blast_R) and a plasmid expressing a single guide RNA (sgRNA) were cloned and transfected together with a plasmid expressing a Cas9 endonuclease into S2-R cells. SV40-Blast_R was inserted into the gene locus (exon 2) near the start codon to disrupt the gene as early as possible (Figure 23A). After transfection, cells were selected with blasticidin for up to three weeks and single colonies were picked to generate clonal cell lines (3.3.3). To ensure that the interrupted *FST* sequence led to a non-functional protein, western blot analysis was performed (Figure 23B). All clones without detectable FST (1, 9, 10, 21, 25, 26 and 28) were identified and then screened with PCR to check if the blasticidin resistance was inserted in one (heterozygous) or both (homozygous) alleles. Clones 1, 10 and 26 were heterozygous while clone 21 showed the correct band sizes for a homozygous insertion (Figure 23C). Sequencing of clone 1 and 26 (6.5) revealed a deletion after the Cas9 endonuclease cleavage site, explaining the complete loss of FST protein in

western blot analysis. Additionally, little to no *FST* mRNA was detected in RT-qPCR for clone 1, 21 and 26 (Figure 23D). In the end, these three candidates fulfilled all criteria for a defined knockout of the *FST* gene and were suitable for subsequent live-cell microscopy experiments.

Besides FST, TGFBR3 emerged as potential key player for the switch in ligand sensitivity. For the overexpression of *TGFBR3* in proliferating cells, the approach from Konermann et al., 2015, was followed where instead of a functional Cas9 a dead Cas9 (dCas9) fused to the transcription activation domain VP64 was used (3.3.4). With the help of a specific sgRNA, this complex was guided to the endogenous locus of *TGFBR3* (within 200 bp upstream of the transcriptional start site (TSS)) and initiated the upregulation of the receptor expression. For a stronger overexpression, the activation efficiency could be further improved by adding additional activation domains (p65 and HSF1) which bind to the scaffold of the sgRNA via specific aptamers and RNA binding domains, respectively (Figure 23E). Since the goal was to mimic growth factor deprivation, I aimed to raise the TGFBR3 level to the same amount observed in quiescent cells. First, both overexpression approaches were tested in wild-type MCF10A cells. To this end, two stable cell lines were created by lentiviral transduction, one expressing only dCas9-VP64 and the other additionally expressing the MS2-p65-HSF1 transcriptional activator. As a negative control, an sgRNA targeting the *ACVR2B* instead of the *TGFBR3* locus was used. The western blot analysis revealed that the overexpression of *TGFBR3* was successful and the transcriptional activation with VP64 alone was sufficient to raise the TGFBR3 level to the same amount observed in quiescent cells. Therefore, S2-R cells were only transduced with the lentiviral vector lentiSAMv2, containing sgRNA and dCas9-VP64 complex. As shown in the western blot analysis, the TGFBR3 level had more than doubled upon transduction and again reached values similar to those observed in quiescent cells (Figure 23F). Besides the two single perturbations, I wanted to investigate combinatory effects as well. To this end, the overexpression of *TGFBR3* was also carried out in *FST* knockout cells. Finally, the different cell lines were used for time-lapse microscopy.

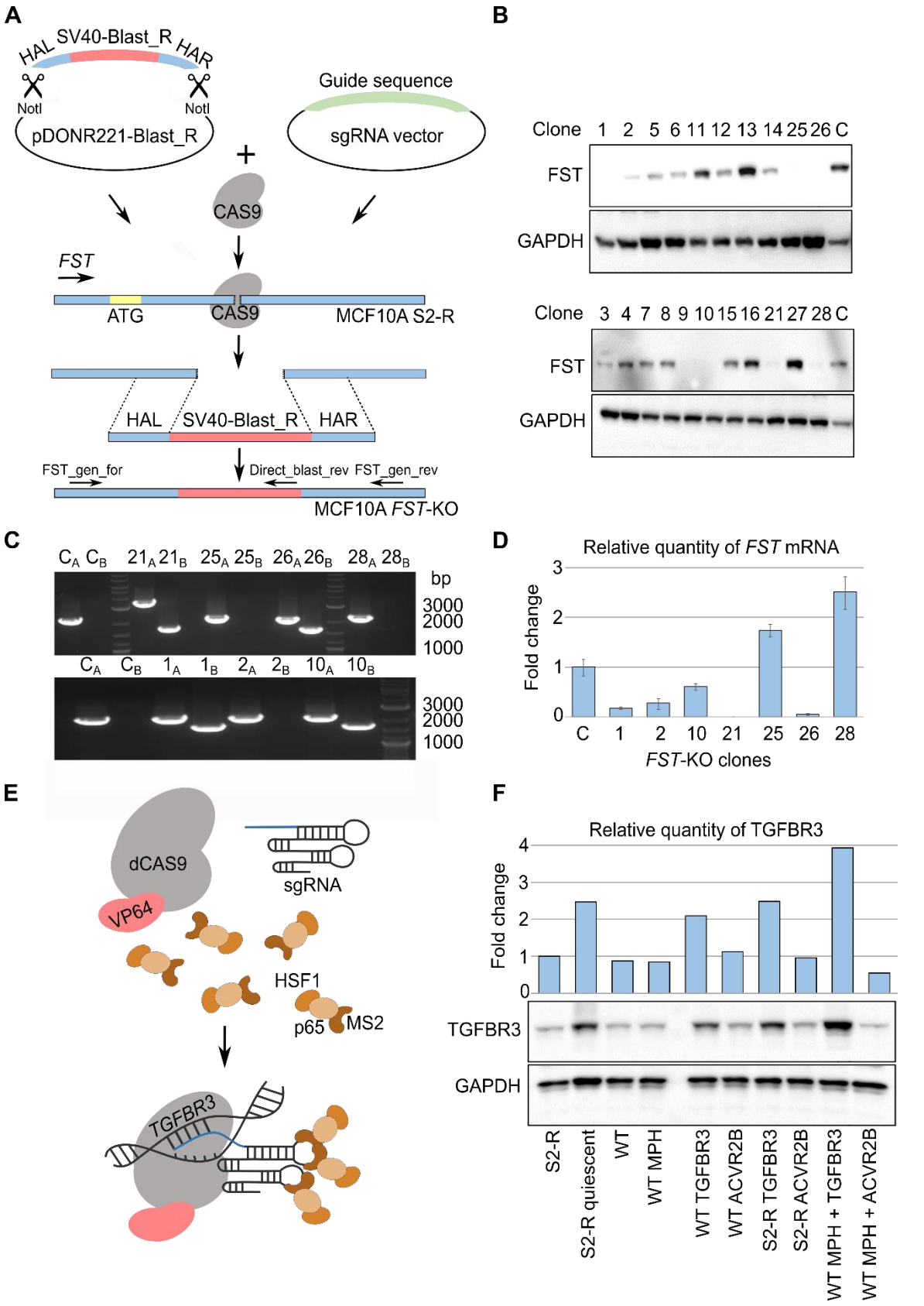

Figure 23: Knockout of *FST* and overexpression of *TGFBR3* were successfully introduced into S2-R cells.

(A) Schematic representation of the CRISPR/Cas9 knockout of *FST*. To generate the vector containing the repair template, homology arms were amplified from genomic DNA of MCF10A and the SV40-Blast_R sequence was amplified from the vector

pVE10 (6.4). Through overlapping ends and assembly cloning (3.3.7), the sequences were joined together. The vector pDONR221-Blast_R (6.4) was then cut with the restriction enzyme NotI, releasing the donor DNA from the backbone. Afterwards, the linearized donor DNA, vectors encoding Cas9 endonuclease and the sgRNA were transfected into S2-R cells. In the presence of a repair template, the Cas9-induced double-strand breaks (DSB) could be repaired precisely by homology-directed repair (HDR), resulting in the desired knock-in of SV40-Blast_R into the *FST* locus. Interrupting the gene close to the start codon will result in a non-functional protein or the protein will not be translated at all. **(B)** Western blot analysis of different knock-in clones and S2-R cells (control). FST bands with a molecular weight of ~65 kDa were observed in S2-R cells and multiple knock-in clones. FST was not detectable in clone 1, 9, 10, 21, 25, 26 and 28. GAPDH with a molecular weight of ~37 kDa served as loading control. **(C)** PCR products of potential *FST* knockout clones. Agarose gels showing the DNA fragments produced by PCR amplification. The primers FST_gen forward and reverse (marked in **(A)**) were utilized to amplify the genomic region containing the Cas9 endonuclease site (first band X_A). If the donor DNA was inserted into the *FST* locus, the PCR amplification generated one fragment (3.4 kbp) for homozygous and two fragments (3.4 kbp + 2.2 kbp) for heterozygous genotypes. The primers FST_gen forward and Direct_blast reverse (marked in **(A)**) were utilized to amplify a part of the inserted blasticidin (second band X_B). Upon successful integration of the donor DNA, the PCR amplification generated a fragment of 1.7 kbp size. Genomic DNA of S2-R cells served as a control. DNA Ladder 1 kb Plus (New England BioLabs) was used as a marker. **(D)** Quantification of *FST* expression after blasticidin knock-in by RT-qPCR. S2-R cells served as a control. Actin was used as an internal control. Error bars indicate standard deviation of technical triplicates. **(E)** Schematic representation of the transcriptional activation through dCas9 (modified after Konermann et al., 2015). The dCas9 is fused to the activation domain VP64 and can be guided to the TSS of the target gene by sgRNAs. The additional activation domains p65 and HSF1 can bind to the MS2-binding loop in the sgRNA backbone to further increase transcriptional upregulation. **(F)** Western blot analysis of TGFBR3 after transcriptional activation in wild-type MCF10A and S2-R cells. Utilizing a lentiviral system, cells were either transduced only with the dCas9-VP64-sgRNA vector (lentiSAMv2) or with lentiSAMv2 and the additional activation domains p65 and HSF1 (lentiMPHv2). Besides an sgRNA targeting the *TGFBR3* locus, an sgRNA targeting the *ACVR2B* locus was used as a control. TGFBR3 bands with a molecular weight of ~110 kDa were observed. GAPDH was used as a loading control. Quantification of densitometric band intensities with ImageJ shows a similar receptor level between quiescent cells and proliferating cells transduced with the lentiSAMv2-TGFBR3 vector. To control for technical variability target protein signals were normalized to the loading control.

3.1.1.5 PERTURBATIONS OF *FST* AND *TGFBR3* ARE NOT SUFFICIENT TO EMULATE GROWTH FACTOR DEPRIVATION

After generating the three different cell lines S2-R-*FST*$^{-/-}$, -*TGFBR3*-OE and -*FST*$^{-/-}$-*TGFBR3*-OE, I investigated SMAD2 dynamics to determine if the single or combined perturbations have the same effect on the signaling pathway as a 48-h growth factor deprivation. To this end, cells were stimulated with TGFb or GDF11 and imaged using time-lapse microscopy. Additionally, the impact of transcriptional feedbacks on SMAD dynamics was tested in S2-R and *FST* knockout cells by utilizing the transcription inhibitor 5,6-dichlorobenzimidazole 1-β-D-ribofuranoside (DRB). Afterwards, I determined the nuc/cyt SMAD2 ratio and compared the effect sizes (differences of medians) of the perturbations and the growth factor deprivation (Figure 24A). As previously observed, GDF11-mediated SMAD signaling was amplified while TGFb-mediated SMAD signaling was attenuated

in quiescent cells. Surprisingly, the perturbations had only minor effects on SMAD signaling. In contrast to my expectations, the knockout of *FST* and the overexpression of *TGFBR3* did not enhance GDF11-mediated SMAD signaling. Only the treatment with DRB slightly increased SMAD2 activation. Since DRB has toxic effects, cells treated with the transcription inhibitor could only be followed for 6 h instead of 24 h. In cells stimulated with TGFb, a slight attenuation of the signaling was observed after overexpressing *TGFBR3*. Furthermore, the DRB treatment showed an amplification of the TGFb signaling (Figure 24A). As I was looking for potential key players that could explain the switch in ligand sensitivity, only DRB treatment in GDF11-stimulated cells and *TGFBR3* overexpression in TGFb-treated cells changed SMAD signaling in the desired direction (Figure 24B and C). To investigate whether the observed effects were significant, I performed permutation testing and determined the confidence intervals of the effect sizes over time (Figure 24D and E). Even though the perturbations altered the signaling output statistically significantly, the extent of the effects caused by growth factor deprivation could not be emulated, suggesting that either another key protein or a complete network rewiring was responsible. However, since a change of over 60 genes involved in SMAD signaling was observed in the RNA sequencing and the single/dual perturbation of *FST* and *TGFBR3* had only minor effects, a complete pathway-rewiring seemed more likely. In addition, a single protein would not only have to increase GDF11-mediated signaling but also decrease TGFb-mediated signaling at the same time. To summarize, the *FST* knockout and the *TGFBR3* overexpression in S2-R cells were successful, however, SMAD2 translocation was only slightly affected by these modifications, although both proteins are direct regulators of the pathway. Therefore, my results indicated that SMAD signaling is very robust against single perturbations and that a more wide-ranging rewiring of the network is necessary to alter dynamics to the extent of a growth factor deprivation. Nonetheless, it should be noted that only two gene perturbations were tested and the hypothesis of a key player regulating this phenomenon could not be rejected.

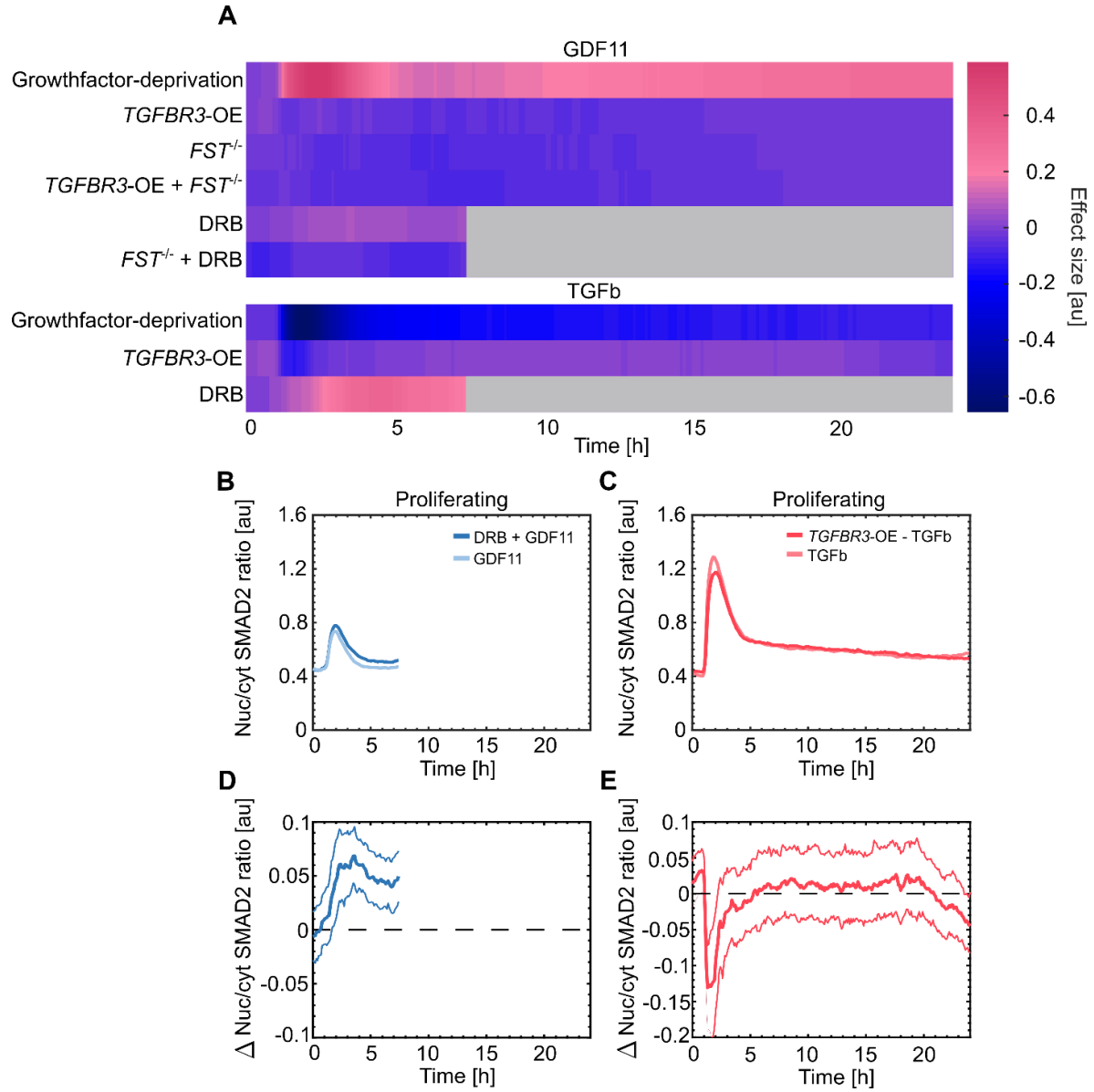

Figure 24: Single and combined perturbations changed SMAD2 signaling dynamics only slightly.

(A) Heatmap showing the effect sizes of different perturbations on SMAD2 translocation over time upon TGFb and GDF11 stimulation. Cells were imaged in live-cell microscopy for 24 h and stimulated with 100 pM TGFb or 10 nM GDF11. Cells were imaged 1 h prior to ligand stimulation. Cells treated with DRB were only tracked for 6 h instead of 24 h. Each vertical line represents one time point, and the effect sizes (differences of medians) are shown as indicated in the legend. Effect sizes represent the magnitude of the experimental effect. **(B)** Median nuc/cyt SMAD2 ratio of proliferating S2-R cells treated with 100 µM DRB and 10 nM GDF11 or 10 nM GDF11 alone over 6 h. **(C)** Median nuc/cyt SMAD2 ratio of proliferating S2-R-*TGFBR3*-OE cells and S2-R cells treated with 100 pM TGFb over 24 h. **(D-E)** Effect size (bold line) and 95 % confidence intervals (thin lines) are shown for the experiments described in **(B-C)**. To estimate the confidence intervals, permutation testing (1,000 permutations) was performed.

3.1.2 SMAD-MEDIATED CELL FATES IN QUIESCENT AND PROLIFERATING CELLS

After revealing that MCF10A cells adjust their sensitivity for ligands of the TGFb superfamily according to the proliferation state, the question has been raised whether different ligands also have different consequences for the physiological response of the cell. Ligands of the TGFb superfamily regulate cell fate decisions during embryogenesis and in the adult organism. Cellular responses like apoptosis, cell cycle arrest and EMT are often associated with SMAD signaling. However, it is poorly understood how the simple and straight forward pathway can determine such a broad range of cell fate decisions. Additionally, it has yet to be answered whether and how the pathway differentiates between varying ligands. I hypothesized that SMAD signaling is rather quantitative than qualitative and that ligands can only be distinguished by SMAD dynamics they initiate.

3.1.2.1 DYNAMICS OF SMAD2 CORRELATE WITH CELLULAR RESPONSES

To investigate cellular outcomes and correlate them with SMAD2 dynamics, long-term stimulations were carried out. Since phenotypic changes are often governed by complex gene regulatory programs and can take several days to develop (Katakura et al., 1999; Zhang et al., 2014; Peixoto et al., 2019), I imaged proliferating and quiescent S2-R cells for up to 120 h in live-cell microscopy. By using high and low concentrations of GDF11 and TGFb, a strong and weak SMAD2 activation for each ligand was achieved. To ensure sustained ligand stimulations, every 48 h the medium was replaced with freshly prepared medium containing GDF11 or TGFb. As shown in Figure 25B, stimulation with 250 pM TGFb caused a strong and sustained SMAD2 response over 120 h, while treatment with 5 pM TGFb initiated a transient response in proliferating cells. Expectedly, for both GDF11 concentrations only minor activation of the signaling pathway was observed. In quiescent cells, responsiveness was reversed resulting in strong GDF11-mediated signaling and weak TGFb-mediated signaling (Figure 25A). After determining the dynamics of SMAD2, the next step was to associate them with phenotypic changes. To this end, cell divisions, motility and cell death were quantified and investigated. One of the first and most striking observations was the increase of dying cells in the quiescent condition treated with GDF11. Usually, only a small fraction of cells died during a 120-h microscopy experiment, however, if stimulated with high doses GDF11, more than 60 % of the cells died (Figure 25C). The same effect, but to a lesser extent, was observed for cells treated with low GDF11 and high TGFb concentrations. Interestingly, the phenomenon was not seen in proliferating cells. In order to further characterize the observed cell death and ensure that cells underwent apoptosis and not necrosis, a western blot analysis of cleaved caspase 7 was carried out. Similar to the live-cell microscopy experiment, cells were

growth factor deprived and stimulated with GDF11 or TGFb. To make sure that all dead cells were included in the analysis, the supernatant was centrifuged and lysed as well. Measuring the amount of cleaved caspase 7 showed that indeed cells underwent apoptosis and that GDF11 treatment had the biggest effect on cell death (Figure 25E). Judging from this experiment alone, the amount of ligand and strength of the signaling seemed to be more decisive than the type of ligand. After characterizing apoptosis, the motility of the cells was analyzed as an increase in movement can be an indicator for EMT (Lamouille and Derynck, 2007). By calculating the motility score (3.3.14.2), I observed an increase for all stimulated cells except for the condition with 100 pM GDF11. Again, the cellular response showed a high correlation with SMAD2 dynamics, as a stronger pathway activation led to more cell movement (Figure 25D). However, this time, the phenotypic changes were only apparent in proliferating cells and not in quiescent cells. One possible reason could be that cells that experienced higher SMAD2 activation underwent apoptosis before exhibiting signs of EMT. To further characterize the increase in motility, I analyzed known biomarkers for EMT such as *SNAI1*, *VIM* and *CDH1* (Zeisberg and Neilson, 2009) by RT-qPCR. All three genes were considerably up- or downregulated if cells were treated with TGFb for a long period of time, indicating that indeed EMT led to increased levels of motility. GDF11-treated cells showed only minor changes in gene expression, which explains the moderate increase in cell motion (Figure 25F). As now two out of three cell fates were observed, I measured the number of cell divisions over time to look for evidence of cytostasis. Interestingly, only the condition with a high TGFb stimulation displayed a decrease in cell division rate, suggesting that strong and sustained SMAD2 activation is necessary to trigger this outcome (Figure 25D). However, it should be noted that cells did not completely stop dividing but rather slowed down cell cycle progression. One potential explanation could be the decrease of *MYC* in TGFb-treated cells (Figure 25F), as MYC promotes the cell cycle by inducing cyclins and CDKs (García-Gutiérrez et al., 2019). Ultimately, I was able to quantify all three phenotypic changes in MCF10A cells by performing long-term ligand stimulations with TGFb and GDF11.

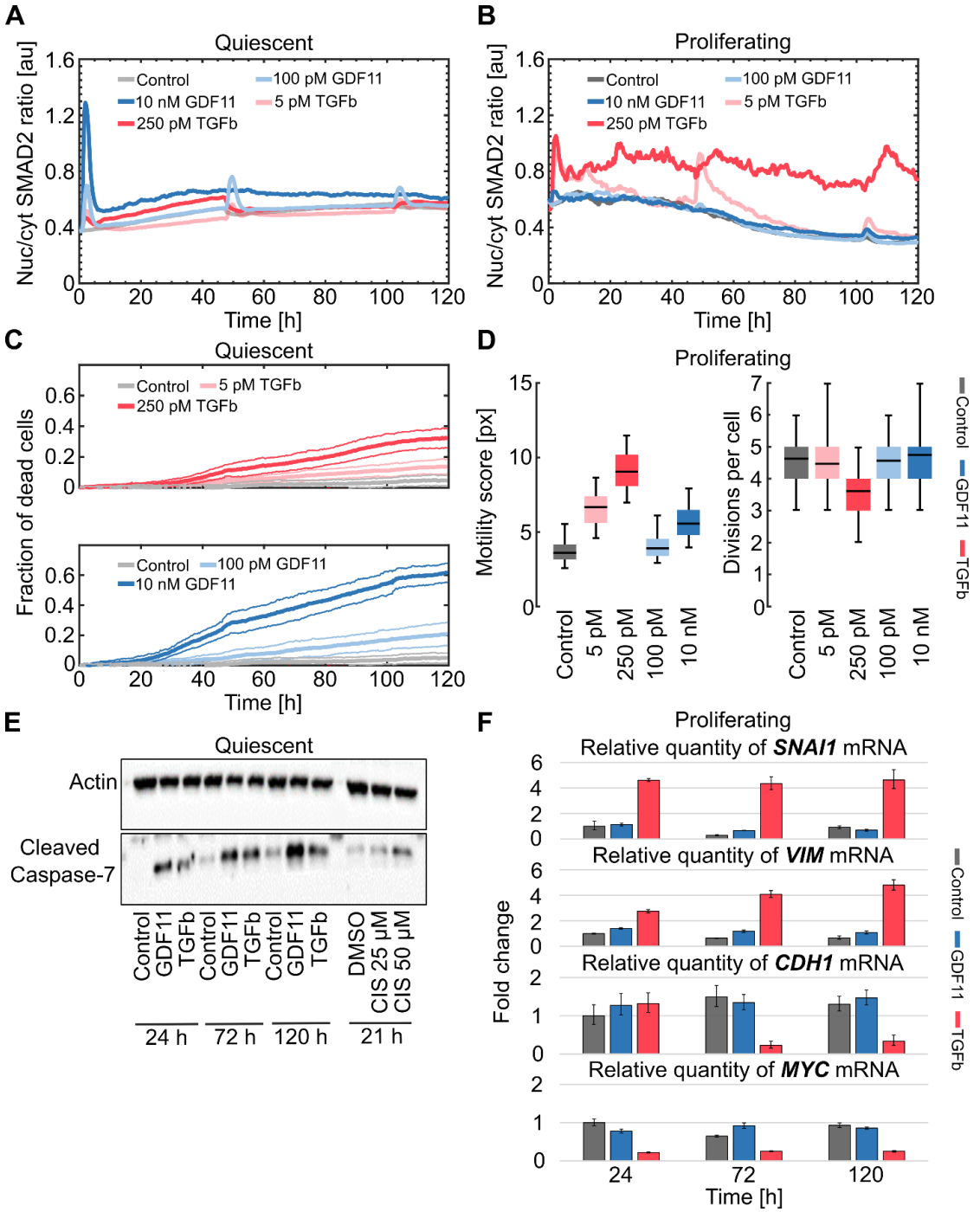

Figure 25: Long-term stimulation and associated cellular responses correlated with SMAD2 dynamics.

(A-B) Median nuc/cyt SMAD2 ratio of quiescent **(A)** and proliferating **(B)** S2-R cells treated with different GDF11 or TGFb concentrations over 120 h. Cells were imaged 1 h prior to ligand stimulation. Every 48 h, medium was exchanged with fresh medium containing respective ligand concentrations. **(C)** Fraction of quiescent cells that died during the 120-h experiment. A dead cell was identified in cell tracks by measuring the diameter of the nucleus. If a nucleus was fragmented during apoptosis and the diameter of the nucleus fell below a certain threshold, it was determined as a dying cell. The data of two biological replicates was used. Bold line represents the median fraction of dead cells and the thin lines represent the standard deviation. **(D)** Movement and cell divisions over time in proliferating cells. Mean distance moved per cell in a fixed time interval (20 min) is shown in the first boxplot. Motility score is shown in pixels (0.24 µm/pixel). Number of cell divisions for each cell over time

was calculated and shown in the second boxplot. The data of two biological replicates was used. The generated boxes include data between the 25th and 75th percentiles. The black line indicates the mean and whiskers extend to maximum values within 1.5× the interquartile range. **(E)** Western blot analysis of cleaved caspase 7 in quiescent S2-R cells. Cells were stimulated with 5 nM GDF11 or 250 pM TGFb for 24 h, 72 h and 120 h. Cleaved caspase 7 bands with a molecular weight of ~20 kDa were observed. Cells treated with cisplatin (25 µM or 50 µM) served as positive control. Actin was used as a loading control. **(F)** Quantification of *SNAI1*, *VIM*, *CDH1* and *MYC* mRNA by RT-qPCR. The RNA for the cDNA synthesis was isolated from proliferating S2-R cells stimulated with 5 nM GDF11 or 250 pM TGFb for 24 h, 72 h and 120 h. Actin was used as an internal control. Error bars indicate standard deviation of technical triplicates.

To further investigate the hypothesis that the strength of the signaling is the most important factor for the cellular outcome, single-cell analyses of the long-term experiments were carried out next. To this end, the area under the curve (AUC) of the nuc/cyt SMAD2 ratio for each individual cell was determined. Afterwards, AUCs were associated with cellular responses like motility and cell divisions. As shown in Figure 26A and B, the AUC correlated well with the cell movement. Cells with a higher AUC also covered more distance over 120 h. For instance, TGFb-treated cells displayed high motility and high AUCs, whereas GDF11-treated cells showed only minor increases. Regarding cell divisions, again a correlation with the signaling strength was observed. For example, it could be shown that, without considering the different treatments, the cells with the 400 highest AUCs were dividing less frequently than the cells with the 400 lowest AUCs (Figure 26C). These results hinted once more at dynamic-dependent, rather than ligand-dependent cell fates as TGFb- and GDF11-treated cells were represented in both, the high and low AUC group. However, it should be noted that only a small fraction of TGFb- and GDF11-treated cells were among the 400 lowest and highest AUCs, respectively (Figure 26D). Since in dividing cells the response to GDF11 is much lower compared to the response to TGFb, this distribution was to be expected. To perform a statistically significant analysis, the number of GDF11-treated cells in the high AUC group and the number of TGFb-treated cells in the low AUC group would have to be increased. As none of the three SMAD-associated cell fates were observed in both proliferation states, it was also not possible to compare quiescent cells showing a strong response to GDF11 with proliferating cells showing a strong response to TGFb. Therefore, it was considered that the analysis of global gene expression in quiescent and proliferating cells could be carried out to investigate whether gene induction mediated by SMAD signaling is rather quantitative than qualitative. For example, if SMAD signaling does indeed not differentiate between different ligands, a similar set of genes would be regulated in GDF11- and TGFb-treated cells and a strong correlation between gene induction and SMAD2 dynamics would be observed.

Taken together, apoptosis, EMT and cytostasis, all cellular fates often associated with SMAD signaling, were observed in MCF10A cells. Interestingly, while apoptosis was only detected in quiescent cells, EMT and cell cycle slowdown were measured exclusively in proliferating cells. All phenotypic changes

showed a high correlation with the amount of activated SMAD2, which indicated that cell fate decisions are mainly determined by dynamic patterns of SMAD2. However, to uncover if the signaling pathway is rather simple and does not differentiate between different ligands, genome-wide changes in gene expression in response to TGFb and GDF11 stimulations were investigated next.

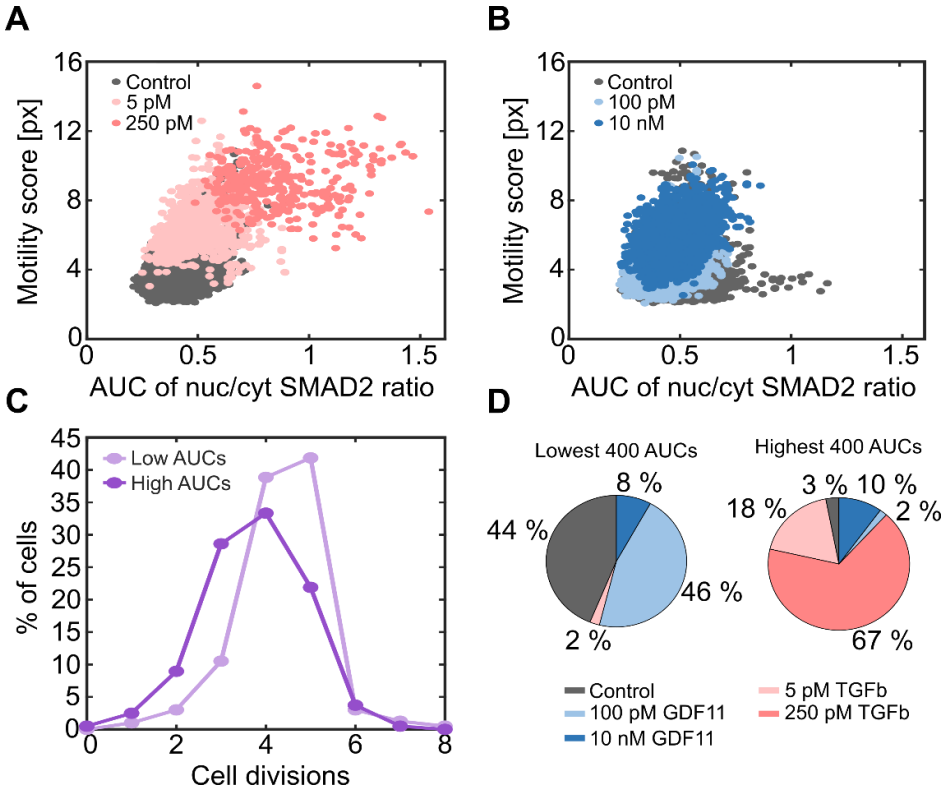

Figure 26: Single-cell analysis of motility and cell division in proliferating cells showed correlations between SMAD2 dynamics and cellular responses.

The analysis was performed in close collaboration with Lorenz Ripka (IMB Mainz). **(A-B)** Scatter plot showing the motility score of each cell analyzed in the long-term microscopy experiments and the AUC of the nuc/cyt SMAD2 ratio. Each dot represents one single cell. Left TGFb-treated cells **(A)** and right GDF11-treated cells **(B)** are shown. **(C)** The number of divisions of cells with the 400 lowest and 400 highest AUCs was determined without considering the different treatments. The reason why the 400 highest/lowest cells were chosen was that when the distribution of the AUCs was examined, the strongest outliers from both experiments corresponded to about 400 cells. **(D)** Pie charts showing the distribution of the different conditions among the 400 highest and lowest AUCs. All plots include the data of two biological replicates.

3.1.2.2 SMAD SIGNALING IS A QUANTITATIVE RATHER THAN QUALITATIVE PATHWAY

My previous results suggested that SMAD signaling does not differentiate between ligands but rather mediates a response in dependence of the amount and duration of SMAD2 in the nucleus. To strengthen this hypothesis, instead of phenotypic changes, the modulation of gene expression would be used as a readout to study the physiological consequences of ligand stimulations. As a proof of

concept, the gene expression of EMT and cell cycle markers in quiescent cells treated with GDF11 was investigated by RT-qPCR. It was speculated that even though the non-dividing cells did not exhibit these cell fates, the corresponding genes would still be modulated due to the quantitative nature of the SMAD signaling pathway. Indeed, as shown in Figure 27A, genes that were only slightly regulated by GDF11-mediated signaling in proliferating cells (Figure 25F) were now strongly modulated by the stimulus. Based on these findings, a large-scale approach to globally study gene expression patterns in quiescent and proliferating cells was carried out by using RNA sequencing. To this end, S2-R cells were treated with high doses of TGFb or GDF11 for 3 h and 6 h. Considering the SMAD2 dynamics observed in live-cell microscopy (Figure 20B-E), these time points should represent the period between the first peak and the onset of the second SMAD2 activation. Thereby, the effects of both responses on gene expression were analyzed. To investigate if a similar set of genes was regulated by the two ligands, scatter plots were generated showing the log2 fold change of all genes. Since the GDF11 condition was plotted against the TGFb condition, all genes along the diagonal are equally regulated by the different stimuli. Additionally, a linear model was incorporated. The slope of this linear model (m) is an indicator of the relative strength of the overall signal induction. A slope greater than 1 indicates a stronger induction through GDF11 than TGFb and vice versa. To test for statistical significance, the combined p-values of both conditions were used, which refer to the differential expression compared to control cells. The combined p-values were also included in the linear model. Thereby, genes with lower p-values were emphasized more strongly. Also, the correlation coefficient (r) was calculated, indicating the strength of association between GDF11- and TGFb-mediated gene regulation. Strikingly, in all conditions, almost every gene was close to the diagonal and the correlation coefficient was always above 0.6 (Figure 27B-E). Usually, values between 0.7 and 0.9 are described as strongly associated (Mukaka, 2012). This already showed that most genes were regulated similarly by the two ligands. Taking a closer look at the linear model revealed that in proliferating cells the gene expression is stronger induced by the TGFb treatment as the slope is below 1 (Figure 27B and C). In accordance with the SMAD2 dynamics, the opposite was observed when cells were growth factor deprived (Figure 27D and E). Interestingly, when quiescent cells treated with GDF11 and proliferating cells stimulated with TGFb were compared, gene expression seemed to be stronger induced in the TGFb condition even though both exhibit an equally great first SMAD2 response (Figure 27F and G). This might be due to the stronger second response mediated by TGFb or fundamental differences between the two cell states. Taken together, the results again suggested that SMAD signaling is quantitative rather than qualitative. Not only were the same genes regulated, but SMAD2 dynamics were also strongly correlated with gene expression. Together with the previous observation of the phenotypic changes, I concluded that the dynamic behavior of SMAD2 is more decisive than the type of ligand and that

ligands of the TGFb superfamily mediate diverse cellular outcomes through different dynamical patterns of SMAD molecules.

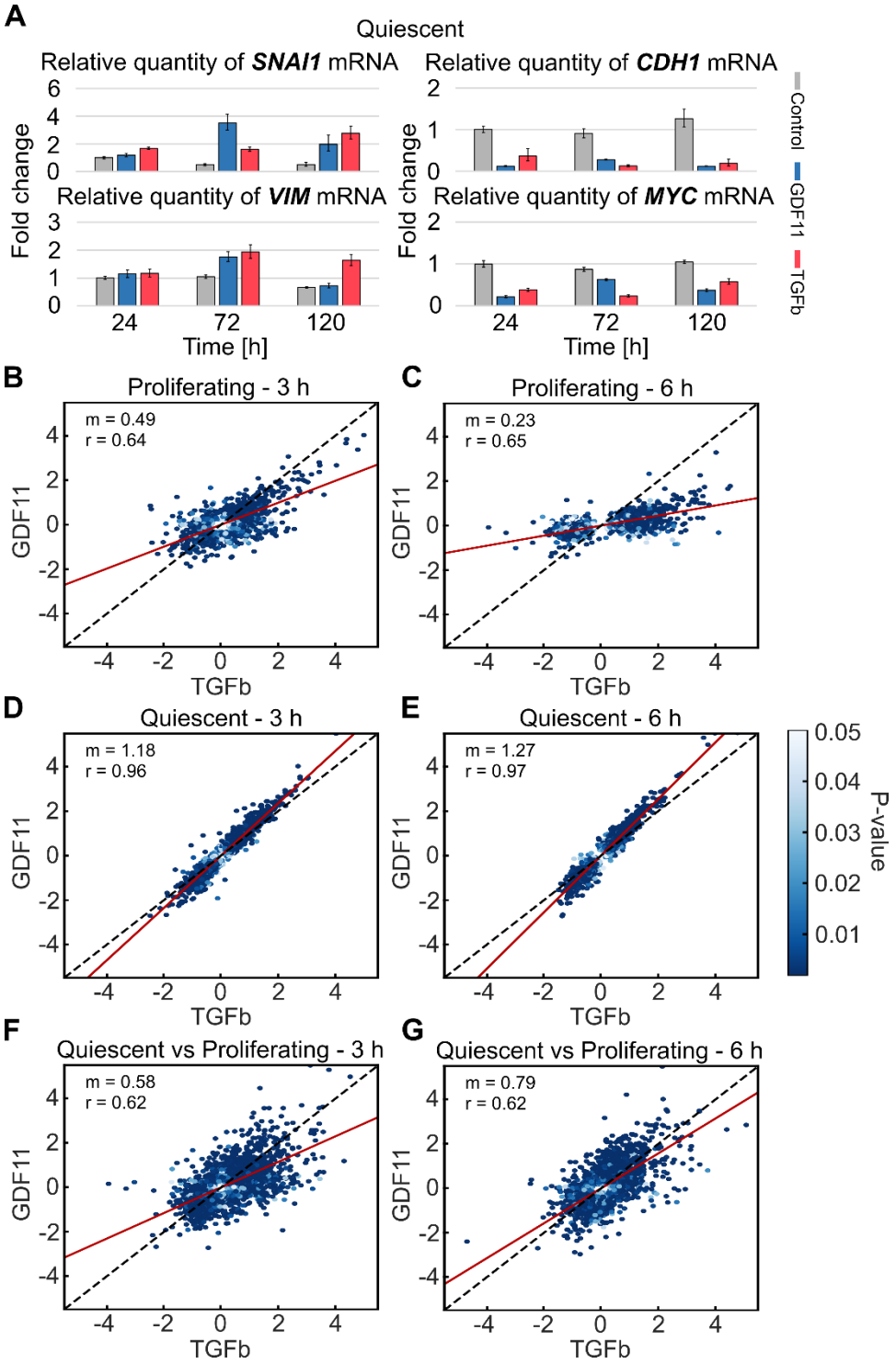

Figure 27: RNA sequencing revealed strong correlation of TGFb- and GDF11-induced gene expression.

The analysis was performed in close collaboration with Lorenz Ripka (IMB Mainz) **(A)** Quantification of *SNAI1*, *VIM*, *CDH1* and *MYC* mRNA by RT-qPCR. The RNA for the cDNA synthesis was isolated from quiescent S2-R cells stimulated with 5 nM GDF11 or 250 pM TGFb for 24 h, 72 h and 120 h. Actin was used as an internal control. Error bars indicate standard deviation of

technical triplicates. **(B-G)** Scatterplots showing the log2 fold change of the measured genes after stimulation with 10 nM GDF11 or 100 pM TGFb. Genes in proliferating **(B-C)** and quiescent **(D-E)** S2-R cells were analyzed. Additionally, the gene expression of quiescent cells treated with GDF11 and proliferating cells stimulated with TGFb was compared **(F-G)**. Each dot represents one gene. X-axis shows the log2 fold change of genes from TGFb-treated cells. Y-axis shows the log2 fold change of genes from GDF11-treated cells. Since a strong correlation of the fold changes between the two conditions was observed, it was possible to predict the fold change under GDF11 stimulation from the fold change under TGFb stimulation for the same gene with a linear model. The slope of this linear fit indicates the relative strength of the gene regulation mediated by both ligands. A slope greater than 1 indicates a stronger gene expression through GDF11 and a slope less than 1 indicates a stronger gene expression through TGFb. To test for statistical significance, the combined p-values of both conditions were calculated and shown as indicated in the legend. Also, the combined p-values were included in the linear model. To this end, 1-p was used as a weight for each data point. Thereby, genes with a low p-value were considered more than genes with a high p-value. P-values refer to the differential expression compared to control cells.

3.2 DISCUSSION OF PART 2

In adult organisms most cells are in a quiescent state, but some can re-enter the cell cycle under the right mitogenic conditions. The switch between cell states is important to enable tissue repair and regeneration (Cheung and Rando, 2013; Yao, 2014). However, it needs to be strictly regulated by proliferative and anti-proliferative signals. SMAD signaling is one of the pathways that is crucial for this regulation as perturbation of the pathway can result in an imbalance of proliferation and quiescence and ultimately in severe diseases such as cancer (Kretzschmar, 2000; Nelson et al., 2006; Inman et al., 2015). For this reason, it is important to gain a better understanding of this pathway not only in proliferating but also in quiescent cells. In the present study, I focused on characterizing the dynamics of TGFb- and GDF11-mediated SMAD signaling as well as the associated physiological responses in both proliferation states, using time-resolved measurements at the single-cell level and computer-aided data analysis.

3.2.1 SMAD SIGNALING IN QUIESCENT AND PROLIFERATING CELLS

Quiescent or G0 cells are described as cells outside of the replicative cell cycle that can resume proliferation under the right physiological conditions. Through a 48-h growth factor deprivation, it was possible to bring MCF10A cells into a non-dividing state (Figure 18A) and, as shown in Figure 19B, re-introduction of EGF into the medium caused cells to proliferate again. While I observed that nearly 95 % of the cells were in G0- or G1-phase upon growth factor deprivation (Figure 18B), it was difficult to differentiate between the two cell cycle phases. In general, quiescent cells have not been well characterized and markers canonically used to distinguish between G0- and G1-phase have been questioned (Oki et al., 2014). For example, Ki67 is often used as a marker for proliferation, as initial studies indicated that the protein is absent in quiescent cells and only detectable in G1-, S- and G2-phase (Gerdes et al., 1984). However, more recent studies revealed that Ki67 levels are highly heterogeneous in individual cells and dependent on the time a cell is remaining in G0. Therefore, Ki67 is not suitable as a binary marker of proliferation versus quiescence (Miller et al., 2018). Since I showed that cells were arrested in G0/G1 after removal of growth factors and that they proliferated again when stimulated with EGF, I labeled these conditions as quiescent, even though I did not distinguish between the two cell cycle phases.

After validating that 48 h in growth factor-deprived medium was sufficient to arrest cells in a quiescent state, I performed western blot analysis, immunofluorescence and live-cell time-lapse microscopy experiments to investigate how SMAD signaling is affected by the cell state. The dynamic behavior of SMAD in proliferating MCF10A cells was already well described in previous studies (Strasen et al.,

2018), however, how SMAD signaling behaves in quiescent cells was mostly undiscovered. Surprisingly, the response to TGFb was much higher in proliferating cells compared to quiescent cells (Figure 18D and E). As quiescence was mainly induced by EGF deprivation (Part 1 of this study and Chou et al., 1999), I examined if re-introduction of the growth factor is sufficient to reverse the observed effects on SMAD signaling. Indeed, stimulation with EGF was sufficient to rescue TGFb signaling (Figure 19A). Therefore, absent EGF was not only responsible for the G0/G1 arrest but also for the attenuation of SMAD activation. This raised the question whether the EGF pathway had a direct effect on SMAD signaling, for example through MAPK, or whether an altered cell cycle state influenced SMAD dynamics. As I compared a dividing population, including cells in G1-, S- and G2-phase, with a population that contained almost exclusively cells in G0/G1-phase, cell cycle phase-specific effects seemed plausible. Moreover, the cell cycle has wide-ranging effects on cellular physiology and can modulate gene expression levels (Buettner et al., 2015). To test this hypothesis, I treated quiescent cells with the CDK4/6 inhibitor palbociclib to keep cells in G0/G1-phase despite the re-introduction of EGF. Even though cells could not progress through the cell cycle, EGF treatment rescued SMAD dynamics, indicating that a loss of mitogenic signaling was responsible for SMAD attenuation instead of cell cycle effects (Figure 19C). Using pharmacological inhibitors, I was able to show that a sustained MEK/ERK activity was necessary for full SMAD signaling activity. Interestingly, inhibition of the PI3K/AKT pathway, which is also activated by EGF and necessary for cell cycle entry and S-phase progression (Part 1 of this study), did not alter SMAD dynamics (Figure 19D). This proved again that arresting cells in G0/G1-phase alone does not influence the signaling as pharmacological PI3K inhibition usually results in G1 accumulation (Fekete et al., 2012). The interaction between MEK/ERK and SMAD signaling was already discovered in earlier studies. Non-canonical SMAD signaling includes various branches of MAPK pathways and can increase MEK and ERK gene expression (Xie et al., 2004; Zhang, 2009). Furthermore, MEK/ERK can have a direct influence on SMAD signaling through phosphorylation of the SMAD linker region. For instance, the accumulation of SMAD molecules in the nucleus can be disturbed by linker phosphorylations (Kretzschmar et al., 1997; Kretzschmar et al., 1999; Massague, 2003). While this would argue against my results that a sustained MEK/ERK activity is essential for strong and sustained TGFb-mediated SMAD signaling, other studies reported a positive crosstalk between the ERK and SMAD pathway (Hayashida et al., 2003) and that the linker phosphorylation can increase the half-life of receptor phosphorylated SMADs (Hough et al., 2012). Concerning my results, the lack of MEK/ERK activity and the resulting lack of linker phosphorylation could be considered as a reason for the attenuation of SMAD signaling. In our laboratory, work is in progress to create specific cell lines containing mutations in different linker regions of SMAD. These cells could then be used to further validate this hypothesis. However, as the rescue of SMAD dynamics

by EGF took several hours, I assumed that the interaction of SMAD and MAPK signaling was rather mediated by MEK/ERK target genes instead of a direct crosstalk.

Before investigating changes in gene expression, I performed a small-scale ligand screening to determine if the effects of other ligands of the TGFb family were influenced by growth factor deprivation as well. The screening revealed that the response to activin A was not affected by the cell state. Interestingly, myostatin (GDF8)- and GDF11-treated cells showed opposite effects on SMAD signaling compared to cells stimulated with TGFb (Figure 20A). The high analogy between GDF8 and GDF11 could explain why both ligands mediated a similar effect on SMAD signaling (Walker et al., 2016). However, since the SMAD network is a simple and straight forward pathway, the vastly different dynamics upon TGFb, activin A and GDF8/11 treatment were not expected. All tested ligands are known to signal via SMAD2/3 (Rebbapragada et al., 2003; Andersson et al., 2006; Tsuchida et al., 2009), which leaves only a few possible differences between the signaling processes that could explain this phenomenon. One distinction is on the receptor level as they utilize different receptor combinations to initiate SMAD2/3 phosphorylation. For the ligands tested in this study, TGFBR2 (TGFb) and ACVR2A/ACVR2B (activin A, GDF8 and GDF11) serve as type II receptors, whereas TGFBR1 (TGFb, GDF8 and GDF11), ACVR1B (activin A, GDF8 and GDF11) and ACVR1C (activin A) serve as type I receptors. Additionally, some ligands require a co-receptor like TGFBR3 (TGFb and GDF11) for full signaling activity (David and Massagué, 2018). Therefore, a regulation on the receptor level could explain the distinct dynamics despite the same downstream signaling. Another possibility are ligand-specific antagonists like FST or follistatin-like 3 (FSTL3), which can bind and neutralize GDF8, GDF11 and activin A but not TGFb (Schneyer et al., 2008). However, as the ligands mediated such opposing effects on the signaling, I assumed that most likely multiple components of the SMAD pathway need to be altered through growth factor deprivation. To gain a better understanding how cells can switch their ligand sensitivity, I chose GDF11 for further experiments in this study. By investigating the median nuc/cyt SMAD2 ratio of quiescent and proliferating cells upon stimulation with varying concentrations of TGFb and GDF11, the dynamic behavior of SMAD2 was further characterized. As shown in Figure 20B-E, dividing cells treated with GDF11 and non-dividing cells treated with TGFb exhibited similar dynamics, however, quiescent cells stimulated with GDF11 showed only a weak second response instead of a strong sustained response which was usually observed for proliferating cells treated with high TGFb concentrations. To investigate if ligand-depletion is the reason for the transient response, I tested higher concentrations of GDF11 (data not shown), but even a dose of 50 nM did not increase the second response. Again, regulation on the receptor level or specific ligand antagonists could be an explanation. The RNA sequencing revealed that *ACVR2B*

expression (RPKM ~0.6) was extremely low in MCF10A cells compared to *TGFBR2* (RPKM ~20). Thereby, degradation of TGFb- and activin-receptors through negative feedbacks like SMAD7 (Kavsak et al., 2000; Winbanks et al., 2016) could lead to transient responses to GDF11, as only small quantities of ACVR2B were available. Overexpression of ACVR2A and ACVR2B in MCF10A cells could be carried out to examine this hypothesis.

Interestingly, pharmacological inhibition of MEK and EGFR revealed that a sustained lack of MAPK activity was responsible for the increase of GDF11-mediated SMAD signaling in quiescent cells (Figure 20H). This means that MEK activity can increase the response to TGFb and simultaneously decrease the response to GDF11. As both ligands signal via the same molecule SMAD2, a direct interaction by linker phosphorylation again seems less likely than an indirect effect mediated by MEK/ERK target genes. For this reason, and because the rescue with EGF suggested that the SMAD network was rewired on a slow time scale, a global gene expression analysis in proliferating and quiescent cells was performed. After evaluating the RNA sequencing, 63 SMAD pathway-associated genes were identified that fulfilled all criteria of the filtering procedure. Among them, several direct regulators of SMAD signaling such as *TGFBR3*, *FST*, *GDF11* or *AKT1* emerged (Figure 21).

After researching the top genes on the list, it was possible to exclude several candidates. For example, genes that are involved in the maturation of ligands, like latent-transforming growth factor beta-binding protein 1 (*LTBP1*) (Robertson et al., 2015), or genes expressing the ligands itself, like *GDF11* and *GDF8* (*MSTN)*, could be neglected as I used high quantities of recombinant TGFb and GDF11. Furthermore, genes that are associated with the SMAD pathway but do not directly influence the signaling were excluded for now. In this way, two candidates of particular interest were identified. For instance, *FST*, a potent GDF8 and GDF11 antagonist (Gamer et al., 1999; Lee and McPherron, 2001; Khalil et al., 2016) was strongly downregulated in the non-dividing conditions (Figure 21D). To rebuild the rewiring caused by growth factor deprivation, I knocked out *FST* in S2-R cells. All three isoforms of *FST* (FST288, FST303 and FST315) that have similar binding affinities to ligands (Sidis et al., 2006) were targeted and I validated the corresponding clones with western blot analysis, PCR, RT-qPCR and sequencing (Figure 23B-D, 6.5). Surprisingly, the loss of *FST* did not alter GDF11 signaling at all (Figure 24A). Clonal effects could be excluded since multiple clones were examined in live-cell microscopy and all showed similar GDF11-mediated SMAD2 dynamics (data not shown). Taken together, I concluded that the generated cell lines do not express any form of *FST*, which indicated that the knockout of *FST* alone does not affect GDF11 signaling. However, genetic compensations could also be responsible for the unchanged SMAD2 dynamics. The compensation through other genes in response to a knockout/knockdown is a common phenomenon (El-Brolosy and Stainier, 2017). For

example, histone deacetylase 1 (*HDAC1*) and *HDAC2* can compensate each other. When *HDAC1* is inactivated, increased levels of *HDAC2* were observed or vice versa (Jurkin et al., 2011). Another example is the compensation of cyclin D2 through cyclin D3 upregulation in B-lymphocytes from cyclin D2 $^{-/-}$ mice (Lam et al., 2000). The loss of a functional gene is often compensated via a closely related gene. This makes *FSTL3* an interesting candidate for the compensation of the *FST* knockout. Both share several functional properties, as well as a 40–50 % overall primary sequence homology (Schneyer et al., 2001; Saito et al., 2005). To test this hypothesis, *FST*-KO cells could be analyzed for *FSTL3* overexpression. Furthermore, there are other antagonists for GDF11 signaling, like GDF-associated serum protein 1 (*GASP1*) and *GASP2* (Kondás et al., 2008; Khalil et al., 2016), which could also be checked for increased levels.

The other interesting candidate was TGFBR3, a co-receptor modulating TGFb presentation to its type II receptor (Wang et al., 1991). It has been reported that the co-receptor can undergo ectodomain shedding and negatively regulate TGFb-induced SMAD2 activation. During this process, cells release soluble TGFBR3 that binds and sequesters ligands to inhibit TGFb signaling (Elderbroom et al., 2014). Strikingly, *TGFBR3* has also been reported to co-occur with *GDF11* (Wang et al., 2014) and enhance GDF11-mediated SMAD2 activation (Bajikar et al., 2017). Therefore, an abundance of TGFBR3 could not only decrease TGFb signaling but also increase GDF11 signaling at the same time. For this reason, TGFBR3 was overexpressed in the S2-R cell line. To ensure that the type III receptor is functional and to avoid common problems of exogenous overexpression, I increased expression levels of the endogenous gene using the CRISPR/Cas9 system (Figure 23E). Moreover, it was verified that the protein level of TGFBR3 was similar between quiescent cells and the overexpression cell line (Figure 23F). However, the increased levels of TGFBR3 did not achieve the desired effect. Even though the upregulation of the receptor decreased TGFb signaling, the effect was negligible (Figure 24C). Taken together, the transcriptional activation of *TGFBR3* was successful, but the minor effects on signaling outcomes suggested that the switch in ligand sensitivity cannot be explained by changes in the TGFBR3 level. However, it should be considered that the decrease of TGFb signaling due to ectodomain shedding might also require the upregulation of additional co-factors rather than just higher quantities of TGFBR3. For example, it was reported that the shedding of the type III receptor requires metalloproteases and pervanadate (Velasco-Loyden et al., 2004). To test this hypothesis, the supernatant of the overexpression cell line could be screened for soluble TGFBR3. If the amount of soluble receptor is not considerably higher than in control cells, the protein level of potential co-factors could be increased by transcriptional upregulation.

Generally, SMAD signaling seems to be very robust against single perturbations. For instance, the knockout of SMAD7, one of the main feedback regulators of the pathway (Moustakas and Heldin, 2009), increased the overall SMAD2 dynamics but did not change dynamical patterns in MCF10A cells (Strasen et al., 2018). Similar effects were observed after knocking out PPM1A (data not shown), a SMAD phosphatase which terminates TGFb signaling (Lin et al., 2006). Even with a complete loss of the phosphatase, only slight increases of the overall signaling strength were determined. The minor changes detected upon perturbation of *TGFBR3* and *FST* in this work are consistent with these earlier observations. Moreover, even when all transcriptional feedbacks were inhibited by DRB treatments, only small adjustments in SMAD2 dynamics were observed. Interestingly, also the combined perturbations (*FST* knockout and *TGFBR3* overexpression or *FST* knockout and DRB treatment) did not considerably change signaling outcomes (Figure 24A). Taken together, these results suggest that single and double perturbations might not be sufficient to reproduce the divergent signaling response of proliferating and quiescent cells. Therefore, maybe a more comprehensive rewiring of the network involving the modulation of multiple components of SMAD signaling is necessary to shift ligand sensitivity. The up- and downregulation of 63 SMAD-associated genes in quiescent cells further strengthens the hypothesis of a wide-ranging pathway-rewiring. To investigate this idea, gene expression of multiple genes would have to be changed. In recent years, more and more genome-scale knockout or activation screenings using CRISPR/Cas9 were developed (Konermann et al., 2015; Feldman et al., 2019; Ihry et al., 2019). For multiplexed regulation of several genes, a library could be generated containing sgRNAs that target the SMAD-associated genes identified by the RNA sequencing. For example, Konermann et al., 2015, showed that the simultaneous activation of ten genes using ten different sgRNAs is possible. However, it would still be challenging to up- and downregulate dozens of genes in one cell line to prove a pathway-rewiring. Eventually, it is also possible that the correct key protein responsible for the ligand sensitivity switch was not identified yet. Nonetheless, a large-scale screening could again help to determine this key player.

3.2.2 SMAD-MEDIATED CELL FATES IN QUIESCENT AND PROLIFERATING CELLS

After revealing that MCF10A cells adjust their sensitivity for ligands of the TGFb superfamily according to the proliferation state, the question has been raised whether different ligands also have different consequences for the physiological response of the cell. Even though multiple studies uncovered a wealth of information about the SMAD network, it is still poorly understood how the simple and straight forward pathway controls such a broad range of phenotypic outcomes. Moreover, it is unclear if and how the signaling network can differentiate between varying ligands. While there are two

signaling branches with SMAD2/3 and SMAD1/5/8 as well as a small set of serine-threonine receptors, the more than 30 different ligands of the TGFb superfamily suggest a rather converging pathway that cannot distinguish between each ligand. However, the diverse functions reported for the different ligands contradict this hypothesis. Also, it seems irrational to have a wide variety of growth factors but no ligand-specific outcome (Nickel and Mueller, 2019). The promiscuity of ligand-receptor interactions was recently discussed for the BMP signaling pathway (SMAD1/5/8). It was suggested that the effect of a particular ligand on pathway activity depends on which other ligands are present. For example, it was shown that BMP3 antagonistically interacts with almost every other ligand that was tested in this context and that BMP4 and BMP7 can exhibit antagonistic and synergistic interactions. Moreover, BMP4 and BMP10, two potent activators of the pathway, became inhibitory in the presence of the other ligand (Antebi et al., 2017). These complex multi-ligand responses could explain how the converging pathway mediates diverse cellular outcomes and it would be intriguing to extend this approach to cytokines activating SMAD2/3. Another possible hypothesis was that the dynamic behavior of SMADs is more decisive than the type of ligand and that ligands mediate diverse cellular outcomes through different dynamical patterns of SMADs. Thus, ligands would not necessarily need a more complex pathway to mediate a variety of functions but rather intrinsic properties, like different binding affinities or binding kinetics that would change signaling dynamics (Nickel and Mueller, 2019). Since previous studies already revealed that signaling dynamics are associated with cellular responses (Purvis and Lahav, 2013), this seemed to be a possibility. To test this hypothesis, proliferating and quiescent S2-R cells were stimulated with TGFb or GDF11 and screened for cellular outcomes in time-lapse live-cell microscopy (Figure 25). I focused on EMT, apoptosis and cytostasis, three cell fates that are often associated with SMAD signaling (Heldin et al., 2009). To determine changes in these cell fates, I quantified phenotypic features like motility, cell death and cell division. Motility can be used as a readout for EMT, as EMT usually results in enhanced cell movement (Lamouille and Derynck, 2007). After imaging stimulated S2-R cells for 120 h, I was able to observe changes in all three cell fates. While an increase in motility and a decrease in cell division rate were only monitored in proliferating cells, a high fraction of cell death was exclusively observed in quiescent cells. To further characterize the phenotypes, biomarkers of the different cell fates were investigated (Figure 25E and F). For example, *CDH1*, *VIM* and *SNAI1* were selected for EMT (Zeisberg and Neilson, 2009), *MYC* for cytostasis (Rabbitts et al., 1985) and cleaved caspase 7 for apoptosis (Fernandes-Alnemri et al., 1995). Indeed, biomarkers changed according to the observed phenotypes. After providing evidence for all three SMAD-related cell fates, the objective was to associate them with the SMAD2 dynamics. Interestingly, the strength of the signaling correlated well with the cellular outcome, as an increasing pathway activation led to increasing cell death and motility (Figure 25C and D). For the decrease in cell division rate strong

sustained dynamics were necessary (Figure 25D), which is consistent with previous studies in cancer cell lines showing that transient SMAD activation was sufficient to alter cellular motility, while sustained signaling was required to induce cytostasis (Nicolás and Hill, 2003; Giampieri et al., 2009). My results suggested that SMAD signaling is indeed quantitative rather than qualitative. Additionally, single-cell analyses of the 120-h experiments revealed a strong correlation between dynamics and cell fate decisions since cells with a higher AUC also covered a greater distance and divided less frequently (Figure 26A-C). Even though the results indicated a dynamic-dependent cell fate, the question whether ligands are a deciding factor for cellular outcomes had yet to be answered. For instance, in Figure 26C the 400 highest and lowest AUCs were analyzed without considering the different treatments to show that the ligand is of secondary importance. However, because of the different ligand sensitivity in proliferating cells, only a few TGFb- and GDF11-treated cells were among the 400 lowest and highest AUCs, respectively (Figure 26D). Due to this, only a handful of cells that had been treated with different ligands, but exhibited similar dynamics/AUCs, could be analyzed. As all SMAD-associated cell fates were only observed in one of the two proliferation states, it was also not possible to compare the cellular outcome of GDF11 signaling in quiescent cells with the cellular outcome of TGFb signaling in proliferating cells, or vice versa. One way to address this problem could be to research other phenotypic changes which are present in both cell states. For example, SMAD signaling is also involved in the regulation of autophagy, a critical cellular response to environmental changes (Kiyono et al., 2009). Therefore, if this cellular outcome is displayed in both proliferation states, proliferating and quiescent cells could be screened for the accumulation of autophagosomes via a GFP-LC3 reporter (Kabeya et al., 2000). Moreover, it has been reported that A549 cells treated with TGFb for 7 days undergo senescence (Katakura et al., 1999). To differentiate between quiescence and senescence, it could be investigated if cells start to divide again upon EGF stimulation. It would be expected that senescent cells, despite growth factor re-introduction, will not resume proliferation. This approach could be combined with the senescence associated β-galactosidase (SA-bG) assay as it has been shown that SA-bG activity was irreversibly increased in senescent cells but was reversible in quiescent cells that re-entered the cell cycle (Yang and Hu, 2005). Thereby, senescence could possibly serve as another readout. However, it should be kept in mind that long-term stimulations in quiescent cells caused apoptosis, which complicates the investigation of other cell fate decisions. Another possibility to address the uneven distribution of the AUCs, would be to increase GDF11-mediated signaling in proliferating cells through modifications of the SMAD pathway. This would lead to more GDF11-treated cells with high AUCs, which could then be screened for increasing motility and decreasing cell division rate. If ligands are insignificant for the cellular outcome, changes similar to those observed in TGFb-treated cells would be expected. However, as seen in my previous

experiments, SMAD signaling seemed to be quite robust against perturbations. For this reason, I decided to approach this problem by analyzing gene expression patterns in stimulated quiescent and proliferating cells. Thus, instead of phenotypic changes, the modulation of gene expression was used as a readout to study the physiological consequences of ligand stimulations. As a proof of concept, the gene expression of EMT and cell cycle markers in quiescent cells treated with GDF11 was investigated by RT-qPCR. It was speculated that even though non-dividing cells did not exhibit SMAD-associated cell fates, the corresponding genes would still be modulated due to the quantitative nature of the SMAD signaling pathway. Indeed, while these genes were barely up- or downregulated in proliferating cells treated with GDF11, they now showed a high fold change compared to the unstimulated control (Figure 27A). However, the fold change of some of the biomarkers was not as high as in proliferating cells treated with TGFb (Figure 25F and Figure 27A). This might be due to the fact that quiescent cells with strong SMAD2 activation die or that GDF11-mediated SMAD2 dynamics show a rather weak second response. Interestingly, despite the clear regulation of EMT markers in quiescent cells, they did not show any corresponding phenotypic changes. One possible explanation for this phenomenon could be lethal EMT, an event that remodels the transcription factor landscape for EMT-associated apoptosis (David et al., 2016). Thus, instead of increased motility and a mesenchymal phenotype, cell death would be observed in quiescent cells. But why quiescent cells are more likely to promote apoptosis than EMT compared to proliferating cells remains to be answered. Nonetheless, a similar regulation of EMT markers in quiescent cells treated with GDF11 and proliferating cells stimulated with TGFb suggested once more that the SMAD pathway does not directly differentiate between ligands but rather mediates cellular outcomes through dynamical patterns of SMADs. To further validate the quantitative nature of SMAD signaling, gene expression patterns in stimulated quiescent and proliferating cells were globally studied utilizing RNA sequencing. To this end, S2-R cells were stimulated with high doses of TGFb or GDF11 for 3 h and 6 h. Since the first peak of SMAD2 activation usually appeared 2 h upon treatment and the sustained response began approximately 4 h after stimulation (Figure 20C and D), these time points should reflect the effects of both responses on gene expression. Strikingly, in nearly all conditions, a similar set of genes was regulated by TGFb and GDF11 signaling. Moreover, dynamics correlated well with the level of gene induction, as all conditions showed correlation coefficients above 0.6, some even over 0.9 (Figure 27B-G). As a rule of thumb, correlation coefficients between 0.7 and 0.9 are usually described as strongly correlated (Mukaka, 2012). Since also genes with very low fold changes were included in the scatterplots, it would be interesting to use a filter system that only considers genes that are associated with SMAD signaling and that have a minimal fold change. To be more specific, genes that contain SMAD binding elements such as GGCGC and related 5 bp motifs as well as known motifs for SMAD-specific transcription factors

(David and Massagué, 2018) could be selected and then analyzed again. Thereby, only genes that are directly regulated would be investigated and indirect effects of SMAD signaling on gene expression could be excluded. To assess whether genes were more strongly regulated by TGFb or GDF11 stimulations, a linear model was added to the scatterplots. In the linear fit, genes with a higher fold change were indirectly considered more since the combined p-values referring to the differential expression compared to the control were used as a weight for each data point. Usually, genes with an extremely low fold change also had higher p-values and thereby were less relevant for the linear fit. Corresponding to the SMAD2 dynamics, genes were more strongly induced by TGFb stimulation in proliferating cells than by GDF11 stimulation and vice versa in quiescent cells. Interestingly, the gene expression of multiple genes in non-dividing cells was still severely modulated by TGFb treatment, although SMAD2 activation was usually very low (Figure 27D and E). However, this was not the case for GDF11-mediated gene expression in proliferating cells, as can be seen from the moderate slope of the linear model (Figure 27B and C). There could be different explanations for this. First, although GDF11 signaling is strongly increased by growth factor deprivation, a secondary response, similar to that obtained with TGFb stimulation, was never observed. Thus, the sustained response in TGFb-treated cells could be responsible for the decreasing slope of the linear model in proliferating cells. In other words, the lack of a strong GDF11-mediated second response in quiescent cells prevented the linear model from trending more towards GDF11-induced gene expression. Second, GDF11 might require an additional transcription factor to induce its full effect, which is not expressed in proliferating cells. For example, it has been reported that ID2, a helix-loop-helix inhibitor important for mammary gland development (Mori et al., 2000), is required for GDF11-mediated cellular responses (Bajikar et al., 2017). Interestingly, ID2 was considerably upregulated in quiescent cells and fulfilled all requirements of the filtering system (Figure 21A-C), which would support this hypothesis. However, it would argue against the idea of a quantitative signaling and raise the question how ID2 can differentiate between TGFb and GDF11. The transcriptional activation of ID2 via CRISPR/Cas9 in proliferating cells could be utilized to further characterize the role of ID2 in GDF11 signaling. In general, the results of the RNA sequencing strongly suggested that SMAD signaling is quantitative rather than qualitative, as the same genes were regulated upon GDF11 and TGFb stimulation and the strength of the signal correlated well with the level of gene expression. However, it should be noted that only two ligands of the TGFb superfamily were investigated. Thereby, it would be intriguing to investigate other ligands as well. For example, activin A could be used for further validations since it also initiated the activation of SMAD2 in MCF10A cells (Figure 20A). Moreover, as activin A signaling was not influenced by growth factor deprivation, the question whether the proliferation state itself affects gene expression could be answered. In case the cell state does not play an essential role, genes would

correlate almost perfectly between quiescent and proliferating cells stimulated with activin A as they exhibit similar nuc/cyt SMAD2 ratios.

Furthermore, it would be interesting to test the idea of a quantitative signaling by using a mathematical model. For instance, the information about TGFb-mediated dynamics and gene expression could be used to predict the gene induction by GDF11. Hypothetically, if the pathway does not differentiate between different ligands, the dynamics of SMAD2 should be sufficient to predict changes in gene expression. Again, dynamics and gene induction of multiple TGFb superfamily members could help to create and validate a sophisticated model. Besides more comprehensive RNA sequencing and mathematical modeling, the influence of the individual ligands could also be investigated in other ways. For example, instead of comparing more growth factors and their cellular outcomes, ligands could also be completely removed from the equation. One way to achieve this could be the optogenetic regulation of SMAD signaling. With this approach, SMAD molecules can be spatiotemporally controlled without the use of ligands (Li et al., 2018; Humphreys et al., 2020). SMAD2 dynamics like those mediated by GDF11 and TGFb treatment could be replicated by light stimulations and subsequent cellular responses could be investigated. It would be intriguing to see if SMAD signaling would still be able to cause cytostasis, apoptosis, EMT or changes in gene expression to the same extent.

Taken together, through quantitative and time-resolved dissection of the SMAD signaling pathway at the single-cell level, I uncovered that TGFb mediated a much higher SMAD2 response in proliferating cells compared to quiescent cells and that it was exactly the opposite for GDF11. Furthermore, I observed different SMAD-associated cell fates that correlated well with SMAD2 dynamics, indicating that the signaling pathway is quantitative rather than qualitative. In essence, these discoveries contribute to a better understanding of the interplay of SMAD signaling and the cell cycle as well as to a deeper insight of SMAD-associated cell fates. But why is a profound knowledge of this network so important? Efficient information processing by the SMAD signaling pathway is essential during embryogenesis and in the adult organism as dysregulations of the signaling contribute to severe diseases such as cancer or fibrosis. Moreover, the pathway plays an important role in the regulatory process of quiescence and proliferation to enable tissue repair and regeneration. Thereby, a quantitative understanding of how cells encode and decode information about extracellular ligands and elicit appropriate responses in both cell states is mandatory for therapeutic targeting of the pathway. This study showed the variety of cellular responses that can be mediated by the SMAD signaling pathway and which requirements must be fulfilled for each cell fate. For instance, for TGFb and GDF11, the cells must be quiescent to initiate apoptosis. For cells to undergo EMT, however, the

cells must be proliferating. In view of the dual role of SMAD signaling in cancer, these findings are interesting. Usually, ligands like TGFb can prevent uncontrolled tissue growth by inducing cytostasis and apoptosis, however, in later stages of tumor progression they lose the suppressive abilities but regain EMT-promoting functions which can lead to metastases (Ikushima and Miyazono, 2010). As cancer cells are characterized by permanent and uncontrolled cell division, it corresponds to my observation that these cells undergo EMT rather than apoptosis. A molecular understanding of how the proliferation state influences the decision between EMT and cell death could help to target and inhibit the cancer promoting effects of SMAD signaling. Moreover, the findings that GDF11 induces a considerable degree of apoptosis in quiescent cells might be interesting for cancer therapies in general. For instance, quiescent cancer stem cells have been observed in many human malignancies and are accountable for the resistance against current treatments, such as cytotoxic chemotherapy. While chemotherapy was effective in killing cancer cells in S/G2/M-phases, there was only little effects on cancer cells in G0/G1-phase (Yano et al., 2014; Chen et al., 2016). Thereby, quiescence is adopted as a surviving strategy to escape from different therapies. Current pharmacological strategies are aimed at eradicating quiescent cells, keeping them in a harmless, non-dividing state, or increasing their sensitivity to anti-proliferative drugs by reactivating them (Recasens and Munoz, 2019). If GDF11 triggers the quiescent-dependent apoptosis in various cell types, treatment with the recombinant ligand could be a new therapeutic approach to eradicate quiescent cancer cells.

3.3 MATERIAL AND METHODS OF PART 2

3.3.1 CELL LINES

MCF10A cell lines were cultured in DMEM/F12 growth-medium (2.3.1). When required, the medium was supplemented with selective antibiotics to maintain transgene expression (400 µg/ml geneticin disulphate (G418, ROTH), 50 µg/ml hygromycin B (Thermo Fisher Scientific) or 5 µg/ml blasticidin S hydrochloride (ROTH)). The S2-R cell line has been previously described (Strasen et al., 2018). In short, lentiviral reporter constructs encoding SMAD2-YFP and H2B-CFP under the control of a constitutive human UbCp were generated using the MultiSite-Gateway recombination system (Invitrogen) and transduced utilizing lentiviral particles.

HEK293 cells were grown in DMEM - High Glucose medium and U-2 OS cells in DMEM/F12 medium. Both media were supplemented with 10 % FBS (PAN-Biotech), 100 U/ml Penicilin, 100 µg/ml streptomycine and 2 mM GlutaMAX.

3.3.2 GENERATING A *FST* KNOCKOUT CELL LINE

A *FST* knockout cell line in MCF10A S2-R was created utilizing the CRISPR/Cas9 system. The knockout of *FST* has to affect both alleles of the gene to ensure a complete loss of the corresponding protein. To this end, a donor DNA and an sgRNA were cloned and transfected together with Cas9 endonuclease into S2-R cells. The donor DNA consists of a knock-in sequence (SV40-Blasticidin_R) surrounded by left and right homology arms. The arms are homologous to the genomic DNA upstream and downstream of the desired knock-in location. To create the homology arms, a template (HA-template) was amplified by PCR (3.3.5) from MCF10A genomic DNA using the primer pair FST_gen (listed below). The corresponding DNA fragment was purified from an agarose gel (3.3.6) and utilized as a template to amplify the homology arms with the primer pairs FST_HAL and FST_HAR. The lengths of the homology arms were as follows: 927 bp for the left and 800 bp for the right arm. For the knock-in sequence, the SV40 promotor in front of the blasticidin resistance gene was amplified from the pVE10 vector by utilizing the primer pair FST_Blast. All three PCRs were performed with the Q5 polymerase (New England BioLabs) and the resulting products were purified from an agarose gel. All primers were designed to create 15-35 bp overlapping DNA fragments to join the homology arms, the knock-in sequence and the expression vector pDONR221 (digested with EcoRV and AflII (both New England BioLabs)) together using NEbuilder (New England BioLabs). The resulting product (pDONR221-FST-Blast_R) was multiplied in *E. coli* (3.3.8) and afterwards validated by control digestion (3.3.10) and sequencing (3.3.11) to exclude any mutations. To clone the sgRNA, a 20 bp long guide

sequence (listed below) which is specific to the target gene was designed first. To ensure the smallest possible number of off-target sites, the sgRNA was designed with an online tool of Labun et al., 2019, (CHOPCHOP v3). The target sequence is located in exon 2 (chr5:53482891) near the start codon (chr5:53480791). Next, corresponding oligos were designed and annealed. To this end, 100 pmol of each oligo were diluted in 40 µl of 10 mM Tris-Buffer, denatured and annealed using a PCR machine (peqSTAR, VWR) (program listed at the end). For further use, 2 µl of the oligos were diluted in 38 µl of 10 mM Tris-Buffer. Afterwards, the sgRNA_AL vector (6.4), which contains the crRNA and tracrRNA sequences, was digested with AgeI (New England BioLabs) and joined together with the annealed oligos utilizing NEbuilder. The final sgRNA was multiplied in *E. coli* and afterwards validated by control digestion and sequencing to exclude any mutations. Finally, 495 ng of sgRNA, 10 ng of donor DNA linearized by NotI (New England BioLabs) and 495 ng of Cas9 endonuclease were transfected into S2-R cells. Monoclonal colonies were achieved as described in 3.3.3. To analyze the corresponding clones and determine whether they are heterozygous, homozygous or negative for the insertion, genomic DNA was isolated from the clones using the QIAamp DNA Mini Kit. Afterwards, a PCR with two different primer pairs was performed. The FST_gen forward and reverse primers flank the target and amplify the genomic region containing the Cas9 endonuclease cleavage site. If the donor DNA was inserted into the *FST* locus, the PCR amplification will generate one fragment (3.4 kbp) for homozygous and two fragments (3.4 kbp + 2.2 kbp) for heterozygous genotypes. To check if the donor DNA was inserted correctly, the FST_gen reverse primer was exchanged with the direct-blast primer, which binds within the blasticidin sequence. By utilizing these two primers, the PCR amplification will generate a fragment of 1.7 kbp size upon successful integration. The program for oligo annealing was set up as follows:

Temperature	**Time**	**Cycles**
95 °C	10 min	1
95-85 °C, -2 °C /s		
85 °C	1 min	1
85-75 °C, 0.3 °C/s		
75 °C	1 min	1
75-65 °C, -0.3 °C /s		
65 °C	1 min	1
65-55 °C, -0.3 °C /s		
55 °C	1 min	1
55-45 °C, -0.3 °C /s		
45 °C	1 min	1
45-35 °C, -0.3 °C /s		
35 °C	1 min	1
35-25 °C, -0.3 °C /s		
25 °C	1 min	1

Primer	**Sequence (5'-> 3')**
FST_gen_for	GAGAAGTCTTCTCGACCCAAATCC
FST_gen_rev	AGGCACTTAGGGAGCCCTGTAG
FST_HAL_for	TTGTAAAACGACGGCCAGTCGCGGCCGCGTTGCCCGCCTTTAGAGGAG
FST_HAL_rev	CTAACTGACACACATTCCACACTTGACGGAGCCAGCAGTTC
FST_HAR_for	GTATACCGTCGACCTCTAGCCGCTGCCAGGTCCTGTACAA
FST_HAR_rev	GTAATACGACTCACTATAGGGGATGCGGCCGCCTGCCTTGGTACTGGACTTC
FST_blast_for	GAACTGCTGGCTCCGTCAAGTGTGGAATGTGTGTCAGTTAGG
FST_blast_rev	TTGTACAGGACCTGGCAGCGGCTAGAGGTCGACGGTATACAG
Direct_blast_rev	GCTGGCGACGCTGTAGTCTTC
Guide sequence	**Sequence (5'-> 3')**
FST_sgRNA_for	CACC**TGGCTCCGTCAAGCGAAGAA**GTTTTAGAGCTAGAAATAGCA
FST_sgRNA_rev	AAAC**TTCTTCGCTTGACGGAGCCA**GGTGTTTCGTCCTTTCC

3.3.3 TRANSFECTION AND GENERATION OF MONOCLONAL CELL LINES

For insertion of plasmid DNA into MCF10A cell lines, approximately 18-24 h before transfection 2.5×10^5 cells were seeded in a 12-well plate and cultured in growth-medium. Afterwards, the corresponding DNA was diluted in 50 µl of preheated Opti-MEM I reduced-serum medium (Thermo Fisher Scientific) and 2 µl of P3000 (Lipofectamine 3000 Kit, Thermo Fisher Scientific) were added. The mixture was incubated for 5 min. Meanwhile, 3 µl of Lipofectamine 3000 (Lipofectamine 3000 kit) was added to another 50 µl of preheated Opti-MEM I reduced-serum medium. Afterwards, the two samples were mixed and incubated for 15 min at room temperature. The mixture was added dropwise to different areas of the wells and gently rocked for homogeneous distribution. After 3 days, the cells were trypsinized with 1× Trypsine-EDTA (Thermo Fisher Scientific) and transferred to 15 cm plates with antibiotic-containing medium. The medium was changed twice per week and after 14-21 days, colonies were picked. To this end, colonies were trypsinized, individually aspirated using a 1 ml pipette and transferred to a 12-well plate with antibiotic-containing medium. When confluent, cells were washed with PBS trypsinized and transferred to a 6-well plate. This process was repeated until cells were transferred to 10 cm plates.

3.3.4 GENERATING A *TGFBR3* OVEREXPRESSION CELL LINE

To amplify the TGFBR3 level in S2-R cells, I followed the approach from Konermann et al., 2015, where a dead Cas9-VP64 complex was used to increase the expression of target genes. First, the target sequence was designed utilizing an online tool (*sam.genome-engineering.org/database/*) to avoid off-target effects and ensure that the target sequence (chr1:91886308) is located close to the TSS

(chr1:91886281). Next, corresponding oligos were denatured and annealed using a PCR machine. The annealed oligos with 4 bp overhangs were then joined together with the lentiviral vector lentiSAMv2 (Addgene plasmid #75112) containing the dCas9-VP64 complex using Golden Gate cloning. The detailed reaction setups and programs are listed below. The final lentiviral vector (lentiSAMv2-TGFBR3) was multiplied in *E. coli* and afterwards validated by control digestion and sequencing to exclude any mutations. At the end, S2-R and wild-type MCF10A cells were infected with the corresponding lentiviral particles to create stable cell lines overexpressing TGFBR3. To achieve an even higher expression level of the target gene, cells were additionally infected with the vector lentiMPHv2 (Addgene plasmid #89308) containing the transcriptional activators p65 and HSF1. The reaction mixture and program for oligo annealing were set up as follows:

Component	**Amount**
Each oligo [100 µM]	1 µl
10x T4 ligase buffer (New England BioLabs)	1 µl
T4 PNK (New England BioLabs)	0.5 µl
ddH_2O	6.5 µl

Temperature	**Time**	**Cycles**
37 °C	30 min	1
95 °C	5 min	1
95-25 °C, -5° C/min		1

Guide sequence	**Sequence (5'-> 3')**
TGFBR3_sgRNA_for	CACC**GGAGAGGAGGCGGGAGGCGGG**
TGFBR3_sgRNA_rev	AAAC**CCCGCCTCCCGCCTCCTCTCC**

The reaction mixture and program for the Golden Gate reaction were set up as follows:

Component	**Amount**
2× T7 Ligase Reaction Buffer (New England BioLabs)	1 µl
BSA [20 mg/ml]	0.125 µl
Restriction enzyme BsmBI (New England BioLabs)	1 µl
T7 ligase (New England BioLabs)	0.125 µl
Diluted oligo anneal (1:10)	1 µl
Backbone vector lentiSAMv2	1 µl
ddH_2O	9.25 µl

Temperature	Time	Cycles
37 °C	5 min	15
20 °C	5 min	15

3.3.5 POLYMERASE CHAIN REACTION

The polymerase chain reaction (PCR) was used to amplify DNA fragments using specific primers listed in the respective sections. Q5 High-Fidelity DNA polymerase (New England BioLabs) was used with the following reaction setup and program:

Component	Amount
5× Q5-Buffer (New England BioLabs)	10 µl
dNTP mix (10 mM) (New England BioLabs)	1 µl
Forward primer (10 pmol/µl)	1 µl
Reverse primer (10 pmol/µl)	1 µl
Q5® DNA polymerase	0.5 µl
Template	10-200 ng
ddH_2O	up to 50 µl

Program was adjusted to primers and product length.

Step	Temperature	Time	Cycles
Initial denaturation	98 °C	1.50 min	1
Denaturation	98 °C	10 s	15
Annealing	65 °C	30 s	15
Elongation	72 °C	1.05 min	15
Denaturation	98 °C	10 s	20
Annealing	60 °C	30 s	20
Elongation	72 °C	1.05 min	20
Final elongation	72 °C	7.00 min	1

3.3.6 ANALYSIS AND PURIFICATION OF DNA BY AGAROSE GELS

For separation of DNA fragments, 1.0-1.5 % agarose gels with the fluorescent dye peqGREEN (Peqlab) were prepared. For a 1 % (w/v) agarose gel, 1 g of agarose was dissolved in 100 ml 1× TAE buffer by heating. After the mixture cooled down, 5 µl of peqGREEN were added. The DNA samples were supplemented with 6× loading dye (New England BioLabs). For molecular weight estimation, the 1 kb plus DNA Ladder (New England BioLabs) was used. Running time and used voltage were adjusted to the size of the DNA fragments (approximately 130 V for 30 min). If the DNA fragments were needed for further experiments, bands were extracted and purified with the QIAquick Gel Extraction Kit (Qiagen) according to the manufacturer's instructions. The DNA was eluted with 30 µl EB buffer and quantified using the spectrophotometer NanoDrop 2000c (Thermo Fisher Scientific).

3.3.7 DNA FRAGMENT ASSEMBLY

To assemble multiple overlapping DNA fragments in a single-tube isothermal reaction, NEbuilder assembly was used. The reaction mixture for cloning the donor DNA was set up as follows:

Component	Amount
pDONR221×EcoRV+AflII	31.4 ng
HAL	25 ng
HAR	35 ng
SV40-Blast_R	28.5 ng
2× NEbuilder Master Mix	10 µl
ddH_2O	up to 20 µl

The reaction mixture for cloning the sgRNA was set up as follows:

Component	Amount
sgRNA_AL×AgeI	50 ng
Annealed oligos	2.8 ng
2× NEbuilder Master Mix	5 µl
ddH_2O	up to 10 µl

All reactions were performed at 50 °C for 1 h.

3.3.8 ELECTROPORATION AND CULTIVATION OF *ESCHERICHIA COLI*

For electroporation, electro competent *E. coli* cells (Top10) were thawed on ice and 1 µl of diluted NEbuilder assembly product (1:3) or 2 µl of Golden Gate reaction were added. The cells were transferred into an electroporation cuvette (Bulldog Bio, Inc.). Using an electroporator (Eppendorf AG), a charge of 1.8 kV was applied and afterwards, 1 ml of SOC medium (New England BioLabs) was added. The cells were incubated for 1 h at 37 °C. Subsequently, 50 µl were spread onto antibiotic-containing LB agar (Sigma) plates and incubated over night at 37 °C. The next day, single colonies were picked and grown in 5 ml LB medium (Carl Roth) with appropriate antibiotics (100 µg/ml Ampicillin (AppliChem) or 50 µg/ml Kanamycin (AppliChem)) at 37 °C O/N while shaking.

3.3.9 GENOMIC DNA AND PLASMID DNA ISOLATION

For the isolation and purification of plasmid DNA from overnight cultures, the QIAprep Spin Miniprep Kit (Qiagen) was used. For the isolation of genomic DNA from cultured MCF10A cells, the QIAamp Mini DNA Kit (Qiagen) was used. The isolations were performed according to the manufacturer's instructions. Plasmid DNA was eluted with 30 µl EB buffer and genomic DNA was eluted with 200 µl EB buffer.

3.3.10 DIGESTION OF DNA SAMPLES

To confirm the presence of the desired DNA fragments in plasmids or to prepare the DNA for other processes, a restriction digest was performed. By using appropriate restriction enzymes and associated buffers, DNA molecules were cleaved at selected sites. The reaction mixture was set up as follows:

Component	**Amount**
DNA (200-1,000 ng)	10 µl
10× Cutsmart Buffer (New England BioLabs)	2 µl
Enzyme I (10 U/µl)	0.5 µl
Enzyme II (10 U/µl)	0.5 µl
ddH_2O	up to 20 µl

3.3.11 SEQUENCING

SEQLAB Gmbh in Göttingen carried out the Sanger DNA sequencing. For this purpose, 60-100 ng/µl plasmid DNA and 2 pmol/µl of an appropriate primer were diluted in 15 µl pure water.

3.3.12 LIVE-CELL TIME-LAPSE IMAGING

For live-cell imaging experiments, I used 24-well imaging plates (ibidi). I seeded 3×10^4 cells per well and incubated them in growth-medium for 40 - 46 h. Afterwards, cells were incubated for at least 48 h in serum- and growth factor-free medium to ensure that cells go into a quiescent state. To compare proliferating and quiescent cells, additional cells were seeded and incubated in growth-medium. At least 1 h before the experiment, I changed medium to microscopy- or deprivation-microscopy-medium. Cells were imaged with the same setup as described in 2.3.2. Over 24 h, images were taken every 6 min. For long-term experiments (120 h), images were taken every 20 min and medium was exchanged every 48 h to ensure sustained ligand stimulation.

3.3.13 LIGAND AND INHIBITOR TREATMENT

Inhibitor and ligand treatments were performed in the appropriate medium. Recombinant TGFb, GDF8 and GDF11 were stored at -80 °C in 4 mM HCl and 1 mg/ml bovine serum. Recombinant activin A and GDF3 were stored at -80 °C in 1 mg/ml bovine serum. If not indicated differently, inhibitors were diluted in DMSO and stored at -20 °C. Ligands and inhibitors were used as indicated below. Before the treatment, cells were imaged for 1 h. Usually, the ligands/inhibitors were prepared in 125 µl of medium and added to the cells to achieve the desired concentration in a final volume of 625 µl. Restimulations were carried out by aspirating the old medium and changing to new medium containing the desired

ligand/inhibitor concentration. Control cells were treated with medium only or medium containing DMSO.

Inhibitors and ligands	Used concentration
Gefitinib EGFR inhibitor	10 µM
Ly294002 PI3K inhibitor	50 µM
Palbociclib CDK4/6 inhibitor in Sodium DL-Lactate	10 µM
Selumetinib (AZD6244) MEK1/2 inhibitor	1 µM
Activin A	1 nM and 20 nM
GDF3 (Peprotech)	1 nM and 20 nM
GDF8 (Peprotech)	1 nM and 20 nM
GDF11 (Peprotech)	various concentrations
TGFb (Peprotech)	various concentrations

3.3.14 DATA ANALYSIS OF LIVE-CELL MICROSCOPY EXPERIMENTS

Cells were tracked as described in 2.3.5. Afterwards, the integrated nuclear fluorescence intensity was quantified and the fluorescence intensity in the cytoplasm was measured using a 4-pixel wide annulus around the nucleus. To ensure that each annulus only measured the corresponding cytoplasm, the annulus was prevented from overlapping with neighboring cytoplasmic and nuclear regions. However, it could not be excluded that it contained extracellular areas. The median fluorescence intensity for each cell over time was measured within the area of the annulus. Together with the median fluorescence intensity of the nucleus, the nuc/cyt SMAD2 ratio was calculated.

3.3.14.1 QUANTIFICATION OF CELL DIVISIONS

To quantify divisions of individual cells, the shape and size of the nucleus as well as the integrated H2B-CFP fluorescence intensity were tracked and analyzed. If the size and intensity decrease by approximately 50 % within a certain time window, the event is considered a cell division. As nuclear envelope breakdown during mitosis could influence measurements of SMAD translocation, the data between 20 min before and 40 min after mitosis were removed by interpolation. To further minimize disturbing factors in the analysis, spikes which appear in all cells simultaneously were removed by interpolation as they usually indicate a flickering of the fluorescent lamp.

3.3.14.2 QUANTIFICATION OF CELL MOTILITY

To quantify the motility of individual cells, Euclidean distances between two subsequent positions of a single cell were calculated based on the x and y coordinates measured in pixels. When the distance covered between two time points exceeded a certain threshold (three times the average distance covered over all cells), the trajectories were ignored for the following analysis. In order to calculate the

motility score, the mean distance covered during two consecutive time points was determined for each cell.

3.3.15 IMMUNOFLUORESCENCE

For immunofluorescence experiments, 2 × 10^5 wild-type MCF10A cells were seeded on coverslips coated with poly-L-lysine (Sigma) and incubated in growth-medium for 2 days. After a 48-h growth factor and serum deprivation, cells were stimulated with TGFb or GDF11 and fixed at indicated time points with 2 % paraformaldehyde in PBS for 10 minutes. Permeabilization, antibody staining, and Hoechst staining were performed as described in 2.3.8. Coverslips were embedded in Prolong Antifade (Thermo Fisher Scientific) and stored over night at room temperature. The next day, images were acquired with the same objective and filter sets as described in 2.3.2. Again, automated segmentation was performed in MATLAB (MathWorks) with algorithms from CellProfiler (Carpenter et al., 2006).

Antibody	**Dilution**
Rabbit monoclonal anti-total SMAD2 (Cell Signaling Technology)	1:100
Goat polyclonal anti-rabbit AlexaFluor™ 647 (Thermo Fisher Scientific)	1:1,000

3.3.16 CELL CYCLE ANALYSIS

Cells were seeded and treated as described in 3.3.12. Proliferating and quiescent cells were incubated with 10 mM EdU (EdU Click-647) for 1 h. EdU was washed off with PBS and cells were fixed with 2 % paraformaldehyde in PBS for 10 min at room temperature. Afterwards, cells were washed with PBS, permeabilized with 0.1 % Triton X-100 in PBS and blocked with 10 % goat serum in PBS. For EdU detection, a reaction cocktail was prepared according to the manufacturer's instructions and added to the cells. After 30 min incubation at room temperature, cells were washed and counterstained with 0.4 mg/ml DAPI in deionized water for 5 min. Cells were washed with deionized water and imaged with a widefield microscope (Axiovert 200M with a 10× objective, Zeiss). Cells were automatically scanned and the EdU signal intensity was plotted against the DAPI signal intensity by utilizing the program MetaCyte (MetaSystems). To determine the number of cells in G1-, S-, and G2-phase, the cell cycle distribution generated by MetaCyte was used.

3.3.17 WESTERN BLOT ANALYSIS

For quantification of protein levels, 6 × 10^5 wild-type MCF10A or S2-R cells were seeded on 6 cm tissue culture plates and incubated in growth-medium for 2 days. After a 48-h growth factor and serum deprivation, cells were stimulated for the indicated time points and then harvested in 2 ml PBS by scraping. Cells were centrifuged and frozen in liquid nitrogen. For protein extraction, cells were lysed

on ice with 50 µl lysis buffer (RIPA) containing 1 % protease inhibitor (Carl Roth), 1 % phosphatase inhibitor (Sigma), 50 mM Tris (Carl Roth), 100 mM NaCl (Carl Roth), 1 % Triton X-100, 0.5 % Na-Deoxycholate (Carl Roth) and 0.1 % SDS (Carl Roth). Cell debris was removed by centrifugation at 4 °C and protein concentration was determined by Bradford protein assay (Roti-Nanoquant, Carl Roth). Afterwards, proteins were denatured with NuPAGE 4× Sample buffer (Invitrogen) and 50 mM reducing agent (DTT, Sigma) for 10 min at 70 °C. Each protein sample (10-20 µg) was loaded on a 10 % SDS-PAGE gel and separated for 1 h at 180 V using the Mini Trans-Blot® Cell System (Biorad) with running buffer containing 25 mM Tris/HCl (Carl Roth), 0.2 M glycine (Carl Roth) and 0.5 % SDS. For molecular weight estimation 7 µl of Precision Plus ProteinTM Dual Color Standards (Biorad) were loaded on the gel. After the run was finished, proteins were transferred to a polyvinylidene difluoride (PVDF) membrane (Carl Roth) for 1.5 h at 200 mA using the same chamber with transfer buffer containing 25 mM Tris, 192 mM glycine and 20 % methanol. To cover unspecific reaction sites, the membrane was blocked with 5 % nonfat-dried milk or BSA in TBS-T for 1 h at room temperature. In the next step, the primary antibodies (listed below) were diluted in the respective blocking solution and incubated with the membrane overnight at 4° C. The next day the membrane was washed with TBS-T and incubated with an HRP (horseradish peroxidase) conjugated goat anti-rabbit/mouse secondary antibody for 1 h at room temperature. Washing steps were performed as before and finally the detection of the transferred proteins was carried out by using the Amersham ECL Prime Western Blotting Detection Kit (GE Healthcare). Chemiluminescent images were captured with a Fusion Fx documentation system (Vilber Lourmat). Western blot bands were quantified with Image J's gel analysis tool.

Antibody	**Dilution**
Mouse monoclonal anti-Actin (Thermo Fisher Scientific)	1:5,000
Mouse monoclonal anti-FST (Santa Cruz)	1:300
Rabbit monoclonal anti-GAPDH (Sigma Aldrich)	1:5,000
Rabbit monoclonal anti-pSMAD2 (Cell Signaling Technology)	1:1,000
Rabbit monoclonal anti-TGFBR3 (Cell Signaling Technology)	1:1,000
Rabbit monoclonal anti-cleaved caspase 7 (Cell Signaling Technology)	1:1,000
Goat polyclonal anti-mouse, HRP conjugated (Thermo Fisher Scientific)	1:10,000
Goat polyclonal anti-rabbit, HRP conjugated (Invitrogen)	1:10,000

3.3.18 RNA ISOLATION AND CDNA SYNTHESIS

For RNA isolation, S2-R cells were seeded, stimulated and harvested as described in 3.3.17. Total RNA was isolated from the cells using the High Pure RNA Isolation Kit by Roche according to the manufacturer´s instructions. The RNA was eluted in 30 µl EB buffer and the concentration was determined using the spectrophotometer NanoDrop 2000c. For each sample, 1 µg of RNA was

converted into cDNA by using the reverse transcriptase and oligo dT primer (NEB First Strand cDNA Synthesis Kit). To this end, the following components were mixed and heated for 5 min at 70 °C.

Component	Amount
RNA	1 µg
dNTP mix (10 mM)	1 µl
Oligo dT	2 µl
DEPC-treated H_2O	8 µl

Afterwards, the components listed below were added and the resulting mixture was incubated for 1 h at 42 °C.

Component	Amount
5× Reaction Buffer	4 µl
DTT (1 M)	2 µl
RNase inhibitor	1 µl
Reverse transcriptase	1 µl

Enzymes were inactivated at 80 °C for 5 min and 180 µl DEPC-treated H_2O were added for dilution.

3.3.19 REAL-TIME QUANTITATIVE PCR

The RT-qPCR was performed in the StepOnePlus™ Real-Time PCR System (Thermo Fisher Scientific) using a 96-well plate (Applied Biosystems) and an adhesive foil (Biozym). All samples were carried out in triplicates. The real-time PCR was performed with the following reaction setup and program:

Component	Amount
cDNA	3 µl
SYBR Green Master Mix (Roche)	12.5 µl
forward primer (640 nM)	4.75 µl
reverse primer (640 nM)	4.75 µl

Step	Temperature	Time	Cycles
Holding stage	95 °C	10 min	1
Cycling stage 1	95 °C	15 s	40
Cycling stage 2	60 °C	1 min	40
Melt curve stage 1	95 °C	15 s	1
Melt curve stage 2	60 °C	1 min	1
Melt curve stage 3	60-95 °C, +0.3 °C	15 s	10

To determine the level of expression for each gene of interest, the comparative CT (ΔΔCT) method was used. First, the difference between the CT value of a housekeeping gene (Actin) and the CT value of

the gene of interest was calculated resulting in the ΔCT value. Then, the difference in the ΔCT values between the experimental and control samples is calculated resulting in the ΔΔCT value.

RT-qPCR primer	Sequence (5'-> 3')
Actin_for	GGCACCCAGCACAATGAAGATCAA
Actin_rev	TAGAAGCATTTGCGGTGGACGATG
CDH1_for	TCCAAAGCCTCAGGTCAT
CDH1_rev	CTCCTCCGAAGAAACAGC
FST_for	TGCTCTGCCAGTTCATGG
FST_rev	CTTGACGGACCCAGCAGT
MYC_for	TATTCTGCCCATTTGGGGACA
MYC_rev	TTGGTGAAGCTAACGTTGAGG
SNAI1_for	GCTCGAAAGGCCTTCAACTGCAAA
SNAI1_rev	AGGCAGAGGACACAGAACCAGAAA
VIM_for	AGGAAATGGCTCGTCACCTTCGTGATTA
VIM_rev	GGAGTGTCGGTTGTTAAGAACTAGAGCT

3.3.20 RNA SEQUENCING

For the RNA sequencing, S2-R cells were seeded, stimulated and harvested as described in 3.3.17. Afterwards, RNA was isolated as described in 3.3.18. Two biological replicates for each condition were prepared. The RNA sequencing itself and subsequent data processing were performed by the IMB Genomics Core Facility (Mainz). Further data evaluation was carried out by Lorenz Ripka (IMB Mainz). To generate the next generation sequencing (NGS) libraries the TruSeq stranded mRNA LT Sample Prep Kit (Illumina) was used according to the manufacturer's instructions. Libraries were prepared with a starting amount of 500 ng RNA, amplified in 11 PCR cycles, and profiled using a DNA 1000 kit and a 2100 Bioanalyzer (both Agilent). Afterwards, the libraries were quantified in a Qubit 2.0 Fluorometer using the dsDNA HS Assay Kit (both Thermo Fisher). All libraries were pooled in equimolar ratios and sequenced on the NextSeq 500 sequencing system (Illumina) with the following parameters: high-output flow cell, single-read mode and 84 cycles plus 7 cycles index read. The poly(A) RNA sequencing was conducted in a non-strand specific mode with a coverage of 50 bp reads. Utilizing the software bcl2fastq (v.2.19.1.403, Illumina), samples were demultiplexed and FastQ files were generated. The raw sequence reads were assessed with FastQC (v.0.11.5, Babraham Bioinformatics) and then aligned to the human reference genome GRCh38.p7 (GTF annotation file from Gencode human release 25) using the STAR aligner (Dobin et al., 2013, v.2.5.2b). The mapped data were summarized on the gene level using the software featureCounts (v.1.6.2, Subread). Further data evaluation, normalization and pairwise differential expression analyses were carried out in R (v.3.5.0) using the Bioconductor package DESeq2 (v.1.20.0) following the recommended analysis workflow. To

calculate the robust reads per kilobase of transcript per million mapped reads (RPKMs) for each gene, the Bioconductor packages GenomicRanges (v.1.32.1) and rtracklayer (v.1.40.6) with the above-mentioned GTF annotation file and robust fragments per million (FPM) data computed by DESeq2 were used. To calculate fold changes, this package uses a maximum likelihood model with the assumption of a negative binomial distribution of reads fitted to the read counts of all samples available for a given combination of conditions. Additionally, based on those models, p-values were calculated for each fold change that refer to the differential expression compared to a reference condition. This part (3.3.20) was written in collaboration with Lorenz Ripka (IMB Mainz).

4 CONCLUSION

The overall objective of this study was to gain an improved understanding of the interplay between different signaling pathways through quantitative and time-resolved dissection of the MEK/ERK, PI3K/AKT and SMAD networks at the single-cell level. With this approach, I was able to disentangle the contributions of the MAPK and PI3K/AKT pathways to mitogenic signaling during different cell cycle phases. Furthermore, I discovered that MAPK signaling strongly affected the SMAD network and shaped ligand-specific signaling dynamics of SMAD2, which is most likely mediated through gene expression changes. Interestingly, these dynamics are more decisive for cellular responses than the ligands themselves, suggesting a quantitative rather than qualitative signaling pathway. Thus, MAPK activity not only affected activation patterns of SMAD molecules but also SMAD-associated cell fate decisions such as apoptosis and EMT. Conversely, SMAD signaling decreased the expression of cell cycle regulators like *MYC* and thereby counteracted the pro-mitotic signals mediated by MEK/ERK and PI3K/AKT pathways. This shows how tightly different signaling pathways are connected and how they interact to orchestrate changes in gene expression and signaling dynamics to ultimately control important cellular outcomes such as proliferation, quiescence, migration and apoptosis.

The interplay between MAPK and SMAD pathways has been investigated before and there is broad evidence that SMAD signaling is integrated in a complex network with other signaling pathways that modify initial SMAD signals (Javelaud and Mauviel, 2005). For example, it has been shown that ligands like TGFb not only signal through SMAD proteins but also activate signaling networks involving MAPK and PI3K. Conversely, these pathways can modulate the outcome of ligand-induced SMAD signaling by regulating R-SMADs through phosphorylation of the corresponding linker-regions, regulating I-SMADs or altering gene expression (Zhang and Derynck, 1999; Lutz and Knaus, 2002; Wakefield and Roberts, 2002; Derynck and Zhang, 2003). Many studies have shown that the expression of SMAD pathway-associated genes can be modified through other networks. For instance, MEK activity is required for the expression of *TGFB1* and positively regulates *SMAD3* gene transcription (Yue and Mulder, 2000; Ross et al., 2007). Furthermore, EGF can induce the expression of I-SMADs and the kinase JNK has a repressive effect on the *TGFB1* gene (Afrakhte et al., 1998; Ventura et al., 2004). These observations are compatible with my results that showed that multiple SMAD pathway-associated genes are differentially expressed without sustained MAPK activity.

Although there are already numerous studies showing crosstalk between the SMAD and MAPK signaling pathways, my work additionally provides time-resolved single-cell measurements of SMAD activity and thus reveals that the interaction of the corresponding pathway with mitogenic signals

leads to an increase or decrease in SMAD2 signaling dynamics depending on the ligand. These results highlight how simple and straight forward pathways gain complexity by interacting with other signaling networks. While I shed some light on the interplay between the MEK/ERK, PI3K/AKT and SMAD pathways, it should be mentioned that further studies need to follow in order to grasp signaling crosstalk in its entirety. As there are many more pathways affecting SMAD signaling such as the WNT, Notch, p53 and NF-κB pathways (Elston and Inman, 2012; Luo, 2017), which can additionally influence one another (Dotto, 2009; Kim et al., 2011; Konrath et al., 2020), a complete understanding of the convoluted interplay constitutes a great challenge. Nonetheless, since comprehending complex biological systems provides valuable knowledge and should be the ambition of systems biology, it is crucial to further research pathway interactions to ultimately understand the larger picture. But why is it important to gain a profound knowledge of the interplay of signaling networks? A good example to answer this question is the interaction of the SMAD and MAPK pathways in cancer progression. Usually, in healthy tissues these pathways operate in opposite directions, however, in different cancers the corresponding pathways are simultaneously activated and promote the malignant state (Chapnick et al., 2011). For instance, the crosstalk between SMAD and MAPK pathways is required for the formation of metastasis. Consistent with my results, it has been reported that none of the two pathways is capable of inducing the transition from an epithelial to mesenchymal phenotype alone (Janda et al., 2002). Interestingly, Janda et al., 2002, also showed that TGFb-induced apoptosis requires a sustained lack of PI3K signaling. Although my results also only showed apoptosis in growth factor-deprived cells and thus without active PI3K, I did not observe an increase in cell death when cells were treated for 48 h with a PI3K inhibitor and subsequently with TGFb or GDF11 (data not shown). Therefore, further pathway interactions may regulate the induction of apoptosis in MCF10A cells. Understanding such molecular details and the relative contributions of each signaling pathway to cell fate decisions is thereby essential to devise therapeutic interventions that counteract altered cellular outcomes. While there are already plenty of inhibitors and antagonistic antibodies of the ERK and SMAD pathways under evaluation in clinical trials (Yingling et al., 2004; Arteaga, 2006; Roberts and Der, 2007), it may be advantageously to utilize a combinatorial approach when considering the interplay between the different pathways. The information provided by my work, such as that MAPK and PI3K/AKT activity are required for proper cell cycle entry and progression, or that the cell state changes SMAD-associated dynamics and cellular responses, may be of use in the development of such combinatorial therapies.

Simultaneously targeting mitogenic signals and the SMAD pathway could be of particular interest in tissues that rely heavily on both networks during their development and in the adult organism and that

often exhibit dysregulations of both signaling networks in cancer. The mammary gland is a perfect example for such a tissue, as it constantly employs the corresponding pathways to facilitate the switch between proliferation states and as approximately 90 % of breast cancer deaths are associated with invasion and distant metastasis (Wang and Zhou, 2011).

The results of this study were all obtained in breast epithelial cells and thereby most relatable to the mammary tissue. However, it should be kept in mind that all experiments in this work were performed *in vitro* under isolated conditions. Therefore, as a next step it would be intriguing to put my observations into context with the mammary gland *in vivo*, where many other factors interact to regulate biological mechanisms. While I have already included different proliferation states into the equation by investigating pathways in quiescent cells without abundant growth factors, there are many more parameters to consider. For instance, the development of the mammary gland is mainly controlled by signals from the mesenchyme and circulating hormones such as estrogen, progesteron and growth hormones (Macias and Hinck, 2012). In my experimental approach, growth control was primarily regulated by EGF. Thus, it would be interesting to see how hormonal cues affect the interplay between different pathways and ultimately cell fate decisions. Furthermore, examining the activity of MAPK, PI3K/AKT, SMAD or other pathways during the development of the mammary gland could give deeper insight into how different networks interact to precisely regulate proliferation, quiescence, migration and apoptosis.

Taken together, although extensive biochemical and genetic studies already characterized most signaling pathways in molecular detail, their relative contribution and interplay in governing cell fate decisions remain largely unexplored. The present thesis shows how important the crosstalk between pathways is, since interfering with different interactions can lead to a strong delay in cell cycle progression or even trigger completely different cell fates. Further studies combining time-resolved quantitative experiments with computer-aided analysis and correlating the data to cellular outcomes will provide the insight for comprehending the bigger picture of pathway interplay.

5 REFERENCES

Afrakhte, M., Morén, A., Jossan, S., Itoh, S., Sampath, K., Westermark, B., Heldin, C.H., Heldin, N.E., and Dijke, P. ten (1998). Induction of inhibitory Smad6 and Smad7 mRNA by TGF-beta family members. Biochemical and Biophysical Research Communications *249*, 505-511. https://doi.org/10.1006/bbrc.1998.9170.

Albeck, J.G., Mills, G.B., and Brugge, J.S. (2013). Frequency-Modulated Pulses of ERK Activity Transmit Quantitative Proliferation Signals. Molecular Cell *49*, 249-261. https://doi.org/10.1016/j.molcel.2012.11.002.

Andersson, O., Reissmann, E., and Ibáñez, C.F. (2006). Growth differentiation factor 11 signals through the transforming growth factor-beta receptor ALK5 to regionalize the anterior-posterior axis. EMBO Reports *7*, 831-837. https://doi.org/10.1038/sj.embor.7400752.

Ankers, J.M., Spiller, D.G., White, M.R., and Harper, C.V. (2008). Spatio-temporal protein dynamics in single living cells. Current Opinion in Biotechnology *19*, 375-380. https://doi.org/10.1016/j.copbio.2008.07.001.

Antebi, Y.E., Linton, J.M., Klumpe, H., Bintu, B., Gong, M., Su, C., McCardell, R., and Elowitz, M.B. (2017). Combinatorial Signal Perception in the BMP Pathway. Cell *170*, 1184-1196.e24. https://doi.org/10.1016/j.cell.2017.08.015.

Arima, Y., Inoue, Y., Shibata, T., Hayashi, H., Nagano, O., Saya, H., and Taya, Y. (2008). Rb depletion results in deregulation of e-cadherin and induction of cellular phenotypic changes that are characteristic of the epithelial-to-mesenchymal transition. Cancer Research *68*, 5104-5112. https://doi.org/10.1158/0008-5472.CAN-07-5680.

Arora, M., Moser, J., Phadke, H., Basha, A.A., and Spencer, S.L. (2017). Endogenous Replication Stress in Mother Cells Leads to Quiescence of Daughter Cells. Cell Reports *19*, 1351-1364. https://doi.org/10.1016/j.celrep.2017.04.055.

Arteaga, C.L. (2006). Inhibition of TGFbeta signaling in cancer therapy. Current Opinion in Genetics & Development *16*, 30-37. https://doi.org/10.1016/j.gde.2005.12.009.

Bajikar, S.S., Wang, C.-C., Borten, M.A., Pereira, E.J., Atkins, K.A., and Janes, K.A. (2017). Tumor-Suppressor Inactivation of GDF11 Occurs by Precursor Sequestration in Triple-Negative Breast Cancer. Developmental Cell *43*, 418-435.e13. https://doi.org/10.1016/j.devcel.2017.10.027.

Barker, N. (2014). Adult intestinal stem cells: critical drivers of epithelial homeostasis and regeneration. Nature reviews. Molecular cell biology *15*, 19-33. https://doi.org/10.1038/nrm3721.

Barr, A.R., Cooper, S., Heldt, F.S., Butera, F., Stoy, H., Mansfeld, J., Novák, B., and Bakal, C. (2017). DNA damage during S-phase mediates the proliferation-quiescence decision in the subsequent G1 via p21 expression. Nature Communications *8*, 14728. https://doi.org/10.1038/ncomms14728.

Belinky, F., Nativ, N., Stelzer, G., Zimmerman, S., Iny Stein, T., Safran, M., and Lancet, D. (2015). PathCards: multi-source consolidation of human biological pathways. Database : The Journal of Biological Databases and Curation *2015*. https://doi.org/10.1093/database/bav006.

Benary, M., Bohn, S., Lüthen, M., Nolis, I.K., Blüthgen, N., and Loewer, A. (2020). Disentangling Pro-mitotic Signaling during Cell Cycle Progression using Time-Resolved Single-Cell Imaging. Cell Reports *31*, 107514. https://doi.org/10.1016/j.celrep.2020.03.078.

Bendris, N., Lemmers, B., Blanchard, J.-M., and Arsic, N. (2011). Cyclin A2 mutagenesis analysis: A new insight into CDK activation and cellular localization requirements. PloS one *6*, e22879. https://doi.org/10.1371/journal.pone.0022879.

Bewick, V., Cheek, L., and Ball, J. (2004). Statistics review 12: Survival analysis. Critical Care *8*, 389. https://doi.org/10.1186/cc2955.

Bianconi, E., Piovesan, A., Facchin, F., Beraudi, A., Casadei, R., Frabetti, F., Vitale, L., Pelleri, M.C., Tassani, S., and Piva, F., et al. (2013). An estimation of the number of cells in the human body. Annals of Human Biology *40*, 463-471. https://doi.org/10.3109/03014460.2013.807878.

Boer, L. de, Oakes, V., Beamish, H., Giles, N., Stevens, F., Somodevilla-Torres, M., Desouza, C., and Gabrielli, B. (2008). Cyclin A/cdk2 coordinates centrosomal and nuclear mitotic events. Oncogene *27*, 4261-4268. https://doi.org/10.1038/onc.2008.74.

Bruce, D.L., and Sapkota, G.P. (2012). Phosphatases in SMAD regulation. FEBS Letters *586*, 1897-1905. https://doi.org/10.1016/j.febslet.2012.02.001.

Buettner, F., Natarajan, K.N., Casale, F.P., Proserpio, V., Scialdone, A., Theis, F.J., Teichmann, S.A., Marioni, J.C., and Stegle, O. (2015). Computational analysis of cell-to-cell heterogeneity in single-cell RNA-sequencing data reveals hidden subpopulations of cells. Nature Biotechnology *33*, 155-160. https://doi.org/10.1038/nbt.3102.

Burch, P.M., Yuan, Z., Loonen, A., and Heintz, N.H. (2004). An extracellular signal-regulated kinase 1- and 2-dependent program of chromatin trafficking of c-Fos and Fra-1 is required for cyclin D1 expression during cell cycle reentry. Molecular and Cellular Biology *24*, 4696-4709. https://doi.org/10.1128/MCB.24.11.4696-4709.2004.

Cantley, L.C. (2002). The phosphoinositide 3-kinase pathway. Science (New York, N.Y.) *296*, 1655-1657. https://doi.org/10.1126/science.296.5573.1655.

Carpenter, A.E., Jones, T.R., Lamprecht, M.R., Clarke, C., Kang, I.H., Friman, O., Guertin, D.A., Chang, J.H., Lindquist, R.A., and Moffat, J., et al. (2006). CellProfiler: image analysis software for identifying and quantifying cell phenotypes. Genome Biology *7*, R100. https://doi.org/10.1186/gb-2006-7-10-r100.

Chalaux, E., López-Rovira, T., Rosa, J.L., Pons, G., Boxer, L.M., Bartrons, R., and Ventura, F. (1999). A zinc-finger transcription factor induced by TGF-β promotes apoptotic cell death in epithelial Mv1Lu cells. FEBS Letters *457*, 478-482. https://doi.org/10.1016/S0014-5793(99)01051-0.

Chambard, J.-C., Lefloch, R., Pouysségur, J., and Lenormand, P. (2007). ERK implication in cell cycle regulation. Biochimica et Biophysica Acta *1773*, 1299-1310. https://doi.org/10.1016/j.bbamcr.2006.11.010.

Chang, C. (2016). Agonists and Antagonists of TGF-β Family Ligands. Cold Spring Harbor Perspectives in Biology *8*. https://doi.org/10.1101/cshperspect.a021923.

Chang, H., Brown, C.W., and Matzuk, M.M. (2002). Genetic analysis of the mammalian transforming growth factor-beta superfamily. Endocrine Reviews *23*, 787-823. https://doi.org/10.1210/er.2002-0003.

Chapnick, D.A., Warner, L., Bernet, J., Rao, T., and Liu, X. (2011). Partners in crime: the TGFβ and MAPK pathways in cancer progression. Cell & bioscience *1*, 42. https://doi.org/10.1186/2045-3701-1-42.

Chen, H.B., Shen, J., Ip, Y.T., and Xu, L. (2006). Identification of phosphatases for Smad in the BMP/DPP pathway. Genes & Development *20*, 648-653. https://doi.org/10.1101/gad.1384706.

Chen, J.-Y., Lin, J.-R., Cimprich, K.A., and Meyer, T. (2012). A two-dimensional ERK-AKT signaling code for an NGF-triggered cell-fate decision. Molecular Cell *45*, 196-209. https://doi.org/10.1016/j.molcel.2011.11.023.

Chen, W., Dong, J., Haiech, J., Kilhoffer, M.-C., and Zeniou, M. (2016). Cancer Stem Cell Quiescence and Plasticity as Major Challenges in Cancer Therapy. Stem Cells International *2016*, 1740936. https://doi.org/10.1155/2016/1740936.

Chen, X., Weisberg, E., Fridmacher, V., Watanabe, M., Naco, G., and Whitman, M. (1997). Smad4 and FAST-1 in the assembly of activin-responsive factor. Nature *389*, 85-89. https://doi.org/10.1038/38008.

Chen, Y.-G. (2009). Endocytic regulation of TGF- signaling. Cell Research *19*, 58-70. https://doi.org/10.1038/cr.2008.315.

Cheng, Q., Du, J., Xie, L., Liu, X., Li, Z., Zuo, F., Wu, J., and Xu, J. (2018). Inhibition of SOX4 induces melanoma cell apoptosis via downregulation of NF-κB p65 signaling. Oncology Reports *40*, 369-376. https://doi.org/10.3892/or.2018.6443.

Cheung, T.H., and Rando, T.A. (2013). Molecular regulation of stem cell quiescence. Nature reviews. Molecular cell biology *14*, 329-340. https://doi.org/10.1038/nrm3591.

Chou, J.L., Fan, Z., DeBlasio, T., Koff, A., Rosen, N., and Mendelsohn, J. (1999). Constitutive overexpression of cyclin D1 in human breast epithelial cells does not prevent G1 arrest induced by deprivation of epidermal growth factor. Breast Cancer Research and Treatment *55*, 267-283. https://doi.org/10.1023/a:1006217413089.

Clijsters, L., Ogink, J., and Wolthuis, R. (2013). The spindle checkpoint, APC/C(Cdc20), and APC/C(Cdh1) play distinct roles in connecting mitosis to S phase. The Journal of Cell Biology *201*, 1013-1026. https://doi.org/10.1083/jcb.201211019.

Clurman, B.E., Sheaff, R.J., Thress, K., Groudine, M., and Roberts, J.M. (1996). Turnover of cyclin E by the ubiquitin-proteasome pathway is regulated by cdk2 binding and cyclin phosphorylation. Genes & Development, 1979-1990. https://doi.org/10.1101/gad.10.16.1979.

Cohen, A.A., Geva-Zatorsky, N., Eden, E., Frenkel-Morgenstern, M., Issaeva, I., Sigal, A., Milo, R., Cohen-Saidon, C., Liron, Y., and Kam, Z., et al. (2008). Dynamic proteomics of individual cancer cells in

response to a drug. Science (New York, N.Y.) *322*, 1511-1516. https://doi.org/10.1126/science.1160165.

Cohen-Saidon, C., Cohen, A.A., Sigal, A., Liron, Y., and Alon, U. (2009). Dynamics and variability of ERK2 response to EGF in individual living cells. Molecular Cell *36*, 885-893. https://doi.org/10.1016/j.molcel.2009.11.025.

Dangi, S., Cha, H., and Shapiro, P. (2003). Requirement for phosphatidylinositol-3 kinase activity during progression through S-phase and entry into mitosis. Cellular Signalling *15*, 667-675. https://doi.org/10.1016/S0898-6568(03)00002-0.

David, C.J., Huang, Y.-H., Chen, M., Su, J., Zou, Y., Bardeesy, N., Iacobuzio-Donahue, C.A., and Massagué, J. (2016). TGF-β Tumor Suppression through a Lethal EMT. Cell *164*, 1015-1030. https://doi.org/10.1016/j.cell.2016.01.009.

David, C.J., and Massagué, J. (2018). Contextual determinants of TGFβ action in development, immunity and cancer. Nature reviews. Molecular cell biology *19*, 419-435. https://doi.org/10.1038/s41580-018-0007-0.

Derynck, R., and Zhang, Y.E. (2003). Smad-dependent and Smad-independent pathways in TGF-beta family signalling. Nature *425*, 577-584. https://doi.org/10.1038/nature02006.

Dobin, A., Davis, C.A., Schlesinger, F., Drenkow, J., Zaleski, C., Jha, S., Batut, P., Chaisson, M., and Gingeras, T.R. (2013). STAR: ultrafast universal RNA-seq aligner. Bioinformatics (Oxford, England) *29*, 15-21. https://doi.org/10.1093/bioinformatics/bts635.

Dong, J., Peng, J., Zhang, H., Mondesire, W.H., Jian, W., Mills, G.B., Hung, M.-C., and Meric-Bernstam, F. (2005). Role of glycogen synthase kinase 3beta in rapamycin-mediated cell cycle regulation and chemosensitivity. Cancer Research *65*, 1961-1972. https://doi.org/10.1158/0008-5472.CAN-04-2501.

Dotto, G.P. (2009). Crosstalk of Notch with p53 and p63 in cancer growth control. Nature reviews. Cancer *9*, 587-595. https://doi.org/10.1038/nrc2675.

Ekholm, S.V., Zickert, P., Reed, S.I., and Zetterberg, A. (2001). Accumulation of cyclin E is not a prerequisite for passage through the restriction point. Molecular and Cellular Biology *21*, 3256-3265. https://doi.org/10.1128/MCB.21.9.3256-3265.2001.

El-Brolosy, M.A., and Stainier, D.Y.R. (2017). Genetic compensation: A phenomenon in search of mechanisms. PLoS Genetics *13*, e1006780. https://doi.org/10.1371/journal.pgen.1006780.

Elderbroom, J.L., Huang, J.J., Gatza, C.E., Chen, J., How, T., Starr, M., Nixon, A.B., and Blobe, G.C. (2014). Ectodomain shedding of TβRIII is required for TβRIII-mediated suppression of TGF-β signaling and breast cancer migration and invasion. Molecular Biology of the Cell *25*, 2320-2332. https://doi.org/10.1091/mbc.E13-09-0524.

Elston, R., and Inman, G.J. (2012). Crosstalk between p53 and TGF-β Signalling. Journal of signal transduction *2012*, 294097. https://doi.org/10.1155/2012/294097.

Elzen, N. den, and Pines, J. (2001). Cyclin A is destroyed in prometaphase and can delay chromosome alignment and anaphase. The Journal of Cell Biology *153*, 121-136. https://doi.org/10.1083/jcb.153.1.121.

Engelman, J.A., Luo, J., and Cantley, L.C. (2006). The evolution of phosphatidylinositol 3-kinases as regulators of growth and metabolism. Nature reviews. Genetics *7*, 606-619. https://doi.org/10.1038/nrg1879.

Fausto, N. (2004). Liver regeneration and repair: Hepatocytes, progenitor cells, and stem cells. Hepatology (Baltimore, Md.) *39*, 1477-1487. https://doi.org/10.1002/hep.20214.

Fekete, M., Santiskulvong, C., Eng, C., and Dorigo, O. (2012). Effect of PI3K/Akt Pathway Inhibition-Mediated G(1) Arrest on Chemosensitization in Ovarian Cancer Cells. Anticancer Research *32*, 445-452.

Feldman, D., Singh, A., Schmid-Burgk, J.L., Carlson, R.J., Mezger, A., Garrity, A.J., Zhang, F., and Blainey, P.C. (2019). Optical Pooled Screens in Human Cells. Cell *179*, 787-799.e17. https://doi.org/10.1016/j.cell.2019.09.016.

Feng, X.-H., and Derynck, R. (2005). Specificity and versatility in TGF-beta signaling through SMADS. Annual Review of Cell and Developmental Biology *21*, 659-693. https://doi.org/10.1146/annurev.cellbio.21.022404.142018.

Fernandes-Alnemri, T., Takahashi, A., Armstrong, R., Krebs, J., Fritz, L., Tomaselli, K.J., Wang, L., Yu, Z., Croce, C.M., and Salveson, G. (1995). Mch3, a novel human apoptotic cysteine protease highly related to CPP32. Cancer Research *55*, 6045-6052.

Fornetti, J., Flanders, K.C., Henson, P.M., Tan, A.-C., Borges, V.F., and Schedin, P. (2016). Mammary epithelial cell phagocytosis downstream of TGF-β3 is characterized by adherens junction reorganization. Cell Death and Differentiation *23*, 185-196. https://doi.org/10.1038/cdd.2015.82.

Gamer, L.W., Wolfman, N.M., Celeste, A.J., Hattersley, G., Hewick, R., and Rosen, V. (1999). A novel BMP expressed in developing mouse limb, spinal cord, and tail bud is a potent mesoderm inducer in Xenopus embryos. Developmental Biology *208*, 222-232. https://doi.org/10.1006/dbio.1998.9191.

García-Gutiérrez, L., Delgado, M.D., and León, J. (2019). MYC Oncogene Contributions to Release of Cell Cycle Brakes. Genes *10*. https://doi.org/10.3390/genes10030244.

Gerdes, J., Lemke, H., Baisch, H., Wacker, H.H., Schwab, U., and Stein, H. (1984). Cell cycle analysis of a cell proliferation-associated human nuclear antigen defined by the monoclonal antibody Ki-67. Journal of immunology (Baltimore, Md. : 1950) *133*, 1710-1715.

Giampieri, S., Manning, C., Hooper, S., Jones, L., Hill, C.S., and Sahai, E. (2009). Localized and reversible TGFbeta signalling switches breast cancer cells from cohesive to single cell motility. Nature Cell Biology *11*, 1287-1296. https://doi.org/10.1038/ncb1973.

Gillies, T.E., Pargett, M., Minguet, M., Davies, A.E., and Albeck, J.G. (2017). Linear Integration of ERK Activity Predominates over Persistence Detection in Fra-1 Regulation. Cell Systems *5*, 549-563.e5. https://doi.org/10.1016/j.cels.2017.10.019.

Gotoh, Y., Nishida, E., Yamashita, T., Hoshi, M., Kawakami, M., and Sakai, H. (1990). Microtubule-associated-protein (MAP) kinase activated by nerve growth factor and epidermal growth factor

in PC12 cells. Identity with the mitogen-activated MAP kinase of fibroblastic cells. European Journal of Biochemistry *193*, 661-669. https://doi.org/10.1111/j.1432-1033.1990.tb19384.x.

Guo, Q., Betts, C., Pennock, N., Mitchell, E., and Schedin, P. (2017). Mammary Gland Involution Provides a Unique Model to Study the TGF-β Cancer Paradox. Journal of Clinical Medicine *6*. https://doi.org/10.3390/jcm6010010.

Hay, N., and Sonenberg, N. (2004). Upstream and downstream of mTOR. Genes & Development *18*, 1926-1945. https://doi.org/10.1101/gad.1212704.

Hayashida, T., Decaestecker, M., and Schnaper, H.W. (2003). Cross-talk between ERK MAP kinase and Smad-signaling pathways enhances TGF-beta-dependent responses in human mesangial cells. FASEB Journal : Official Publication of the Federation of American Societies for Experimental Biology *17*, 1576-1578. https://doi.org/10.1096/fj.03-0037fje.

Heinrich, R., Neel, B.G., and Rapoport, T.A. (2002). Mathematical models of protein kinase signal transduction. Molecular Cell *9*, 957-970. https://doi.org/10.1016/s1097-2765(02)00528-2.

Heldin, C.-H., Landström, M., and Moustakas, A. (2009). Mechanism of TGF-beta signaling to growth arrest, apoptosis, and epithelial-mesenchymal transition. Current Opinion in Cell Biology *21*, 166-176. https://doi.org/10.1016/j.ceb.2009.01.021.

Hernandez-Aya, L.F., and Gonzalez-Angulo, A.M. (2011). Targeting the phosphatidylinositol 3-kinase signaling pathway in breast cancer. The Oncologist *16*, 404-414. https://doi.org/10.1634/theoncologist.2010-0402.

Hershko, A. (1999). Mechanisms and regulation of the degradation of cyclin B. Philosophical Transactions of the Royal Society of London. Series B, Biological sciences *354*, 1571-5; discussion 1575-6. https://doi.org/10.1098/rstb.1999.0500.

Hill, C.S. (2016). Transcriptional Control by the SMADs. Cold Spring Harbor Perspectives in Biology *8*. https://doi.org/10.1101/cshperspect.a022079.

Hinck, L., and Näthke, I. (2014). Changes in cell and tissue organization in cancer of the breast and colon. Current Opinion in Cell Biology *26*, 87-95. https://doi.org/10.1016/j.ceb.2013.11.003.

Hough, C., Radu, M., and Doré, J.J.E. (2012). Tgf-beta induced Erk phosphorylation of smad linker region regulates smad signaling. PloS one *7*, e42513. https://doi.org/10.1371/journal.pone.0042513.

Humphreys, P.A., Woods, S., Smith, C.A., Bates, N., Cain, S.A., Lucas, R., and Kimber, S.J. (2020). Optogenetic Control of the BMP Signaling Pathway. ACS Synthetic Biology *9*, 3067-3078. https://doi.org/10.1021/acssynbio.0c00315.

Hur, W., Rhim, H., Jung, C.K., Kim, J.D., Bae, S.H., Jang, J.W., Yang, J.M., Oh, S.-T., Kim, D.G., and Wang, H.J., et al. (2010). SOX4 overexpression regulates the p53-mediated apoptosis in hepatocellular carcinoma: clinical implication and functional analysis in vitro. Carcinogenesis *31*, 1298-1307. https://doi.org/10.1093/carcin/bgq072.

Ihry, R.J., Salick, M.R., Ho, D.J., Sondey, M., Kommineni, S., Paula, S., Raymond, J., Henry, B., Frias, E., and Wang, Q., et al. (2019). Genome-Scale CRISPR Screens Identify Human Pluripotency-Specific Genes. Cell Reports *27*, 616-630.e6. https://doi.org/10.1016/j.celrep.2019.03.043.

Ikushima, H., and Miyazono, K. (2010). TGFbeta signalling: a complex web in cancer progression. Nature reviews. Cancer *10*, 415-424. https://doi.org/10.1038/nrc2853.

Imamura, T., Takase, M., Nishihara, A., Oeda, E., Hanai, J., Kawabata, M., and Miyazono, K. (1997). Smad6 inhibits signalling by the TGF-beta superfamily. Nature *389*, 622-626. https://doi.org/10.1038/39355.

Inman, G.J., Nicolás, F.J., and Hill, C.S. (2002). Nucleocytoplasmic Shuttling of Smads 2, 3, and 4 Permits Sensing of TGF-β Receptor Activity. Molecular Cell *10*, 283-294. https://doi.org/10.1016/S1097-2765(02)00585-3.

Inman, J.L., Robertson, C., Mott, J.D., and Bissell, M.J. (2015). Mammary gland development: cell fate specification, stem cells and the microenvironment. Development (Cambridge, England) *142*, 1028-1042. https://doi.org/10.1242/dev.087643.

Janda, E., Lehmann, K., Killisch, I., Jechlinger, M., Herzig, M., Downward, J., Beug, H., and Grünert, S. (2002). Ras and TGFbeta cooperatively regulate epithelial cell plasticity and metastasis: dissection of Ras signaling pathways. The Journal of Cell Biology *156*, 299-313. https://doi.org/10.1083/jcb.200109037.

Javelaud, D., and Mauviel, A. (2005). Crosstalk mechanisms between the mitogen-activated protein kinase pathways and Smad signaling downstream of TGF-beta: implications for carcinogenesis. Oncogene *24*, 5742-5750. https://doi.org/10.1038/sj.onc.1208928.

Johnson, H.E., and Toettcher, J.E. (2019). Signaling Dynamics Control Cell Fate in the Early Drosophila Embryo. Developmental Cell *48*, 361-370.e3. https://doi.org/10.1016/j.devcel.2019.01.009.

Jones, S.M., and Kazlauskas, A. (2001). Growth-factor-dependent mitogenesis requires two distinct phases of signalling. Nature Cell Biology *3*, 165-172. https://doi.org/10.1038/35055073.

Jurkin, J., Zupkovitz, G., Lagger, S., Grausenburger, R., Hagelkruys, A., Kenner, L., and Seiser, C. (2011). Distinct and redundant functions of histone deacetylases HDAC1 and HDAC2 in proliferation and tumorigenesis. Cell Cycle (Georgetown, Tex.) *10*, 406-412. https://doi.org/10.4161/cc.10.3.14712.

Kabeya, Y., Mizushima, N., Ueno, T., Yamamoto, A., Kirisako, T., Noda, T., Kominami, E., Ohsumi, Y., and Yoshimori, T. (2000). LC3, a mammalian homologue of yeast Apg8p, is localized in autophagosome membranes after processing. The EMBO Journal *19*, 5720-5728. https://doi.org/10.1093/emboj/19.21.5720.

Kanehisa, M., Sato, Y., Kawashima, M., Furumichi, M., and Tanabe, M. (2016). KEGG as a reference resource for gene and protein annotation. Nucleic Acids Research *44*, D457-62. https://doi.org/10.1093/nar/gkv1070.

Katakura, Y., Nakata, E., Miura, T., and Shirahata, S. (1999). Transforming growth factor beta triggers two independent-senescence programs in cancer cells. Biochemical and Biophysical Research Communications *255*, 110-115. https://doi.org/10.1006/bbrc.1999.0129.

Katsimpardi, L., Litterman, N.K., Schein, P.A., Miller, C.M., Loffredo, F.S., Wojtkiewicz, G.R., Chen, J.W., Lee, R.T., Wagers, A.J., and Rubin, L.L. (2014). Vascular and neurogenic rejuvenation of the

aging mouse brain by young systemic factors. Science (New York, N.Y.) *344*, 630-634. https://doi.org/10.1126/science.1251141.

Kavsak, P., Rasmussen, R.K., Causing, C.G., Bonni, S., Zhu, H., Thomsen, G.H., and Wrana, J.L. (2000). Smad7 Binds to Smurf2 to Form an E3 Ubiquitin Ligase that Targets the TGFβ Receptor for Degradation. Molecular Cell *6*, 1365-1375. https://doi.org/10.1016/S1097-2765(00)00134-9.

Khalil, A.M., Dotimas, H., Kahn, J., Lamerdin, J.E., Hayes, D.B., Gupta, P., and Franti, M. (2016). Differential Binding Activity of TGF-β Family Proteins to Select TGF-β Receptors. The Journal of Pharmacology and Experimental Therapeutics *358*, 423-430. https://doi.org/10.1124/jpet.116.232322.

Kim, N.H., Kim, H.S., Kim, N.-G., Lee, I., Choi, H.-S., Li, X.-Y., Kang, S.E., Cha, S.Y., Ryu, J.K., and Na, J.M., et al. (2011). p53 and microRNA-34 are suppressors of canonical Wnt signaling. Science Signaling *4*, ra71. https://doi.org/10.1126/scisignal.2001744.

Kiyono, K., Suzuki, H.I., Matsuyama, H., Morishita, Y., Komuro, A., Kano, M.R., Sugimoto, K., and Miyazono, K. (2009). Autophagy is activated by TGF-beta and potentiates TGF-beta-mediated growth inhibition in human hepatocellular carcinoma cells. Cancer Research *69*, 8844-8852. https://doi.org/10.1158/0008-5472.CAN-08-4401.

Kolek, O., Gajkowska, B., Godlewski, M.M., and Motyl, T. (2003). Antiproliferative and apoptotic effect of TGF-β1 in bovine mammary epithelial BME-UV1 cells. Comparative Biochemistry and Physiology Part C: Toxicology & Pharmacology *134*, 417-430. https://doi.org/10.1016/S1532-0456(02)00249-1.

Komatsu, N., Aoki, K., Yamada, M., Yukinaga, H., Fujita, Y., Kamioka, Y., and Matsuda, M. (2011). Development of an optimized backbone of FRET biosensors for kinases and GTPases. Molecular Biology of the Cell *22*, 4647-4656. https://doi.org/10.1091/mbc.E11-01-0072.

Kondás, K., Szláma, G., Trexler, M., and Patthy, L. (2008). Both WFIKKN1 and WFIKKN2 have high affinity for growth and differentiation factors 8 and 11. The Journal of Biological Chemistry *283*, 23677-23684. https://doi.org/10.1074/jbc.M803025200.

Konermann, S., Brigham, M.D., Trevino, A.E., Joung, J., Abudayyeh, O.O., Barcena, C., Hsu, P.D., Habib, N., Gootenberg, J.S., and Nishimasu, H., et al. (2015). Genome-scale transcriptional activation by an engineered CRISPR-Cas9 complex. Nature *517*, 583-588. https://doi.org/10.1038/nature14136.

Konrath, F., Mittermeier, A., Cristiano, E., Wolf, J., and Loewer, A. (2020). Single cell trajectories (Technical University of Darmstadt).

Kretzschmar, M. (2000). Transforming growth factor-β and breast cancer: Transforming growth factor-β/SMAD signaling defects and cancer. Breast Cancer Research *2*, 107. https://doi.org/10.1186/bcr42.

Kretzschmar, M., Doody, J., and Massagué, J. (1997). Opposing BMP and EGF signalling pathways converge on the TGF-beta family mediator Smad1. Nature *389*, 618-622. https://doi.org/10.1038/39348.

Kretzschmar, M., Doody, J., Timokhina, I., and Massagué, J. (1999). A mechanism of repression of TGFbeta/ Smad signaling by oncogenic Ras. Genes & Development *13*, 804-816. https://doi.org/10.1101/gad.13.7.804.

Labun, K., Montague, T.G., Krause, M., Torres Cleuren, Y.N., Tjeldnes, H., and Valen, E. (2019). CHOPCHOP v3: expanding the CRISPR web toolbox beyond genome editing. Nucleic Acids Research *47*, W171-W174. https://doi.org/10.1093/nar/gkz365.

Lahav, G., Rosenfeld, N., Sigal, A., Geva-Zatorsky, N., Levine, A.J., Elowitz, M.B., and Alon, U. (2004). Dynamics of the p53-Mdm2 feedback loop in individual cells. Nature genetics *36*, 147-150. https://doi.org/10.1038/ng1293.

Lam, E.W., Glassford, J., Banerji, L., Thomas, N.S., Sicinski, P., and Klaus, G.G. (2000). Cyclin D3 compensates for loss of cyclin D2 in mouse B-lymphocytes activated via the antigen receptor and CD40. The Journal of Biological Chemistry *275*, 3479-3484. https://doi.org/10.1074/jbc.275.5.3479.

Lamouille, S., and Derynck, R. (2007). Cell size and invasion in TGF-beta-induced epithelial to mesenchymal transition is regulated by activation of the mTOR pathway. The Journal of Cell Biology *178*, 437-451. https://doi.org/10.1083/jcb.200611146.

Lea, N.C., Orr, S.J., Stoeber, K., Williams, G.H., Lam, E.W.-F., Ibrahim, M.A.A., Mufti, G.J., and Thomas, N.S.B. (2003). Commitment point during G0--G1 that controls entry into the cell cycle. Molecular and Cellular Biology *23*, 2351-2361. https://doi.org/10.1128/mcb.23.7.2351-2361.2003.

Lee, S.J., and McPherron, A.C. (2001). Regulation of myostatin activity and muscle growth. Proceedings of the National Academy of Sciences of the United States of America *98*, 9306-9311. https://doi.org/10.1073/pnas.151270098.

Legewie, S. (2009). Systems biological analyses of intracellular signal transduction (Humboldt-Universität zu Berlin, Mathematisch-Naturwissenschaftliche Fakultät I).

Leung, J.Y., Ehmann, G.L., Giangrande, P.H., and Nevins, J.R. (2008). A role for Myc in facilitating transcription activation by E2F1. Oncogene *27*, 4172-4179. https://doi.org/10.1038/onc.2008.55.

Lev Bar-Or, R., Maya, R., Segel, L.A., Alon, U., Levine, A.J., and Oren, M. (2000). Generation of oscillations by the p53-Mdm2 feedback loop: a theoretical and experimental study. Proceedings of the National Academy of Sciences of the United States of America *97*, 11250-11255. https://doi.org/10.1073/pnas.210171597.

Li, Y., Lee, M., Kim, N., Wu, G., Deng, D., Kim, J.M., Liu, X., Heo, W.D., and Zi, Z. (2018). Spatiotemporal Control of TGF-β Signaling with Light. ACS Synthetic Biology *7*, 443-451. https://doi.org/10.1021/acssynbio.7b00225.

Liang, J., and Slingerland, J.M. (2003). Multiple Roles of the PI3K/PKB (Akt) Pathway in Cell Cycle Progression. Cell Cycle *2*, 336-342. https://doi.org/10.4161/cc.2.4.433.

Lin, X., Duan, X., Liang, Y.-Y., Su, Y., Wrighton, K.H., Long, J., Hu, M., Davis, C.M., Wang, J., and Brunicardi, F.C., et al. (2006). PPM1A functions as a Smad phosphatase to terminate TGFbeta signaling. Cell *125*, 915-928. https://doi.org/10.1016/j.cell.2006.03.044.

Lloyd, A.C. (2013). The regulation of cell size. Cell *154*, 1194-1205. https://doi.org/10.1016/j.cell.2013.08.053.

Loewer, A., and Lahav, G. (2011). We are all individuals: causes and consequences of non-genetic heterogeneity in mammalian cells. Current Opinion in Genetics & Development *21*, 753-758. https://doi.org/10.1016/j.gde.2011.09.010.

Love, M.I., Huber, W., and Anders, S. (2014). Moderated estimation of fold change and dispersion for RNA-seq data with DESeq2. Genome Biology *15*, 550. https://doi.org/10.1186/s13059-014-0550-8.

Luo, K. (2017). Signaling Cross Talk between TGF-β/Smad and Other Signaling Pathways. Cold Spring Harbor Perspectives in Biology *9*. https://doi.org/10.1101/cshperspect.a022137.

Lutz, M., and Knaus, P. (2002). Integration of the TGF-β pathway into the cellular signalling network. Cellular Signalling *14*, 977-988. https://doi.org/10.1016/S0898-6568(02)00058-X.

Ma, X., and Bai, Y. (2012). IGF-1 activates the P13K/AKT signaling pathway via upregulation of secretory clusterin. Molecular Medicine Reports *6*, 1433-1437. https://doi.org/10.3892/mmr.2012.1110.

Macias, H., and Hinck, L. (2012). Mammary gland development. Wiley interdisciplinary reviews. Developmental biology *1*, 533-557. https://doi.org/10.1002/wdev.35.

Macias, M.J., Martin-Malpartida, P., and Massagué, J. (2015). Structural determinants of Smad function in TGF-β signaling. Trends in Biochemical Sciences *40*, 296-308. https://doi.org/10.1016/j.tibs.2015.03.012.

Maddika, S., Ande, S.R., Wiechec, E., Hansen, L.L., Wesselborg, S., and Los, M. (2008). Akt-mediated phosphorylation of CDK2 regulates its dual role in cell cycle progression and apoptosis. Journal of Cell Science *121*, 979. https://doi.org/10.1242/jcs.009530.

Marshall, C. (1995). Specificity of receptor tyrosine kinase signaling: Transient versus sustained extracellular signal-regulated kinase activation. Cell *80*, 179-185. https://doi.org/10.1016/0092-8674(95)90401-8.

Massague, J. (2003). Integration of Smad and MAPK pathways: a link and a linker revisited. Genes & Development *17*, 2993-2997. https://doi.org/10.1101/gad.1167003.

Massagué, J. (2012). TGFβ signalling in context. Nature reviews. Molecular cell biology *13*, 616-630. https://doi.org/10.1038/nrm3434.

Massagué, J., and Polyak, K. (1995). Mammalian antiproliferative signals and their targets. Current Opinion in Genetics & Development *5*, 91-96. https://doi.org/10.1016/s0959-437x(95)90059-4.

Massagué, J., Seoane, J., and Wotton, D. (2005). Smad transcription factors. Genes & Development *19*, 2783-2810. https://doi.org/10.1101/gad.1350705.

Matsuo, S.E., Leoni, S.G., Colquhoun, A., and Kimura, E.T. (2006). Transforming growth factor-beta1 and activin A generate antiproliferative signaling in thyroid cancer cells. The Journal of Endocrinology *190*, 141-150. https://doi.org/10.1677/joe.1.06713.

Meloche, S., Seuwen, K., Pagès, G., and Pouysségur, J. (1992). Biphasic and synergistic activation of p44mapk (ERK1) by growth factors: correlation between late phase activation and mitogenicity. Molecular Endocrinology *6*, 845-854. https://doi.org/10.1210/mend.6.5.1603090.

Miettinen, P.J., Ebner, R., Lopez, A.R., and Derynck, R. (1994). TGF-beta induced transdifferentiation of mammary epithelial cells to mesenchymal cells: involvement of type I receptors. The Journal of Cell Biology *127*, 2021-2036. https://doi.org/10.1083/jcb.127.6.2021.

Miller, I., Min, M., Yang, C., Tian, C., Gookin, S., Carter, D., and Spencer, S.L. (2018). Ki67 is a Graded Rather than a Binary Marker of Proliferation versus Quiescence. Cell Reports *24*, 1105-1112.e5. https://doi.org/10.1016/j.celrep.2018.06.110.

Moelling, K., Schad, K., Bosse, M., Zimmermann, S., and Schweneker, M. (2002). Regulation of Raf-Akt Cross-talk. The Journal of Biological Chemistry *277*, 31099-31106. https://doi.org/10.1074/jbc.M111974200.

Mori, S., Nishikawa, S.I., and Yokota, Y. (2000). Lactation defect in mice lacking the helix-loop-helix inhibitor Id2. The EMBO Journal *19*, 5772-5781. https://doi.org/10.1093/emboj/19.21.5772.

Moustakas, A., and Heldin, C.-H. (2009). The regulation of TGFbeta signal transduction. Development (Cambridge, England) *136*, 3699-3714. https://doi.org/10.1242/dev.030338.

Mukaka, M.M. (2012). Statistics corner: A guide to appropriate use of correlation coefficient in medical research. Malawi Medical Journal : The Journal of Medical Association of Malawi *24*, 69-71.

Murphy, L.O., Smith, S., Chen, R.-H., Fingar, D.C., and Blenis, J. (2002). Molecular interpretation of ERK signal duration by immediate early gene products. Nature Cell Biology *4*, 556-564. https://doi.org/10.1038/ncb822.

Nelson, C.M., Vanduijn, M.M., Inman, J.L., Fletcher, D.A., and Bissell, M.J. (2006). Tissue geometry determines sites of mammary branching morphogenesis in organotypic cultures. Science (New York, N.Y.) *314*, 298-300. https://doi.org/10.1126/science.1131000.

Nguyen, A.V., and Pollard, J.W. (2000). Transforming growth factor beta3 induces cell death during the first stage of mammary gland involution. Development (Cambridge, England) *127*, 3107-3118.

Nguyen, T.T., Scimeca, J.C., Filloux, C., Peraldi, P., Carpentier, J.L., and van Obberghen, E. (1993). Co-regulation of the mitogen-activated protein kinase, extracellular signal-regulated kinase 1, and the 90-kDa ribosomal S6 kinase in PC12 cells. Distinct effects of the neurotrophic factor, nerve growth factor, and the mitogenic factor, epidermal growth factor. Journal of Biological Chemistry *268*, 9803-9810. https://doi.org/10.1016/S0021-9258(18)98418-8.

Nickel, J., and Mueller, T.D. (2019). Specification of BMP Signaling. Cells *8*. https://doi.org/10.3390/cells8121579.

Nicolás, F.J., and Hill, C.S. (2003). Attenuation of the TGF-beta-Smad signaling pathway in pancreatic tumor cells confers resistance to TGF-beta-induced growth arrest. Oncogene *22*, 3698-3711. https://doi.org/10.1038/sj.onc.1206420.

Ohtani, K., DeGregori, J., and Nevins, J.R. (1995). Regulation of the cyclin E gene by transcription factor E2F1. Proceedings of the National Academy of Sciences *92*, 12146. https://doi.org/10.1073/pnas.92.26.12146.

Ohtsubo, M., Theodoras, A.M., Schumacher, J., Roberts, J.M., and Pagano, M. (1995). Human cyclin E, a nuclear protein essential for the G1-to-S phase transition. Molecular and Cellular Biology *15*, 2612-2624. https://doi.org/10.1128/mcb.15.5.2612.

Oki, T., Nishimura, K., Kitaura, J., Togami, K., Maehara, A., Izawa, K., Sakaue-Sawano, A., Niida, A., Miyano, S., and Aburatani, H., et al. (2014). A novel cell-cycle-indicator, mVenus-p27K-, identifies quiescent cells and visualizes G0-G1 transition. Scientific Reports *4*, 4012. https://doi.org/10.1038/srep04012.

Peixoto, P., Etcheverry, A., Aubry, M., Missey, A., Lachat, C., Perrard, J., Hendrick, E., Delage-Mourroux, R., Mosser, J., and Borg, C., et al. (2019). EMT is associated with an epigenetic signature of ECM remodeling genes. Cell Death & Disease *10*, 205. https://doi.org/10.1038/s41419-019-1397-4.

Plotnikov, A., Zehorai, E., Procaccia, S., and Seger, R. (2011). The MAPK cascades: signaling components, nuclear roles and mechanisms of nuclear translocation. Biochimica et Biophysica Acta *1813*, 1619-1633. https://doi.org/10.1016/j.bbamcr.2010.12.012.

Purvis, J.E., Karhohs, K.W., Mock, C., Batchelor, E., Loewer, A., and Lahav, G. (2012). p53 dynamics control cell fate. Science (New York, N.Y.) *336*, 1440-1444. https://doi.org/10.1126/science.1218351.

Purvis, J.E., and Lahav, G. (2013). Encoding and decoding cellular information through signaling dynamics. Cell *152*, 945-956. https://doi.org/10.1016/j.cell.2013.02.005.

Quereda, V., Porlan, E., Cañamero, M., Dubus, P., and Malumbres, M. (2016). An essential role for Ink4 and Cip/Kip cell-cycle inhibitors in preventing replicative stress. Cell Death and Differentiation *23*, 430-441. https://doi.org/10.1038/cdd.2015.112.

Rabbitts, P.H., Watson, J.V., Lamond, A., Forster, A., Stinson, M.A., Evan, G., Fischer, W., Atherton, E., Sheppard, R., and Rabbitts, T.H. (1985). Metabolism of c-myc gene products: c-myc mRNA and protein expression in the cell cycle. The EMBO Journal *4*, 2009-2015. https://doi.org/10.1002/j.1460-2075.1985.tb03885.x.

Ramesh, S., Wildey, G.M., and Howe, P.H. (2009). Transforming growth factor beta (TGFbeta)-induced apoptosis: the rise & fall of Bim. Cell Cycle *8*, 11-17. https://doi.org/10.4161/cc.8.1.7291.

Rebbapragada, A., Benchabane, H., Wrana, J.L., Celeste, A.J., and Attisano, L. (2003). Myostatin signals through a transforming growth factor beta-like signaling pathway to block adipogenesis. Molecular and Cellular Biology *23*, 7230-7242. https://doi.org/10.1128/mcb.23.20.7230-7242.2003.

Recasens, A., and Munoz, L. (2019). Targeting Cancer Cell Dormancy. Trends in pharmacological sciences *40*, 128-141. https://doi.org/10.1016/j.tips.2018.12.004.

Regot, S., Hughey, J.J., Bajar, B.T., Carrasco, S., and Covert, M.W. (2014). High-Sensitivity Measurements of Multiple Kinase Activities in Live Single Cells. Cell *157*, 1724-1734. https://doi.org/10.1016/j.cell.2014.04.039.

Ren, S., and Rollins, B.J. (2004). Cyclin C/cdk3 promotes Rb-dependent G0 exit. Cell *117*, 239-251. https://doi.org/10.1016/s0092-8674(04)00300-9.

Ribeiro, A., Bronk, S.F., Roberts, P.J., Urrutia, R., and Gores, G.J. (1999). The transforming growth factor beta(1)-inducible transcription factor TIEG1, mediates apoptosis through oxidative stress. Hepatology (Baltimore, Md.) *30*, 1490-1497. https://doi.org/10.1002/hep.510300620.

Roberts, P.J., and Der, C.J. (2007). Targeting the Raf-MEK-ERK mitogen-activated protein kinase cascade for the treatment of cancer. Oncogene *26*, 3291-3310. https://doi.org/10.1038/sj.onc.1210422.

Robertson, I.B., Horiguchi, M., Zilberberg, L., Dabovic, B., Hadjiolova, K., and Rifkin, D.B. (2015). Latent TGF-β-binding proteins. Matrix Biology : Journal of the International Society for Matrix Biology *47*, 44-53. https://doi.org/10.1016/j.matbio.2015.05.005.

Robson, C.N., Gnanapragasam, V., Byrne, R.L., Collins, A.T., and Neal, D.E. (1999). Transforming growth factor-beta1 up-regulates p15, p21 and p27 and blocks cell cycling in G1 in human prostate epithelium. The Journal of Endocrinology *160*, 257-266. https://doi.org/10.1677/joe.0.1600257.

Robson, E.J.D., Khaled, W.T., Abell, K., and Watson, C.J. (2006). Epithelial-to-mesenchymal transition confers resistance to apoptosis in three murine mammary epithelial cell lines. Differentiation; Research in Biological Diversity *74*, 254-264. https://doi.org/10.1111/j.1432-0436.2006.00075.x.

Ross, K.R., Corey, D.A., Dunn, J.M., and Kelley, T.J. (2007). SMAD3 expression is regulated by mitogen-activated protein kinase kinase-1 in epithelial and smooth muscle cells. Cellular Signalling *19*, 923-931. https://doi.org/10.1016/j.cellsig.2006.11.008.

Rubinfeld, H., and Seger, R. (2005). The ERK cascade: a prototype of MAPK signaling. Molecular Biotechnology *31*, 151-174. https://doi.org/10.1385/MB:31:2:151.

Ryu, H., Chung, M., Dobrzyński, M., Fey, D., Blum, Y., Lee, S.S., Peter, M., Kholodenko, B.N., Jeon, N.L., and Pertz, O. (2015). Frequency modulation of ERK activation dynamics rewires cell fate. Molecular Systems Biology *11*, 838. https://doi.org/10.15252/msb.20156458.

Sage, J. (2004). Cyclin C Makes an Entry into the Cell Cycle. Developmental Cell *6*, 607-608. https://doi.org/10.1016/S1534-5807(04)00137-6.

Saito, S., Sidis, Y., Mukherjee, A., Xia, Y., and Schneyer, A. (2005). Differential biosynthesis and intracellular transport of follistatin isoforms and follistatin-like-3. Endocrinology *146*, 5052-5062. https://doi.org/10.1210/en.2005-0833.

Sakaue-Sawano, A., Kurokawa, H., Morimura, T., Hanyu, A., Hama, H., Osawa, H., Kashiwagi, S., Fukami, K., Miyata, T., and Miyoshi, H., et al. (2008). Visualizing Spatiotemporal Dynamics of Multicellular Cell-Cycle Progression. Cell *132*, 487-498. https://doi.org/10.1016/j.cell.2007.12.033.

Santen, R.J., Song, R.X., McPherson, R., Kumar, R., Adam, L., Jeng, M.-H., and Yue, W. (2002). The role of mitogen-activated protein (MAP) kinase in breast cancer. The Journal of Steroid Biochemistry and Molecular Biology *80*, 239-256. https://doi.org/10.1016/s0960-0760(01)00189-3.

Schafer, K.A. (1998). The Cell Cycle: A Review. Veterinary Pathology *35*, 461-478. https://doi.org/10.1177/030098589803500601.

Schmidt, M., Fernandez de Mattos, S., van der Horst, A., Klompmaker, R., Kops, G.J.P.L., Lam, E.W.-F., Burgering, B.M.T., and Medema, R.H. (2002). Cell cycle inhibition by FoxO forkhead transcription factors involves downregulation of cyclin D. Molecular and Cellular Biology *22*, 7842-7852. https://doi.org/10.1128/mcb.22.22.7842-7852.2002.

Schmierer, B., and Hill, C.S. (2007). TGFbeta-SMAD signal transduction: molecular specificity and functional flexibility. Nature reviews. Molecular cell biology *8*, 970-982. https://doi.org/10.1038/nrm2297.

Schneyer, A., Tortoriello, D., Sidis, Y., Keutmann, H., Matsuzaki, T., and Holmes, W. (2001). Follistatin-related protein (FSRP): a new member of the follistatin gene family. Molecular and Cellular Endocrinology *180*, 33-38. https://doi.org/10.1016/S0303-7207(01)00501-9.

Schneyer, A.L., Sidis, Y., Gulati, A., Sun, J.L., Keutmann, H., and Krasney, P.A. (2008). Differential antagonism of activin, myostatin and growth and differentiation factor 11 by wild-type and mutant follistatin. Endocrinology *149*, 4589-4595. https://doi.org/10.1210/en.2008-0259.

Schubert, M., Klinger, B., Klünemann, M., Sieber, A., Uhlitz, F., Sauer, S., Garnett, M.J., Blüthgen, N., and Saez-Rodriguez, J. (2018). Perturbation-response genes reveal signaling footprints in cancer gene expression. Nature Communications *9*, 20. https://doi.org/10.1038/s41467-017-02391-6.

Schuster, N., and Krieglstein, K. (2002). Mechanisms of TGF-beta-mediated apoptosis. Cell and Tissue Research *307*, 1-14. https://doi.org/10.1007/s00441-001-0479-6.

Seger, R., and Krebs, E.G. (1995). The MAPK signaling cascade. FASEB j. *9*, 726-735. https://doi.org/10.1096/fasebj.9.9.7601337.

Selimkhanov, J., Taylor, B., Yao, J., Pilko, A., Albeck, J., Hoffmann, A., Tsimring, L., and Wollman, R. (2014). Systems biology. Accurate information transmission through dynamic biochemical signaling networks. Science (New York, N.Y.) *346*, 1370-1373. https://doi.org/10.1126/science.1254933.

Seoane, J., Le, H.-V., Shen, L., Anderson, S.A., and Massagué, J. (2004). Integration of Smad and Forkhead Pathways in the Control of Neuroepithelial and Glioblastoma Cell Proliferation. Cell *117*, 211-223. https://doi.org/10.1016/S0092-8674(04)00298-3.

Shankaran, H., Ippolito, D.L., Chrisler, W.B., Resat, H., Bollinger, N., Opresko, L.K., and Wiley, H.S. (2009). Rapid and sustained nuclear-cytoplasmic ERK oscillations induced by epidermal growth factor. Molecular Systems Biology *5*, 332. https://doi.org/10.1038/msb.2009.90.

Sharrocks, A.D. (2006). Cell cycle: sustained ERK signalling represses the inhibitors. Current Biology : CB *16*, R540-2. https://doi.org/10.1016/j.cub.2006.06.038.

Shi, Y., and Massagué, J. (2003). Mechanisms of TGF-β Signaling from Cell Membrane to the Nucleus. Cell *113*, 685-700. https://doi.org/10.1016/S0092-8674(03)00432-X.

Shi, Y., Wang, Y.F., Jayaraman, L., Yang, H., Massagué, J., and Pavletich, N.P. (1998). Crystal structure of a Smad MH1 domain bound to DNA: insights on DNA binding in TGF-beta signaling. Cell *94*, 585-594. https://doi.org/10.1016/s0092-8674(00)81600-1.

Sidis, Y., Mukherjee, A., Keutmann, H., Delbaere, A., Sadatsuki, M., and Schneyer, A. (2006). Biological activity of follistatin isoforms and follistatin-like-3 is dependent on differential cell surface binding and specificity for activin, myostatin, and bone morphogenetic proteins. Endocrinology *147*, 3586-3597. https://doi.org/10.1210/en.2006-0089.

Simoncini, T., Hafezi-Moghadam, A., Brazil, D.P., Ley, K., Chin, W.W., and Liao, J.K. (2000). Interaction of oestrogen receptor with the regulatory subunit of phosphatidylinositol-3-OH kinase. Nature *407*, 538-541. https://doi.org/10.1038/35035131.

Simoni-Nieves, A., Gerardo-Ramírez, M., Pedraza-Vázquez, G., Chávez-Rodríguez, L., Bucio, L., Souza, V., Miranda-Labra, R.U., Gomez-Quiroz, L.E., and Gutiérrez-Ruiz, M.C. (2019). GDF11 Implications in Cancer Biology and Metabolism. Facts and Controversies. Frontiers in Oncology *9*, 1039. https://doi.org/10.3389/fonc.2019.01039.

Sinha, M., Jang, Y.C., Oh, J., Khong, D., Wu, E.Y., Manohar, R., Miller, C., Regalado, S.G., Loffredo, F.S., and Pancoast, J.R., et al. (2014). Restoring systemic GDF11 levels reverses age-related dysfunction in mouse skeletal muscle. Science (New York, N.Y.) *344*, 649-652. https://doi.org/10.1126/science.1251152.

Spencer, S.L., Cappell, S.D., Tsai, F.-C., Overton, K.W., Wang, C.L., and Meyer, T. (2013). The proliferation-quiescence decision is controlled by a bifurcation in CDK2 activity at mitotic exit. Cell *155*, 369-383. https://doi.org/10.1016/j.cell.2013.08.062.

Spiller, D.G., Wood, C.D., Rand, D.A., and White, M.R.H. (2010). Measurement of single-cell dynamics. Nature *465*, 736-745. https://doi.org/10.1038/nature09232.

Strasen, J., Sarma, U., Jentsch, M., Bohn, S., Sheng, C., Horbelt, D., Knaus, P., Legewie, S., and Loewer, A. (2018). Cell-specific responses to the cytokine TGFβ are determined by variability in protein levels. Molecular Systems Biology *14*, e7733. https://doi.org/10.15252/msb.20177733.

Stuart, T., Butler, A., Hoffman, P., Hafemeister, C., Papalexi, E., Mauck, W.M., Hao, Y., Stoeckius, M., Smibert, P., and Satija, R. (2019). Comprehensive Integration of Single-Cell Data. Cell *177*, 1888-1902.e21. https://doi.org/10.1016/j.cell.2019.05.031.

Suh, J., Kim, N.-K., Lee, S.-H., Eom, J.-H., Lee, Y., Park, J.-C., Woo, K.M., Baek, J.-H., Kim, J.-E., and Ryoo, H.-M., et al. (2020). GDF11 promotes osteogenesis as opposed to MSTN, and follistatin, a MSTN/GDF11 inhibitor, increases muscle mass but weakens bone. Proceedings of the National Academy of Sciences of the United States of America *117*, 4910-4920. https://doi.org/10.1073/pnas.1916034117.

Sung, H., Ferlay, J., Siegel, R.L., Laversanne, M., Soerjomataram, I., Jemal, A., and Bray, F. (2021). Global cancer statistics 2020: GLOBOCAN estimates of incidence and mortality worldwide for 36 cancers in 185 countries. CA: A Cancer Journal for Clinicians. https://doi.org/10.3322/caac.21660.

Suryadinata, R., Sadowski, M., and Sarcevic, B. (2010). Control of cell cycle progression by phosphorylation of cyclin-dependent kinase (CDK) substrates. Bioscience Reports *30*, 243-255. https://doi.org/10.1042/BSR20090171.

Tirosh, I., Izar, B., Prakadan, S.M., Wadsworth, M.H., Treacy, D., Trombetta, J.J., Rotem, A., Rodman, C., Lian, C., and Murphy, G., et al. (2016). Dissecting the multicellular ecosystem of metastatic melanoma by single-cell RNA-seq. Science (New York, N.Y.) *352*, 189-196. https://doi.org/10.1126/science.aad0501.

Traverse, S., Gomez, N., Paterson, H., Marshall, C., and Cohen, P. (1992). Sustained activation of the mitogen-activated protein (MAP) kinase cascade may be required for differentiation of PC12 cells. Comparison of the effects of nerve growth factor and epidermal growth factor. Biochem J *288 (Pt 2)*, 351-355. https://doi.org/10.1042/bj2880351.

Tsuchida, K., Nakatani, M., Hitachi, K., Uezumi, A., Sunada, Y., Ageta, H., and Inokuchi, K. (2009). Activin signaling as an emerging target for therapeutic interventions. Cell Communication and Signaling : CCS *7*, 15. https://doi.org/10.1186/1478-811X-7-15.

Velasco-Loyden, G., Arribas, J., and López-Casillas, F. (2004). The Shedding of Betaglycan Is Regulated by Pervanadate and Mediated by Membrane Type Matrix Metalloprotease-1. Journal of Biological Chemistry *279*, 7721-7733. https://doi.org/10.1074/jbc.M306499200.

Ventura, J.-J., Kennedy, N.J., Flavell, R.A., and Davis, R.J. (2004). JNK regulates autocrine expression of TGF-beta1. Molecular Cell *15*, 269-278. https://doi.org/10.1016/j.molcel.2004.06.007.

Vermeulen, K., van Bockstaele, D.R., and Berneman, Z.N. (2003). The cell cycle: a review of regulation, deregulation and therapeutic targets in cancer. Cell Proliferation *36*, 131-149. https://doi.org/10.1046/j.1365-2184.2003.00266.x.

Wakefield, L.M., and Roberts, A.B. (2002). TGF-β signaling: positive and negative effects on tumorigenesis. Current Opinion in Genetics & Development *12*, 22-29. https://doi.org/10.1016/S0959-437X(01)00259-3.

Walker, R.G., Poggioli, T., Katsimpardi, L., Buchanan, S.M., Oh, J., Wattrus, S., Heidecker, B., Fong, Y.W., Rubin, L.L., and Ganz, P., et al. (2016). Biochemistry and Biology of GDF11 and Myostatin: Similarities, Differences, and Questions for Future Investigation. Circulation Research *118*, 1125-41; discussion 1142. https://doi.org/10.1161/CIRCRESAHA.116.308391.

Wang, C.-C., Bajikar, S.S., Jamal, L., Atkins, K.A., and Janes, K.A. (2014). A time- and matrix-dependent TGFBR3-JUND-KRT5 regulatory circuit in single breast epithelial cells and basal-like premalignancies. Nature Cell Biology *16*, 345-356. https://doi.org/10.1038/ncb2930.

Wang, X.F., Lin, H.Y., Ng-Eaton, E., Downward, J., Lodish, H.F., and Weinberg, R.A. (1991). Expression cloning and characterization of the TGF-beta type III receptor. Cell *67*, 797-805. https://doi.org/10.1016/0092-8674(91)90074-9.

Wang, Y., and Zhou, B.P. (2011). Epithelial-mesenchymal transition in breast cancer progression and metastasis. Chinese journal of cancer *30*, 603-611. https://doi.org/10.5732/cjc.011.10226.

Ward, P.S., and Thompson, C.B. (2012). Signaling in control of cell growth and metabolism. Cold Spring Harbor Perspectives in Biology *4*, a006783. https://doi.org/10.1101/cshperspect.a006783.

Warmflash, A., Zhang, Q., Sorre, B., Vonica, A., Siggia, E.D., and Brivanlou, A.H. (2012). Dynamics of TGF-β signaling reveal adaptive and pulsatile behaviors reflected in the nuclear localization of transcription factor Smad4. Proceedings of the National Academy of Sciences of the United States of America *109*, E1947-56. https://doi.org/10.1073/pnas.1207607109.

Wildey, G.M., Patil, S., and Howe, P.H. (2003). Smad3 potentiates transforming growth factor beta (TGFbeta)-induced apoptosis and expression of the BH3-only protein Bim in WEHI 231 B lymphocytes. The Journal of Biological Chemistry *278*, 18069-18077. https://doi.org/10.1074/jbc.M211958200.

Winbanks, C.E., Murphy, K.T., Bernardo, B.C., Qian, H., Liu, Y., Sepulveda, P.V., Beyer, C., Hagg, A., Thomson, R.E., and Chen, J.L., et al. (2016). Smad7 gene delivery prevents muscle wasting associated with cancer cachexia in mice. Science Translational Medicine *8*, 348ra98. https://doi.org/10.1126/scitranslmed.aac4976.

Worster, D.T., Schmelzle, T., Solimini, N.L., Lightcap, E.S., Millard, B., Mills, G.B., Brugge, J.S., and Albeck, J.G. (2012). Akt and ERK control the proliferative response of mammary epithelial cells to the growth factors IGF-1 and EGF through the cell cycle inhibitor p57Kip2. Science Signaling *5*, ra19. https://doi.org/10.1126/scisignal.2001986.

Xie, L., Law, B.K., Chytil, A.M., Brown, K.A., Aakre, M.E., and Moses, H.L. (2004). Activation of the Erk pathway is required for TGF-beta1-induced EMT in vitro. Neoplasia (New York, N.Y.) *6*, 603-610. https://doi.org/10.1593/neo.04241.

Yagi, K., Furuhashi, M., Aoki, H., Goto, D., Kuwano, H., Sugamura, K., Miyazono, K., and Kato, M. (2002). c-myc is a downstream target of the Smad pathway. The Journal of Biological Chemistry *277*, 854-861. https://doi.org/10.1074/jbc.M104170200.

Yang, N.-C., and Hu, M.-L. (2005). The limitations and validities of senescence associated-beta-galactosidase activity as an aging marker for human foreskin fibroblast Hs68 cells. Experimental Gerontology *40*, 813-819. https://doi.org/10.1016/j.exger.2005.07.011.

Yano, S., Zhang, Y., Miwa, S., Tome, Y., Hiroshima, Y., Uehara, F., Yamamoto, M., Suetsugu, A., Kishimoto, H., and Tazawa, H., et al. (2014). Spatial-temporal FUCCI imaging of each cell in a tumor demonstrates locational dependence of cell cycle dynamics and chemoresponsiveness. Cell Cycle (Georgetown, Tex.) *13*, 2110-2119. https://doi.org/10.4161/cc.29156.

Yao, G. (2014). Modelling mammalian cellular quiescence. Interface Focus *4*, 20130074. https://doi.org/10.1098/rsfs.2013.0074.

Yingling, J.M., Blanchard, K.L., and Sawyer, J.S. (2004). Development of TGF-beta signalling inhibitors for cancer therapy. Nature reviews. Drug discovery *3*, 1011-1022. https://doi.org/10.1038/nrd1580.

Yu, G., Li, F., Qin, Y., Bo, X., Wu, Y., and Wang, S. (2010). GOSemSim: an R package for measuring semantic similarity among GO terms and gene products. Bioinformatics (Oxford, England) *26*, 976-978. https://doi.org/10.1093/bioinformatics/btq064.

Yu, G., Wang, L.-G., Han, Y., and He, Q.-Y. (2012). clusterProfiler: an R package for comparing biological themes among gene clusters. Omics : A Journal of Integrative Biology *16*, 284-287. https://doi.org/10.1089/omi.2011.0118.

Yu, J., Zhang, L., Chen, A., Xiang, G., Wang, Y., Wu, J., Mitchelson, K., Cheng, J., and Zhou, Y. (2008). Identification of the gene transcription and apoptosis mediated by TGF-beta-Smad2/3-Smad4 signaling. Journal of Cellular Physiology *215*, 422-433. https://doi.org/10.1002/jcp.21325.

Yue, J., and Mulder, K.M. (2000). Requirement of Ras/MAPK pathway activation by transforming growth factor beta for transforming growth factor beta 1 production in a Smad-dependent pathway. The Journal of Biological Chemistry *275*, 30765-30773. https://doi.org/10.1074/jbc.M000039200.

Zarzynska, J.M. (2014). Two faces of TGF-beta1 in breast cancer. Mediators of Inflammation *2014*, 141747. https://doi.org/10.1155/2014/141747.

Zeisberg, M., and Neilson, E.G. (2009). Biomarkers for epithelial-mesenchymal transitions. The Journal of Clinical Investigation *119*, 1429-1437. https://doi.org/10.1172/JCI36183.

Zetterberg, A., Larsson, O., and Wiman, K.G. (1995). What is the restriction point? Current Opinion in Cell Biology *7*, 835-842. https://doi.org/10.1016/0955-0674(95)80067-0.

Zhang, J., Tian, X.-J., Zhang, H., Teng, Y., Li, R., Bai, F., Elankumaran, S., and Xing, J. (2014). TGF-β-induced epithelial-to-mesenchymal transition proceeds through stepwise activation of multiple feedback loops. Science Signaling *7*, ra91. https://doi.org/10.1126/scisignal.2005304.

Zhang, W., and Liu, H.T. (2002). MAPK signal pathways in the regulation of cell proliferation in mammalian cells. Cell Research *12*, 9-18. https://doi.org/10.1038/sj.cr.7290105.

Zhang, Y., and Derynck, R. (1999). Regulation of Smad signalling by protein associations and signalling crosstalk. Trends in Cell Biology *9*, 274-279. https://doi.org/10.1016/S0962-8924(99)01579-2.

Zhang, Y.E. (2009). Non-Smad pathways in TGF-β signaling. Cell Research *19*, 128-139. https://doi.org/10.1038/cr.2008.328.

Zhao, Y., Hamza, M.S., Leong, H.S., Lim, C.-B., Pan, Y.-F., Cheung, E., Soo, K.-C., and Iyer, N.G. (2008). Kruppel-like factor 5 modulates p53-independent apoptosis through Pim1 survival kinase in cancer cells. Oncogene *27*, 1-8. https://doi.org/10.1038/sj.onc.1210625.

Zheng, W.-H., and Quirion, R. (2006). Insulin-like growth factor-1 (IGF-1) induces the activation/phosphorylation of Akt kinase and cAMP response element-binding protein (CREB) by activating different signaling pathways in PC12 cells. BMC Neuroscience *7*, 51. https://doi.org/10.1186/1471-2202-7-51.

Zhou, S., Zawel, L., Lengauer, C., Kinzler, K.W., and Vogelstein, B. (1998). Characterization of Human FAST-1, a TGFβ and Activin Signal Transducer. Molecular Cell *2*, 121-127. https://doi.org/10.1016/S1097-2765(00)80120-3.

Zieba, A., Pardali, K., Söderberg, O., Lindbom, L., Nyström, E., Moustakas, A., Heldin, C.-H., and Landegren, U. (2012). Intercellular variation in signaling through the TGF-β pathway and its relation to cell density and cell cycle phase. Molecular & Cellular Proteomics : MCP *11*, M111.013482. https://doi.org/10.1074/mcp.M111.013482.

Zimmermann, S., and Moelling, K. (1999). Phosphorylation and regulation of Raf by Akt (protein kinase B). Science (New York, N.Y.) *286*, 1741-1744. https://doi.org/10.1126/science.286.5445.1741.

Zmajkovicova, K., Jesenberger, V., Catalanotti, F., Baumgartner, C., Reyes, G., and Baccarini, M. (2013). MEK1 is required for PTEN membrane recruitment, AKT regulation, and the maintenance of peripheral tolerance. Molecular Cell *50*, 43-55. https://doi.org/10.1016/j.molcel.2013.01.037.

Zwang, Y., Sas-Chen, A., Drier, Y., Shay, T., Avraham, R., Lauriola, M., Shema, E., Lidor-Nili, E., Jacob-Hirsch, J., and Amariglio, N., et al. (2011). Two phases of mitogenic signaling unveil roles for p53 and EGR1 in elimination of inconsistent growth signals. Molecular Cell *42*, 524-535. https://doi.org/10.1016/j.molcel.2011.04.017.

6 APPENDIX

6.1 LIST OF ABBREVIATIONS

– listed in alphabetical order –

α-ω		
	µg	micrograms
	µl	microliter
	µM	micromolar
A		
	ACVR1B	activin A receptor 1B
	ACVR1C	activin A receptor 1C
	ACVR2A	activin A receptor 2A
	ACVR2B	activin A receptor 2B
	AKTi	AKT inhibitor
	AMH	anti-Muellerian hormone
	Amp	amplitude
	APC	anaphase-promoting complex
	APS	ammonium persulfate
	au	arbitrary unit
	AUC	area under the curve
B		
	BAM	binary sequencing alignment map
	BIM	Bcl-2-like protein 11
	Blast_R	blasticidin resistance
	BMP	bone morphogenetic protein
	BMPR2	BMP receptor 2
	bp	base pairs
	BSA	bovine serum albumine
C		
	Cas9	CRISPR-associated 9
	CDH1	E-cadherin
	CDH2	N-cadherin
	CDK	cyclin-dependent kinases
	CDK1i	CDK1 inhibitor
	CDK4/6i	CDK4/6 inhibitor
	CDKN1A	cyclin-dependent kinase inhibitor 1A (p21)
	CDKN1B	cyclin-dependent kinase inhibitor 1B (p27)
	CDKN2B	cyclin-dependent kinase inhibitor 2B (p15)
	cDNA	complementary DNA
	CFP	cyan fluorescent protein
	CKIs	CDK inhibitors
	cm	centimeter
	CMV	cauliflower mosaic virus
	Co-SMAD	common-mediator SMAD; isoform 4
	CRISPR	clustered regularly interspaced short palindromic repeats

	crRNA	CRISPR RNA
	CT	cycle threshold
D		
	DAPI	4’,6-diamidino-2-phenylindole
	dCas9	dead Cas9
	ddH_2O	double-distilled water
	DEPC-treated H_2O	diethyl pyrocarbonate treated water
	DMEM/F12	Dulbecco's Modified Eagle Medium/Nutrient Mixture F-12
	DMSO	dimethyl sulfoxide
	DNA	deoxyribonucleic acid
	dNTP	deoxyribose nucleotide triphosphate
	DPBS	Dulbecco's phosphate buffered saline
	DRB	5,6-dichlorobenzimidazole 1-β-D-ribofuranoside
	DSB	double-strand breaks
	dsDNA	double-stranded DNA
	DTT	dithiothreitol
E		
	ECL	enhanced chemiluminescence
	EDTA	ethylenediaminetetraacetic acid
	EdU	5-Ethynyl-2’-deoxyuridine
	EGF	epidermal growth factors
	EGFR	EGF receptor
	EGFRi	EGFR inhibitor
	EGR1	early growth response protein 1
	EMT	epithelial to mesenchymal transition
	ERK	extracellular signal-regulated kinase
F		
	FC	fold change
	FIRE	fra-1-based integrative reporter of ERK
	FOXH1	forkhead box protein H1
	FOXO	forkhead box protein O
	FPM	fragments per million
	FRA1/FOSL1	fos-related antigen 1
	FRET	fluorescence resonance energy transfer
	FST	follistatin
	FSTL3	follistatin-like 3
G		
	G1-phase	first gap phase (cell cycle)
	G2-phase	second gap phase (cell cycle)
	GAPDH	glyceraldehyde 3-phosphate dehydrogenase
	GASP1	GDF-associated serum protein 1
	GASP2	GDF-associated serum protein 2
	GDF3	growth differentiation factor 3
	GDF8	growth differentiation factor 8; also called myostatin
	GDF11	growth differentiation factor 11
	GFP	green fluorescent protein

	GO	gene ontology
	GSK3beta	glycogen synthase kinase 3 beta
	GSK3i	GSK3 inhibitor
	GTF	general transfer format
H		
	h	hours
	H2B	histone 2b
	HA	homology arm
	HAL	homology arm left
	HAR	homology arm right
	HCl	hydrogen chloride
	HDAC1	histone deacetylase 1
	HDAC2	histone deacetylase 2
	HDR	homology-directed repair
	HEK293T	human embryonic kidney cells expressing SV40 large T antigen
	HRP	horseradish peroxidase
I		
	ID2	inhibitor of DNA binding 2
	IGF	insulin-like growth factor
	I-SMAD	inhibitory SMADs; isoforms 6 and 7
J		
	JNK	c-Jun N-terminal kinase
	JNKi	JNK inhibitor
K		
	kDa	kilodalton
	KEGG	Kyoto Encyclopedia of Genes and Genomes
	KLF	krueppel-like factors
	KO	knockout
	kV	kilovolt
L		
	LTBP1	latent-transforming growth factor beta-binding protein 1
M		
	m	slope of linear model
	mA	milliampere
	MAPK	mitogen-activated protein kinase
	MCF10A	immortalized human breast epithelial cell line (Michigan Cancer Foundation-10A)
	MEK	MAPK kinase
	MEKi	MEK inhibitor
	mg	milligrams
	MH1	mad homology 1
	MH2	mad homology 2
	min	minutes
	ml	milliliter
	mM	millimolar
	M-phase	mitosis phase (cell cycle)

	mRNA	messenger RNA
	MSCV LTR	murine stem cell virus long terminal repeat
	mTOR	mechanistic target of rapamycin kinase
	MYC	myelocytomatosis oncogene
N		
	NF-κB	nuclear factor 'kappa-light-chain-enhancer' of activated B-cells
	ng	nanograms
	NGF	nerve growth factors
	NGS	next generation sequencing
	NLS	nuclear localization sequence
	nM	nanomolar
	nuc/cyt	nuclear/cytoplasmic
O		
	O/N	over night
	OE	overexpression
P		
	p38i	p38 inhibitor
	PBS	phosphate buffered saline
	PC	principal components
	PCA	principal component analysis
	PCR	polymerase chain reaction
	PDK1	phosphoinositide-dependent kinase 1
	PDP	pyruvate dehydrogenase phosphatase
	PI3K	phosphatidylinositol 3-kinase
	PI3Ki	PI3K inhibitor
	PIP2	phosphatidylinositol-4,5-bisphosphate
	PIP3	phosphatidylinositol-3,4,5-triphosphate
	pM	picomolar
	poly(A)	polyadenylation
	PPM1A	protein phosphatase 1A
	PROGENy	Pathway RespOnsive GENes for activity inference
	pSMAD2	phosphorylated SMAD2
	PTEN	phosphatase and tensin homologue
	PTM	post-translational modification
	PVDF	polyvinylidene difluoride
R		
	r	correlation coefficient
	RAF	rapidly accelerated fibrosarcoma
	RB	retinoblastoma protein
	RFP	red fluorescent protein
	RNA	ribonucleic acid
	RNase	ribonuclease
	RPKM	reads per kilobase of transcript per million mapped reads
	R-SMADs	receptor-regulated SMADs; isoforms 1, 2, 3, 5, 8
	RT-qPCR	real-time quantitative PCR
	Runx1	runt-related transcription factor 1

S		
	s	seconds
	S2-R	MCF10A SMAD2 reporter cell line
	SA-bG	senescence-associated beta-galactosidase
	scRNA-seq	single-cell RNA sequencing
	sd	standard deviation
	SDS	sodium dodecyl sulfate
	sgRNA	single guide RNA
	SMAD	SMA ('small') and MAD ('mothers against decapentaplegic')
	SOC	super optimal broth with catabolite repression
	SOX4	SRY-box transcription factor 4
	S-phase	synthesis phase (cell cycle)
	Sv40	simian virus 40
T		
	TAE	tris-acetate-EDTA
	TBS-T	tris-buffered saline with Tween20
	TEMED	tetramethylethylenediamine
	TGFb	transforming growth factor beta
	TGFBR1	TGFb receptor 1
	TGFBR2	TGFb receptor 2
	TGFBR3	TGFb receptor 3
	tracrRNA	trans-activating crRNA
	TSS	transcriptional start site
U		
	U/ml	units per milliliter
	U-2 OS	human bone osteosarcoma cells
	UbCp	ubiquitin C promoter
	UMAP	uniform manifold approximation and projection
	UMIs	unique molecular identifiers
V		
	V	volt
	VIM	vimentin
W		
	w/v	weight per volume
	WT	wild-type
Y		
	YFP	yellow fluorescent protein
Z		
	ZEB1	zinc-finger-enhancer protein 1

6.2 LIST OF FIGURES

6.3 NUMBER OF TRACKED CELLS IN TIME-LAPSE MICROSCOPY EXPERIMENTS (PART 1)

Experiment	EGF conc. (ng/ml)	Inhibitor	Time of adding inhibitor (hours)	Time of washout (hours)	Time of EdU costaining (hours)	Cells tracked
Related to Figure 8-10						
Stimulation	0	control				1147
Stimulation	0,5	control				1137
Stimulation	1	control				1062
Stimulation	2,5	control				1248
Stimulation	5	control				1022
Stimulation	7,5	control				1013
Stimulation	10	control				876
Stimulation	12,5	control				877
Stimulation	15	control				1061
Stimulation	17,5	control				920
Stimulation	20	control				905
Stimulation	50	control				1175
Related to Figure 9 and 10						
EDU costaining	0	control				2821
EDU costaining	0	control			20	3501
EDU costaining	0,5	control				2531
EDU costaining	0,5	control			20	3206
EDU costaining	1	control				2356
EDU costaining	1	control			20	3119
EDU costaining	2,5	control				2127
EDU costaining	2,5	control			20	2575
Related to Figure 11						
MAPK	0	AZD6244				1324
MAPK	0	control				995
MAPK	0	gefitinib				1373
MAPK	0	sorafenib				1423
MAPK	1	AZD6244				1550
MAPK	1	control				1097
MAPK	1	gefitinib				1601
MAPK	1	sorafenib				1565
MAPK	7,5	AZD6244				1603
MAPK	7,5	control				1264
MAPK	7,5	gefitinib				1524

MAPK	7,5	sorafenib				1441
Related to Figure 11						
PI3K-IKK2	0	control				1403
PI3K-IKK2	0	IKK2				2009
PI3K-IKK2	0	PI3K				1575
PI3K-IKK2	1	control				1580
PI3K-IKK2	1	IKK2				1810
PI3K-IKK2	1	PI3K				1810
PI3K-IKK2	7,5	control				1338
PI3K-IKK2	7,5	IKK2				1780
PI3K-IKK2	7,5	PI3K				1825
Related to Figure 11						
p38	0	control				1071
p38	0	p38				1779
p38	1	control				1398
p38	1	p38				1760
p38	7,5	control				1255
p38	7,5	p38				1648
Related to Figure 11						
AKT	0	AKT				1779
AKT	0	control				1817
AKT	1	AKT				2075
AKT	1	control				2137
AKT	7,5	AKT				1721
AKT	7,5	control				1805
Related to Figure 11						
JNK-GSK	0	control				1765
JNK-GSK	0	GSK3				2027
JNK-GSK	0	JNK				1862
JNK-GSK	1	control				1386
JNK-GSK	1	GSK3				1837
JNK-GSK	1	JNK				2082
JNK-GSK	7,5	control				1621
JNK-GSK	7,5	GSK3				1753
JNK-GSK	7,5	JNK				1796
Related to Figure 12						
CDK	0	CDK4/6 (10 uM Palbocyclin)				2110
CDK	0	CDK1 (10 uM RO3306)				2336
CDK	0	control				2067
CDK	1	CDK4/6 (10 uM Palbocyclin)				2365
CDK	1	CDK1 (10 uM RO3306)				2386
CDK	1	control				2038

CDK	7,5	CDK4/6 (10 uM Palbocyclin)				2155
CDK	7,5	CDK1 (10 uM RO3306)				2595
CDK	7,5	control				1801
Related to Figure 13						
Pulse_02	0	control	0			3108
Pulse_02	7,5	AZD6244	0			2245
Pulse_02	7,5	AZD6244	10			2291
Pulse_02	7,5	AZD6244	15			2429
Pulse_02	7,5	AZD6244	20			1839
Pulse_02	7,5	control	0			1568
Pulse_02	7,5	control	10			1713
Pulse_02	7,5	control	15			1842
Pulse_02	7,5	control	20			1749
Pulse_02	7,5	gefitinib	0			2854
Pulse_02	7,5	gefitinib	10			2668
Pulse_02	7,5	gefitinib	15			3018
Pulse_02	7,5	gefitinib	20			2507
Pulse_02	7,5	PI3K	0			2778
Pulse_02	7,5	PI3K	10			2998
Pulse_02	7,5	PI3K	15			3101
Pulse_02	7,5	PI3K	20			3092
Related to Figure 13 and 17						
EdU_pulse	0	gefitinib				2227
EdU_pulse	7,5	gefitinib		15		1983
EdU_pulse	7,5	control			15	1985
EdU_pulse	7,5	control			22.5	1775
EdU_pulse	7,5	control			32.5	1819
EdU_pulse	7,5	control	15			1918
EdU_pulse	7,5	AZD6244	15		22.5	2394
EdU_pulse	7,5	AZD6244	15		32.5	2155
EdU_pulse	7,5	PI3K	15		22.5	2646
EdU_pulse	7,5	PI3K	15		32.5	2443
EdU_pulse	7,5	AZD6244	20			1877
EdU_pulse	7,5	PI3K	20			2609
Related to Figure 13						
Washout	0	control		0		2441
Washout	7,5	control		0		196
Washout	7,5	control		5		494
Washout	7,5	control		10		584
Washout	7,5	control		15		288
Washout	7,5	MEK		0		2398
Washout	7,5	MEK		5		2016
Washout	7,5	MEK		10		1997

Washout	7,5	MEK		15		1982
Washout	7,5	PI3K		0		1293
Washout	7,5	PI3K		5		2022
Washout	7,5	PI3K		10		2405
Washout	7,5	PI3K		15		2655
Related to Figure 14						
IGF expanded	0	control				3186
IGF expanded	0,1	IGF (2.5 µg/ml)				2287
IGF expanded	0,1	control				2584
IGF expanded	0,175	IGF (2.5 µg/ml)				2528
IGF expanded	0,175	control				2519
IGF expanded	0,25	IGF (2.5 µg/ml)				2402
IGF expanded	0,25	control				2402
IGF expanded	0,5	IGF (2.5 µg/ml)				2815
IGF expanded	0,5	control				2212
Related to Figure 14						
Insulin	0	control				1811
Insulin	1	Insulin (5 µg/ml)				1681
Insulin	1	control				1601
Insulin	7,5	control				1504
Related to Figure 14						
IGF rescue	0	control			20	3545
IGF rescue	0	IGF			20	3710
IGF rescue	0,1	control			20	3853
IGF rescue	0,1	IGF			20	3935
IGF rescue	0,25	control			20	3678
IGF rescue	0,25	IGF			20	4095
IGF rescue	0,5	control			20	4107
IGF rescue	0,5	IGF			20	4365
Related to Figure 14						
IGF	0	control				2242
IGF	0,5	IGF (2.5 µg/ml)				2047
IGF	0,5	control				2148
IGF	50	control				1379
IGF	0	IGF (0.5 µg/ml)				1874
IGF	0	IGF (1 µg/ml)				2388
IGF	0	IGF (2.5 µg/ml)				2244

6.4 PLASMID MAPS

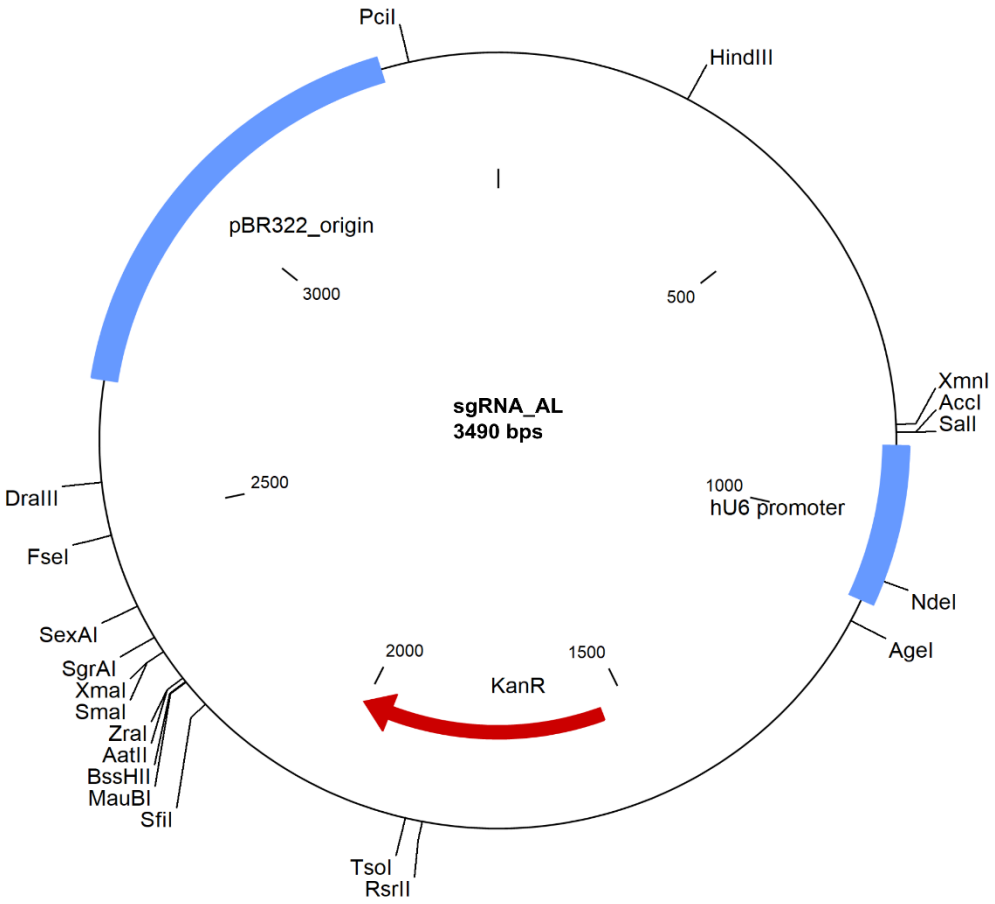

Figure 28: Plasmid map of sgRNA_AL.

Guide sequences were inserted into this plasmid.

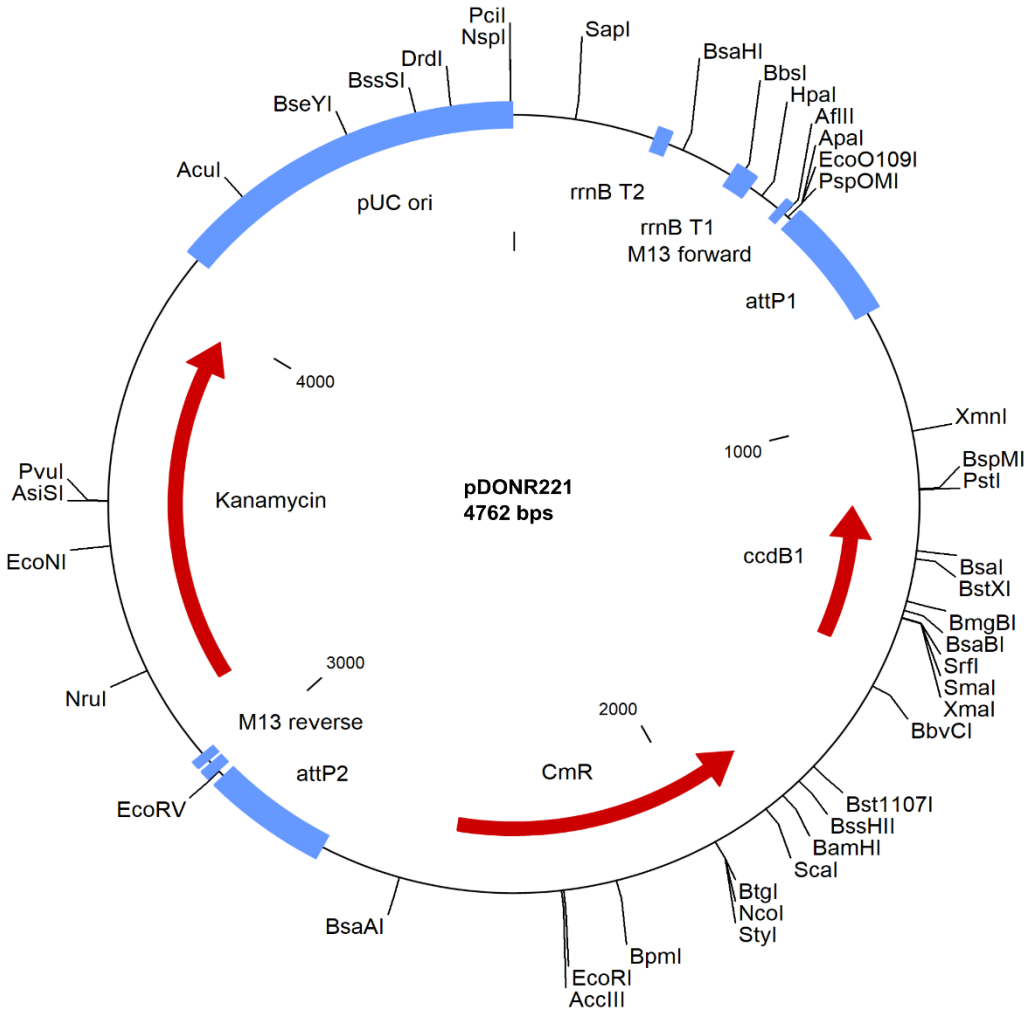

Figure 29: Plasmid map of pDONR221.

This plasmid was used as a backbone for the repair template.

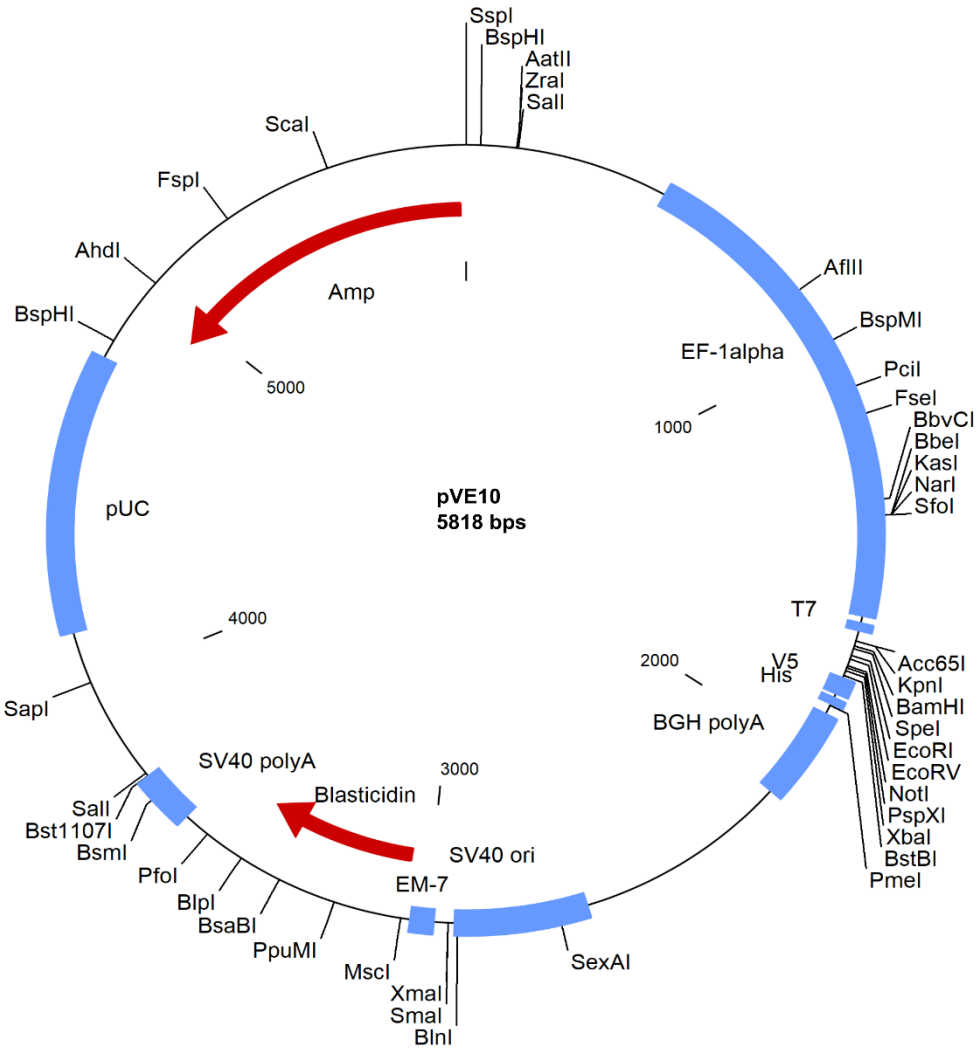

Figure 30: Plasmid map of pVE10.

The SV40-Blast_R sequence was amplified from this plasmid.

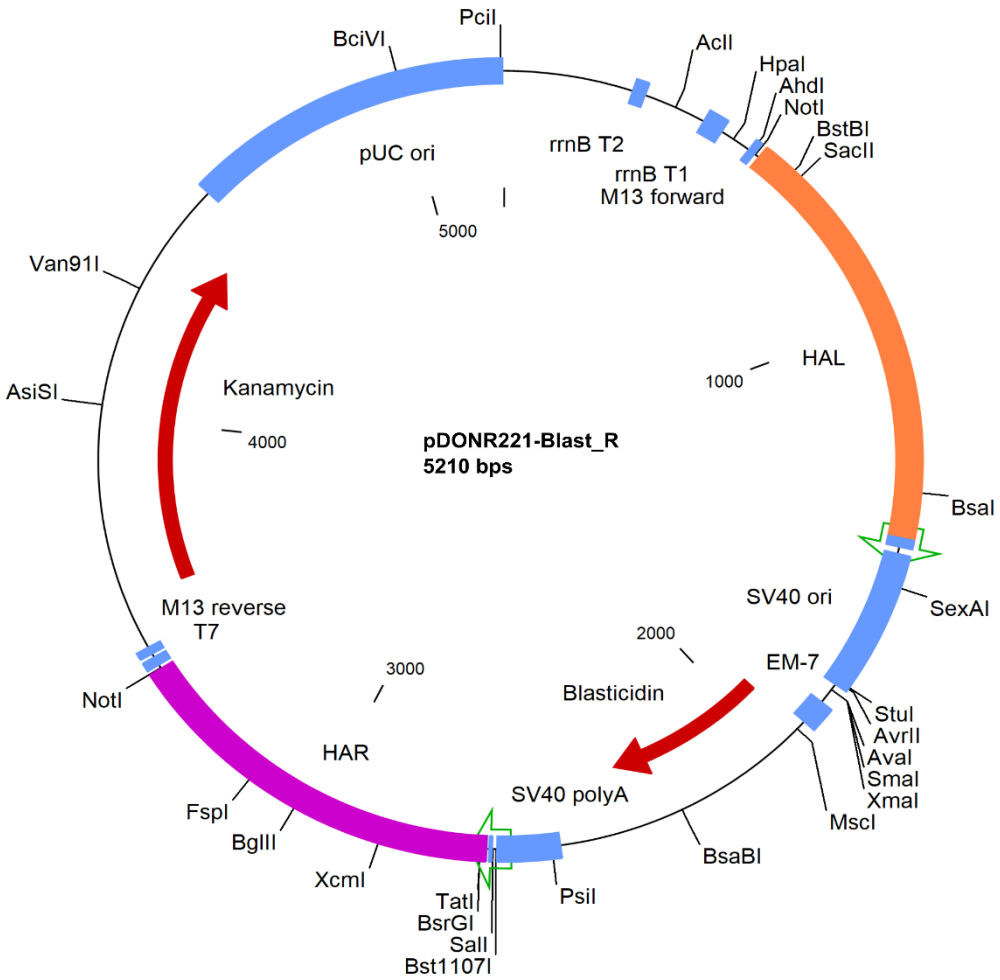

Figure 31: Plasmid map of pDONR221-Blast_R.

The plasmid pDONR221-Blast_R contains the repair template (HAL-SV40-Blast_R-HAR).

6.5 SEQUENCING OF *FST* KNOCKOUT CLONES

```
WT              CCTCCCTCTCGCCCACCTCCCATCTCTGTGATCAGGGCTTCCCCCTCCACTGCCTTCTTT
FST-1           CCTCCCTCTCGCCCACCTCCCATCTCTGTGATCAGGGCTTCCCCCTCCACTGCCTTCTTT
                ************************************************************

WT              TTCCACCCCTCCACCCCTTTCGATTTATTTCCTACTTTTCTCCCGCGTCTCTCTCACTTC
FST-1           TTCCACCCCTCCACCCCTTTCGATTTATTTCCTACTTTTCTCCCGCGTCTCTCTCACTTC
                ************************************************************

WT              CCCTCCTCCACGCTCACCCCCTCCCCATCCCCGCCGGGGTCTCCTTCGCTAGCCACCTCGC
FST-1           CCCTCCTCCACGCTCACCCCCTCCCCATCCCCGCCGGGGTCTCCTTCGCTAGCCACCTCGC
                ************************************************************

WT              TCTCCCTGCCCTGCCACCGCTCACTGCTCACTCACCCACCTCCCCACCCTTGTCTCTTCA
FST-1           TCTCCCTGCCCTGCCACCGCTCACTGCTCACTCACCCACCTCCCCACCCTTGTCTCTTCA
                ************************************************************

WT              CAGCTGGGAACTGCTGGCTCCGTCAAGCGAAGAACGGCCGCTGCCAGGTCCTGTACAAGA
FST-1           CAGCTGGGAACTGCTGGCTCCGTCAAGCGA--AACGGCCGCTGCCAGGTCCTGTACAARA
                ****************************  ************************** *

WT              CCGAACTGAGCAAGGAGGAGTGCTGCAGCACCGGCCGGCTGAGCACCTCGTGGACCGAGG
FST-1           CCGAACTGAGCAAGGAGGAGTGCTGCAGCACCGGCCGGCTGAGCACCTCGTGGACCGAGG
                ************************************************************

WT              AGGACGTGAATGACAACACACTCTTCAAGTGGATGATTTTCAACGGGGGCGCCCCCAACT
FST-1           AGGACGTGAATGACAACACACTCTTCAAGTGGATGATTTTCAACGGGGGCGCCCCCAACT
                ************************************************************

WT              CCTCCCTCTCGCCCACCTCCCATCTCTGTGATCAGGGCTTCCCCCTCCACTGCCTTCTTT
FST-26          CCTCCCTCTCGCCCACCTCCCATCTCTGTGATCAGGGCTTCCCCCTCCACTGCCTTCTTT
                ************************************************************

WT              TTCCACCCCTCCACCCCTTTCGATTTATTTCCTACTTTTCTCCCGCGTCTCTCTCACTTC
FST-26          TTCCACCCCTCCACCCCTTTCGATTTATTTCCTACTTTTCTCCCGCGTCTCTCTCACTTC
                ************************************************************

WT              CCCTCCTCCACGCTCACCCCCTCCCCATCCCCGCCGGGGTCTCCTTCGCTAGCCACCTCGC
FST-26          CCCTCCTCCACGCTCACCC----------------------------------------
                ******************

WT              TCTCCCTGCCCTGCCACCGCTCACTGCTCACTCACCCACCTCCCCACCCTTGTCTCTTCA
FST-26          ------------------------------------CCTCCCCACCCTTGTCTCTTCA
                                                     **********************

WT              CAGCTGGGAACTGCTGGCTCCGTCAAGCGAAGAACGGCCGCTGCCAGGTCCTGTACAAGA
FST-26          CAGCTGGGAACTGCTGGCTCCGTCAAG----------------------CTGTACAAGA
                ***************************                      **********

WT              CCGAACTGAGCAAGGAGGAGTGCTGCAGCACCGGCCGGCTGAGCACCTCGTGGACCGAGG
FST-26          CCGAACTGAGCAAGGAGGAGTGCTGCAGCACCGGCCGGCTGAGCACCTCGTGGACCGAGG
                ************************************************************

WT              AGGACGTGAATGACAACACACTCTTCAAGTGGATGATTTTCAACGGGGGCGCCCCCAACT
FST-26          AGGACGTGAATGACAACACACTCTTCAAGTGGATGATTTTCAACGGGGGCGCCCCCAACT
                ************************************************************
```

Figure 32: Sequencing results of *FST*-KO clones 1 and 26.

The region near the sgRNA binding site was sequenced and both clones showed deletions explaining the loss of the FST protein.

6.6 DATABASE RESOURCES USED FOR SMAD PATHWAY-ASSOCIATED GENES

Database resource	Reference
TGF-beta signaling pathway (KEGG)	[1]
TGF-beta signaling pathway	[2]
TGF-beta Receptor Signaling	[2]
ALK1 signaling (GDF11)	[2]
TGF-beta receptor signaling activates SMADs	[2]
SMAD Signaling Network	[2]
TGF-beta Signaling Pathways	[2]
Transcriptional feedback regulation of TGFb signaling	[3]

[1] Kanehisa et al., 2016 ; [2] Belinky et al., 2015 ; [3] Legewie, 2009

6.7 NUMBER OF TRACKED CELLS IN TIME-LAPSE MICROSCOPY EXPERIMENTS (PART 2)

Condition	Number of tracked cells
Figure 18D + E + G + H	
Quiescent control	1092
Quiescent TGFb	1256
Proliferating control	924
Proliferating TGFb	912
Figure 19A	
Quiescent control	790
Quiescent + EGF	899
Quiescent TGFb	815
Quiescent 4 h EGF	789
Quiescent 6 h EGF	811
Quiescent 8 h EGF	793
Figure 19C	
Quiescent control	235
Quiescent TGFb	303
Quiescent CDK4/6 + TGFb	402
Quiescent EGF + TGFb	478
Quiescent CDK4/6 + EGF + TGFb	779
Figure 19D + 20H	
Quiescent control	764
Quiescent TGFb	781
Proliferating control	796

Proliferating TGFb	704
EGFRi + TGFb	912
MEKi + TGFb	986
Quiescence GDF11	719
EGFRi + GDF11	891
MEKi + GDF11	907
Proliferating GDF11	697
PI3K + TGFb	2694
PI3K + GDF11	3183
Proliferating Control	4076
Figure 20A	
Quiescent control	1136
Quiescent 100 pM TGFb	1515
Quiescent 1 nM GDF11	2081
Quiescent 20 nM GDF11	1801
Quiescent 1 nM GDF8	2065
Quiescent 20 nM GDF8	1726
Quiescent 1 nM GDF3	2006
Quiescent 20 nM GDF3	2019
Quiescent 1 nM activin A	2165
Quiescent 20 nM activin A	2005
Proliferating control	1054
Proliferating 100 pM TGFb	895
Proliferating 1 nM GDF11	851
Proliferating 20 nM GDF11	971
Proliferating 1 nM GDF8	953
Proliferating 20 nM GDF8	1025
Proliferating 1 nM GDF3	925
Proliferating 20 nM GDF3	982
Proliferating 1 nM activin A	1054
Proliferating 20 nM activin A	965
Figure 20B-E + Figure 18A	
Quiescent control	1635
Quiescent 1 pM TGFb	1447
Quiescent 2.5 pM TGFb	1424
Quiescent 5 pM TGFb	1410
Quiescent 25 pM TGFb	1413
Quiescent 100 pM TGFb	1576
Quiescent 100 pM GDF11	1522
Quiescent 500 pM GDF11	1682
Quiescent 1 nM GDF11	1516

Quiescent 2.5 nM GDF11	1380
Quiescent 10 nM GDF11	1379
Proliferating Control	739
Proliferating 1 pM TGFb	744
Proliferating 2.5 pM TGFb	768
Proliferating 5 pM TGFb	702
Proliferating 25 pM TGFb	671
Proliferating 100 pM TGFb	649
Proliferating 100 pM GDF11	763
Proliferating 500 pM GDF11	649
Proliferating 1 nM GDF11	869
Proliferating 2.5 nM GDF11	803
Proliferating 10 nM GDF11	769
Figure 20F + 18F	
Proliferating control	1103
Proliferating GDF11	1128
Proliferating TGFb	1080
Quiescent control	1249
Quiescent GDF11	1248
Quiescent TGFb	1386
Figure 24B + C	
DRB + GDF11	1479
GDF11	1651
TGFb	1049
TGFBR3-OE TGFb	865
Figure 25 + 26 two biological replicates	
Quiescent control	5185
Quiescent 5 pm TGFb	4713
Quiescent 250 pM TGFb	2651
Quiescent 100 pM GDF11	3749
Quiescent 10 nM GDF11	572
Proliferating Control	4478
Proliferating 5 pM TGFb	1230
Proliferating 250 pM TGFb	355
Proliferating 100 pM GDF11	4901
Proliferating 10 nM GDF11	2692

7 ACKNOWLEDGEMENT

First, I would like to thank Prof. Dr. Alexander Löwer for giving me the opportunity to write my thesis in his research group. Thank you for all your support and guidance. I always appreciated that you took so much time to answer my questions and to support all my ideas. Working in your lab really helped me to grow as a scientist.

I would also like to thank Prof. Dr. Ulrike A. Nuber for taking over the second assessment of my thesis and for providing useful advice during TAC meetings.

Gratitude is owed to the whole research group for a great working atmosphere. Thank you for all the fun lunch breaks, for listening to all my complaints and for always giving useful input. Also, thanks for all the assistance in the lab.

I would like to thank my whole family for always supporting me. I want to thank my parents for their care, love and understanding. I am really happy that you are always there for me. I could not have asked for better parents. Also, thanks to my sister for always having a sympathetic ear for me.

Additionally, I would like to thank my friends (For Ever Eumels) for providing a much-needed distraction during this stressful time and their honest (sometimes too honest) friendship. After corona we have a lot of catching up to do and I am looking forward to it!

Finally, I would like to thank my girlfriend Sarah for her endless support. Thank you for your love and that you are always there for me no matter how annoying I am. We are a great team (Bohmpfl)! I am really glad to have you in my life.

8 CURRICULUM VITAE

Stefan Jürgen Bohn
Master of Science (Biology)
Born on 16th March 1991 in Heppenheim (Bergstraße)
Single

Academic Career

11/2016 – 04/2021	**PhD Student, Technical University Darmstadt** • Dissertation: **„**The Interplay of Signaling Dynamics and Cell Cycle Regulation in Single Cells**”**
10/2014 – 09/2016	**Master of Science Technical Biology, Technical University Darmstadt** • Master Thesis: **„**Investigating molecular mechanisms mediating stimulus-dependent SMAD signaling in single cells**”** • Grade: 1.2
10/2011 – 09/2014	**Bachelor of Science Biology, Technical University Darmstadt** • Bachelor Thesis: **„**Produktion eines Anti-Malaria-Nanobodies in Tabak” • Grade: 1.9

School Education

08/2001 – 06/2010	**Abitur, Starkenburg-Gymnasium, Heppenheim (Bergstraße)** Grade: 2.5

Awards

2017	**Masterpreis der Gesellschaft für Biochemie und Molekularbiologie (GBM)**

Puplications

Strasen, J., Sarma, U., Jentsch, M., **Bohn, S.**, Sheng, C., Horbelt, D., Knaus, P., Legewie, S., and Loewer, A. (2018). Cell-specific responses to the cytokine TGFβ are determined by variability in protein levels. Molecular Systems Biology 14, e7733. https://doi.org/10.15252/msb.20177733.

Benary, M., **Bohn, S.**, Lüthen, M., Nolis, I.K., Blüthgen, N., and Loewer, A. (2020). Disentangling Pro-mitotic Signaling during Cell Cycle Progression using Time-Resolved Single-Cell Imaging. Cell Reports 31, 107514. https://doi.org/10.1016/j.celrep.2020.03.078.

9 EHRENWÖRTLICHE ERKLÄRUNG

Ich erkläre hiermit ehrenwörtlich, dass ich die vorliegende Arbeit entsprechend den Regeln guter wissenschaftlicher Praxis selbstständig und ohne unzulässige Hilfe Dritter angefertigt habe.

Sämtliche aus fremden Quellen direkt oder indirekt übernommenen Gedanken sowie sämtliche von Anderen direkt oder indirekt übernommenen Daten, Techniken und Materialien sind als solche kenntlich gemacht. Die Arbeit wurde bisher bei keiner anderen Hochschule zu Prüfungszwecken eingereicht.

Darmstadt, den